JAN. - APR. 2008
Volume XIV Number I

ISSN 0859 144X

THE ASEAN JOURNAL OF RADIOLOGY

Published by The Radiological Society and
The Royal College of Radiologists of Thailand,
Bangkok, Thailand

Started through an educational grant from Bracco since 1995

THE IMAGE OF INNOVATION

JAN. - APR. 2008
Volume XIV Number I

ISSN 0859 144X

THE ASEAN JOURNAL OF RADIOLOGY

Published by The Radiological Society and
The Royal College of Radiologists of Thailand,
Bangkok, Thailand

Chief Editor

Professor Kawee Tungsubutra
Kaweevej Hospital, 318 Tarksin Road, Dhonburi, Bangkok 10600, Thailand.

Asean Journal of Radiology.
Instructions for Authors.

1. The Asean Journal of Radiology publishes the papers on Radiological Sciences, such as research work, review articles, case reports, innovations in Medical Sciences related to all branches of Radiology, and letters to the editor. The aforementioned materials can be written in English only.

2. The authors have to submit 2 copies of the manuscript and a diskette: **to Prof. Dr. Kawee Tungsubutra.** 318 Kaweevej Hospital, Tarksin Road, Dhonburi, Bangkok 10600, Thailand.

3. The original copy to be submitted must be typed in a double space on one side of the page of 8.1/2" x 11.1/2" paper.

4. The format of the article must include :
   a. Title page and address of the author (s)
   b. Abstract
   c. Introduction (Background)
   d. Material and Method
   e. Results and discussion (Tables and Illustrations)
   f. Acknowledgement (if any)
   g. References (Follow the Vancouver style developed by ICMJE)

5. We will provide 5 copies of reprints for the author (s) who submit (s) an article for publication in the Asean Journal.

6. The illustrations and tables must be clearly prepared with legends in English as they are the art works to be reproduced.

7. The authors are reponsible for the contents of the article as to its facts and findings.

8. Ethics.

Paper reporting studies which might be interpreted as human experimentation (e.g. controlled trials) should conform to the standards of the Declaration of Helsinki (see British Medical Journal 1964: 2: 177) and should indicate that, approval that such studies may proceed, has been granted by the local or hospital Ethics Committee.

When reporting experiments on animals indicate whether the institution's or the National Research Council's guide for, or any national law on, the care and use of laboratory animals was followed.

THE ASEAN JOURNAL OF RADIOLOGY

Volume XIV Number I JAN. - APR. 2008

CONTENTS

THE ASEAN JOURNAL OF RADIOLOGY

Volume XIV Number I JAN. - APR. 2008

CONTENTS

A PROSPECTIVE TRIAL OF IODIXANOL 270, 320 (VISIPAQUE) IN PATIENTS WITH RENAL IMPAIRMENT (WHO HAS SERUM CREATININE BETWEEN 1.8-3.0 MH/DL.) UNDERGOING COMPUTED TOMOGRAPHY AND INTRAVENOUS PYELOGRAPHY

Wayupa WONGWIKROM, MD.[1]

OBJECTIVES: This study was designed to determine the nephrotoxicity of iodixanol in patients with renal impairment undergoing computed tomography and intravenous pyelography.

BACKGROUND: Iodixanol, a nonionic, dimeric, iso-osmolar contrast medium (IOCM), may be the alternative use in renal insufficiency patients, as treatment is limited to supportive measures while awaiting the resolution of the renal impairment

MATERIALAND METHODS: The prospective study in patients with high serum creatinine between 1.8-3.0 mg/dl. who are undergoing computed tomography and intravenous pyelography. Most of the patients age are about 50-95 years. Serum creatinine measurement were performed before and after 72 hours (IPD case) or 7 days (OPD case) intravenous injection of Iodixanol. At what level of serum creatinine do radiologists become anxious enough to withhold IV contrast (unless it is essential) -we begin to worry at around 1.7-1.8 and above this, so we design the sample size of patients who have serum creatinine between 1.8- 3.0 mg/dl.

RESULTS: The creatinine concentration increased significantly less in patients who received iodixanol.

CONCLUSIONS: Nephropathy induced by contrast medium may be less likely to develop in high-risk patients when iodixanol is used in patients with high serum creatinine (1.8 - 3.0 mg/dl.) who must be awareness in IV contrast administration use.

Key words: Computed tomography (CT scan), Intravenous pyelography (IVP), Renal insufficiency, serum creatinine, CIN (contrast-induced nephropathy).

INTRODUCTION

Acute renal failure is serious and treatment is costly.[1,2] Nephropathy induced by contrast medium remains one of the most clinically important complications of the use of iodinated contrast medium.[2,3,4,5,6] Most commonly, it is defined as an acute impairment of renal function manifested by an absolute increase in the serum creatinine concentration of at least 0.5 mg per deciliter (44.2 μmol per liter) or by a relative increase of at least 25 percent from the base-line value.[7,8,9,10,11] The serum creatinine concentration typically peaks on the second or third day after exposure to contrast medium and usually returns to the base-line value within two weeks.[6,12] However, renal function may not return to its base-line level,

[1] Head, Department of Radiology, Chonburi Hospital, 20000, Thailand. **Email:** onewayupa@yahoo.com **HP:** 081-9494030 **Chonburi hospital no.** 038-931000, 038-931489, 038-931488

contributing to an increased risk of death.[2,12]

The incidence of nephropathy induced by low-osmolar contrast medium is low in the general population and has been calculated to be less than 2 percent.[3] Patients at increased risk include those with renal impairment and diabetes, especially in combination.[8,10,13] In such patients, the incidence is significantly higher, in the range of 12 to 50 percent.[2,4,8,10,14,15,16,17,18] Large clinical studies and meta-analyses have indicated that the use of low-osmolar contrast medium substantially reduces the risk of nephropathy in high -risk patients as compared with the use of high-osmolar contrast medium.[8,9,11,14,19,20]

Iodixanol, a nonionic, dimeric contrast medium, is iso-osmolar to blood at all concentrations, and its level of general toxicity is lower than that of low-osmolar contrast mediums.[21,22,23] Extensive investigations of iodixanol in low-risk patients (patients without diabetes who have normal renal function) have shown no difference between the frequency of nephropathy associated with iodixanol and that of nephropathy associated with low-osmolar contrast mediums.[3,21,24] This absence of difference may reflect the low risk of nephropathy in low-risk patients.[7]

MATERIAL AND METHODS

The prospective study in patients with high serum creatinine between 1.8-3.0 mg/dl. who undergoing computed tomography and intravenous pyelography. Almost patients's age are about 50-95 years. Serum creatinine measurement was performed before and after 72 hours intravenous injection of Iodixanol. Criteria for exclusion were pregnancy, lactation, intravascular administration of an iodinated contrast medium within the previous seven days, treatment with metformin or nonsteroidal antiinflammatory drugs within the previous 48 hours, intake of nephrotoxic drugs within the previous seven days, history of serious reactions to iodinated contrast mediums, newly discovered unstable diabetes, severe concomitant disease, renal transplantation, or end-stage renal disease necessitating dialysis. Written informed consent was obtained from each patient before enrollment.

Patients protocol: Almost patients's age are about 50-95 years. with high serum creatinine between 1.8-3.0 mg/dl. who undergoing computed tomography and intravenous pyelography.

Study protocol: It was designed to determine the renal effects of a nonionic, iso-osmolar, dimeric contrast medium, iodixanol (270, 320 mg of iodine per milliliter) (Visipaque). Each patient was assigned to receive a nonionic, iso-osmolar, dimeric contrast medium. The volume used varied among patients and was not standardized. All patients were to be well hydrated before computed tomography or intravenous pyelography, according to local regimens. It was recommended, but not required, that patients receive 500 ml of water orally, 500 ml of saline intravenously, or both before the computed tomography or intravenous pyelography, followed by 1 liter of 0.9 percent saline or similar fluids intravenously from the start of the procedure.

The follow-up period was seven days. Serum creatinine was measured before examination (at base line, or day 0) and on days 3- 7 according to IPD or OPD patients.

RESULTS

The prospective study in patients with high serum creatinine between 1.8-3.0 mg/dl. who undergoing computed tomography and intravenous pyelography. Almost patients's age are about 50-95 years. There is 55 % reduced in serum creatinine, 36 % increased in serum creatinine and 9 % unchanged serum creatinine. All the results possibly depend on many factors such as patient status (underlying disease), pre-investigation hydrated patient, post -investigation hydrated patient.

DISCUSSION

Contrast-induced nephropathy (CIN), usually defined as an increase in serum creatinine of 44 μmol litre-1 (0.5 mg dl-1) or a 25% increase from the

baseline value 48 hours after intravascular injection of contrast media, is a common and potentially serious complication of the use of iodinated contrast media in patients at risk of acute renal injury. It is an important cause of hospital-acquired renal failure, may be a difficult differential diagnosis and the incidence does not appear to have changed over the last few decades.

In the general population, the incidence of CIN is estimated to be 1-2%. However, the risk for developing CIN may be as high as 50% in some patient subgroups, such as those with diabetes mellitus and pre-existing renal impairment. The impact of CIN on clinical outcomes has been evaluated most extensively in patients undergoing percutaneous coronary intervention where it is associated with increased mortality both in hospital and at 1 yr. As treatment is limited to supportive measures while awaiting the resolution of the renal impairment, emphasis needs to be directed at prevention.

In the general population, the incidence of contrast-induced kidney impairment is less than two per cent. For patients with diabetes and existing renal impairment, the risk is significantly higher - and the number of patients in this high-risk category is growing, due to the increased incidence of lifestyle-related diabetes and the ageing population.

The contrast media affect kidney function is not clearly understood. However, medical literature suggests several factors could be involved, and indicates that osmolality, or the concentration of particles in solution in the contrast agent as opposed to the blood, may be one of the key factors in high -risk patients.

We designed this study in patients who do need IV contrast administration use which we begin to worry about high serum creatinine (1.8 - 3.0 mg/dl). Before nonionic, iso-osmolar, dimeric contrast (Visipaque) is used. We deny IV contrast administration in this high serum creatinine patient group. Some patients were not received computed tomography or intravenous pyelography and may undergoing to explore in surgical case or wait and wait in IPD. In summary, we have found the limitation of the study is the limited number of patients (small sample size) but we hope that this study may be the alternative way of IV contrast used in patient who has high serum creatinine between 1.8-3.0 mg/dl. and do need the IV contrast investigation.

CONCLUSION

Nephropathy induced by contrast medium may be less likely to develop in high-risk patients when iodixanol, a nonionic, dimeric, iso-osmolar contrast medium is used in patients with high serum creatinine (1.8 - 3.0 mg/dl.) who must be awareness in IV contrast administration used.

Alternative way of IV contrast investigation in patients who have high serum creatinine between 1.8- 3.0 mg/dl. is by using Iodixanol, a nonionic, dimeric, iso-osmolar contrast medium to help the clinician to give faster and better treatment to patients while awaiting the resolution of the renal impairment. Increased turn over rate of IPD patients. Reduce the cost of long time hospitalization.

ACKNOWLEDGEMENTS

The auther would like to express our deep appreciation to Professor Kawee Tungsubutra (Editor-in-Chief) for reviewing the manuscript.

REFERENCES

1. Turney JH. Acute renal failure -- a dangerous condition. JAMA 1996; 275: 1516-1517.
2. Rihal CS, Textor SC, Grill DE, et al. Incidence and prognostic importance of acute renal failure after percutaneous coronary intervention. Circulation 2002; 105: 2259-2264.
3. Berg KJ. Nephrotoxicity related to contrast media. Scand J Urol Nephrol 2000; 34: 317 -322.
4. Cochran ST, Wong WS, Roe DJ. Predicting angiography-induced acute renal function impairment: clinical risk model. AJR Am J Roentgenol 1983; 141: 1027-1033.

5. Morcos SK, Thomsen HS, Webb JA. Contrast-media-induced nephrotoxicity: a consensus report. Eur Radiol 1999;9:1602 -1613.
6. Waybill MM, Waybill PN. Contrast media -induced nephrotoxicity: identification of patients at risk and algorithms for prevention. J Vasc Interv Radiol 2001; 12: 3-9.
7. Barrett BJ, Parfrey PS, Vavasour HM, et al. Contrast nephropathy in patients with impaired renal function: high versus low osmolar media. Kidney Int 1992; 41: 1274-1279.
8. Rudnick MR, Goldfarb S, Wexler L, et al. Nephrotoxicity of ionic and nonionic contrast media in 1196 patients: a randomized trial: the Iohexol Cooperative Study. Kidney Int 1995; 47: 254-261.
9. Taliercio CP, Vlietstra RE, Ilstrup DM, et al. A randomized comparison of the nephrotoxicity of iopamidol and diatrizoate in high risk patients undergoing cardiac angiography. J Am Coll Cardiol 1991; 17: 384-390.
10. Manske CL, Sprafka JM, Strony JT, Wang Y. Contrast nephropathy in azotemic diabetic patients undergoing coronary angiography. Am J Med 1990; 89: 615-620.
11. Wang A, Holcslaw T, Bashore TM, et al. Exacerbation of radiocontrast nephrotoxicity by endothelin receptor antagonism. Kidney Int 2000; 57: 1675-1680.
12. Levy EM, Viscoli CM, Horwitz RI. The effect of acute renal failure on mortality: a cohort analysis. JAMA 1996; 275: 1489-1494.
13. McCullough PA, Wolyn R, Rocher LL, Levin RN, O'Neill WW. Acute renal failure after coronary intervention: incidence, risk factors, and relationship to mortality. Am J Med 1997; 103: 368-375.
14. Lautin EM, Freeman NJ, Schoenfeld AH, et al. Radiocontrast-associated renal dysfunction: a comparison of lower-osmolality and conventional high-osmolality contrast media. AJR Am J Roentgenol 1991; 157: 59-65. [Erratum, AJR Am J Roentgenol 1991; 157: 895.]
15. Morcos SK. Contrast media-induced nephrotoxicity -- questions and answers. Br J Radiol 1998; 71: 357-365.
16. Weisberg LS, Kurnik PB, Kurnik BR. Risk of radiocontrast nephropathy in patients with and without diabetes mellitus. Kidney Int 1994; 45: 259-265.
17. Parfrey PS, Griffiths SM, Barrett BJ, et al. Contrast material-induced renal failure in patients with diabetes mellitus, renal insufficiency, or both: a prospective controlled study. N Engl J Med 1989; 320: 143-149.
18. Schwab SJ, Hlatky MA, Pieper KS, et al. Contrast nephrotoxicity: a randomized controlled trial of a nonionic and an ionic radiographic contrast agent. N Engl J Med 989; 320: 149-153.
19. Barrett BJ. Contrast nephrotoxicity. J Am Soc Nephrol 1994; 5: 125-137.
20. Barrett BJ, Carlisle EJ. Metaanalysis of the relative nephrotoxicity of high- and low -osmolality iodinated contrast media. Radiology 1993; 188: 171-178.
21. Grynne BH, Nossen JO, Bolstad B, Borch KW. Main results of the first comparative clinical studies on Visipaque. Acta Radiol Suppl 1995; 399: 265-270.
22. Jakobsen JA. Renal experience with Visipaque. Eur Radiol 1996; 6: Suppl 2: S16-S19.
23. Davidson CJ, Laskey WK, Hermilller JB, et al. Randomized trial of contrast media utilization in high-risk PTCA: the COURT trial. Circulation 2000; 101: 2172-2177.
24. Murakami R, Tajima H, Kumazaki T, Yamamoto K. Effect of iodixanol on renal function immediately after abdominal angiography: clinical comparison with iomeprol and ioxaglate. Acta Radiol 1998; 39: 368-371.

CASE REPORT: PRIMARY CARDIAC SARCOMA

Chalakot DEJARKOM, MD[1]

ABSTRACT

A 14-years-old female was admitted to the hospital with the chief complaint of having hemoptysis and progressive dyspnea. The imaging studies revealed pericardial, myocardial and mediastinal mass with bilateral lung nodules. The tumor could not be resected through a thoracotomy, only biopsies could be taken. The final diagnosis was cardiac sarcoma. The patient received chemotherapy and three days after that she died from severe hemoptysis and cardiac arrest.

INTRODUCTION

Primary cardiac neoplasms are rare. It is estimated that primary cardiac neoplasms are 100-1,000 times less prevalent than secondary neoplasms of the heart. Even among primary cardiac tumors, the majority is benign and most frequently are atrial myxomas. Sarcomas are the second most common primary cardiac tumor. Reported here is a case of primary cardiac sarcoma in a 14-years-old female.

CASE RERORT

A 14-years-old female was admitted for hemoptysis and progressive dyspnea especially on exertion. Two weeks prior to admission she had dyspnea and weight loss about 2 kg in 2 weeks. She had underlying thalassemia (Hemoglobin E trait). She had no history of asbestos exposure.

On physical examination, she had low grade fever (37-38 c°), dyspnea, and pulse rate was 100 beats/min. She had mild pale. Lung had fine crepitation both lower lungs. Heart showed PMI at 6th intercostal space, mid clavicular line, RV heaving, no thrill, regular rhythm, normal S1, S2, no murmur. JVP was normal.

The laboratory data revealed mild anemia and leukocytosis (Hemoglobin 8.3 g/dl, Hematocrit 25%, WBC 18,100/ml, platelet 211,000/ml). Three days sputum exam for AFB was negative. ESR was 39 mm/hr (0-20).

Electrocardiogram showed inverted T at II, III, AVF, V1-V5 leads.

Chest radiograph showed widening of cardiac shadow, bilateral reticulonodular infiltration with round mass with well defined border at left lower lobe (Figure 1A,1B).

Echocardiogram demonstrated large inhomogeneous mass attach to the right atrium without obstruction during cardiac cycle, suggested cardiac tumor. No pericardial effusion was detected (Figure 2).

A computed tomography scan of the chest revealed heterogeneous enhancing mass involving right atrium, right ventricle, pericardium and mediastinum, representing malignant pericardial tumor with myocardial and mediastinal involvement or myocardial tumor with pericardial and mediastinal involvement. Multiple pulmonary nodules were detected, suggestive of pulmonary metastases (Figure 3).

[1] Department of Radiology, Buddhachinnaraj Hospital, Muang, Phitasanulok, THAILAND. 65000

The patient was sent to performed percutaneous transpericardial window biopsy but unfortunately it failed to demonstrate the pathology.

Then the patient underwent surgery to obtain biopsy or excision of the tumour. Open thoracotomy was performed. Huge semisolid well-circumsribed tumor at anterior mediastinal space with multiple palpable nodules, varying in size of pulmonary nodules and moderate right pleural effusion were demonstrated. The tumor could not be resected, only biopsy was performed.

Tissue from anterior mediastinum showed multiple pieces of brownish tissue in macroscopic masses measuring 3x2x1 cm in aggregation. The histology revealed sheets of tumor cells which are large polygonal as well as rather elongated cells (Figure 4A). Those tumor cells contained enlarged nuclei with prominent nucleoli. No gland or keratin formation was noted. Immunohistochemical studies revealed the tumor cells were immunoreactive for vimentin, but not with CK, CD3, CD45, CD79a, PLAP, Tdt, or CEA (Figure 4B). The final histopathologic diagnosis was malignant lesion, suggestive of sarcoma.

All treatment options were extensively considered and discussed. With the diagnosis of primary cardiac sarcoma with pulmonary metastasis, she was put on palliative chemotherapy. Three days after chemotherapy she died from severe hemoptysis and cardiac arrest.

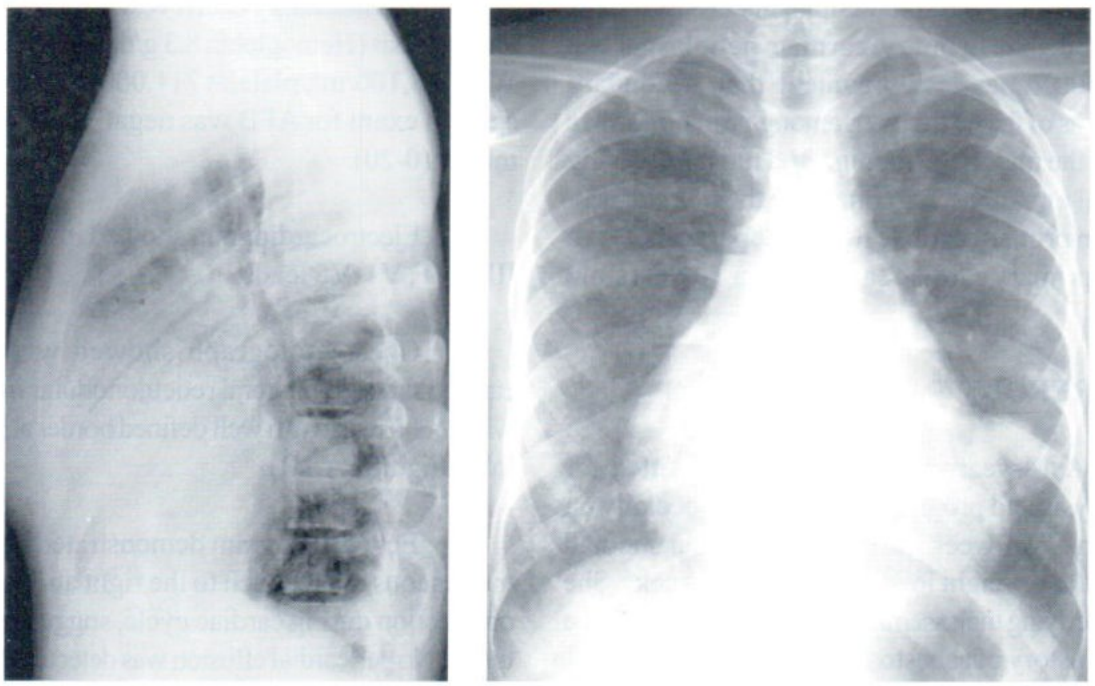

Fig.1A and 1B Chest radiograph (PA, upright and lateral views) showed widening of cardiac shadow, bilateral reticulonodular infiltration with round mass at left lower lobe.

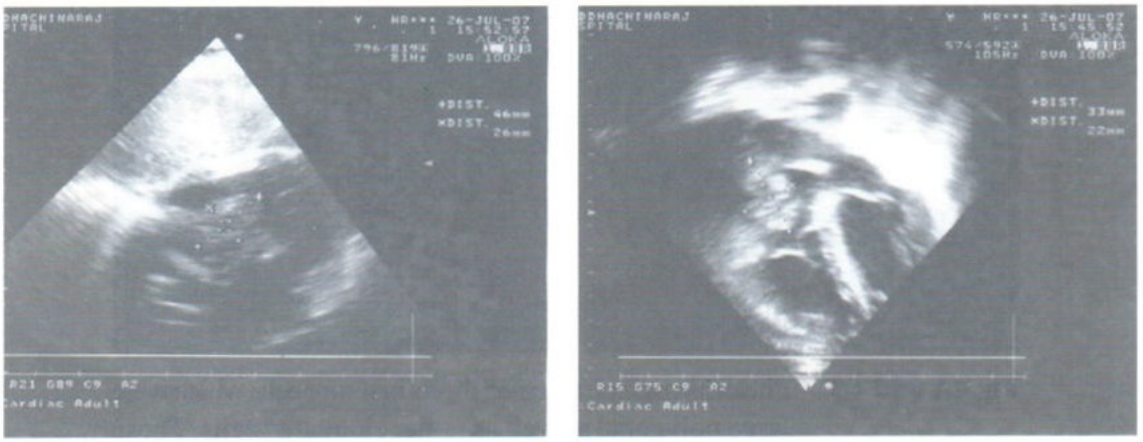

Fig.2 Echocardiogram demonstrated large inhomogeneous mass attach to right atrium without obstruction during cardiac cycle, suggestive of cardiac tumor. No pericardial effusion was detected.

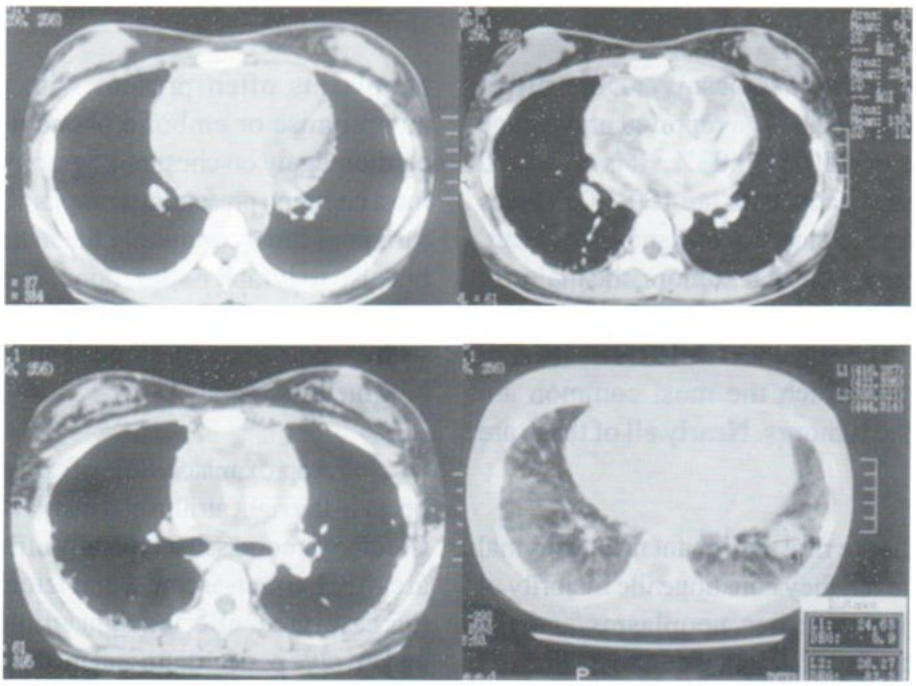

Fig.3 (3A; NECT, 3B and 3C; CECT, 3D; lung window) CTchest revealed heterogeneous enhancing mass involving right atrium, right ventricle, pericardium and mediastinum, which extended from SVC recess into pericardial cavity. Multiple nodular lesions seen in both lungs suggestive of pulmonary metastases.

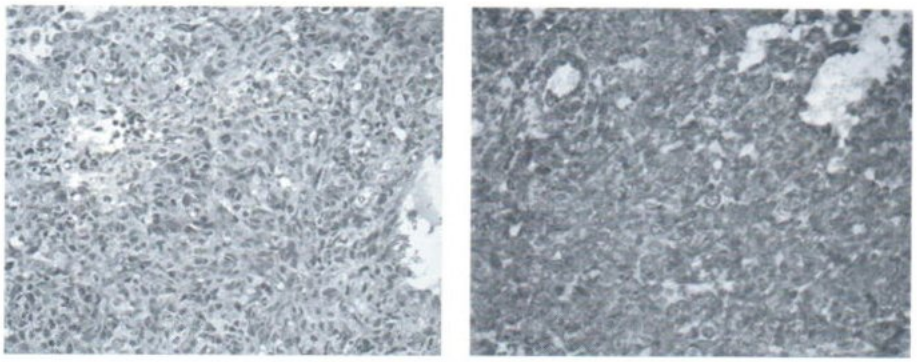

Fig.4A and 4B Photomicrograph revealed sheets of tumor cells which were large polygonal as well as rather elongated cells. Those tumor cells contained enlarged nuclei with prominent nucleoli. No gland or keratin formation was noted (4A). (H&E x40) Immunohistochemical study; the tumor cells revealed cytoplasmic staining with vimentin antibody (4B). (x40)

DISCUSSION

Primary cardiac neoplasms are rare, affect patients of all ages, and have a reported prevalence in autopsy series of 0.001%-0.03%.[1] It is estimated that primary cardiac neoplasms are 100-1,000 times less prevalent than secondary neoplasms of the heart. Even among primary cardiac tumors, the majority (approximate 75%) is benign and most frequently are atrial myxomas.[2] The remainder includes a variety of other tumours, of which the most common are malignant cardiac tumours. Nearly all of these are sarcomas.[3]

Sarcomas are rare malignant mesenchymal neoplasms; however, they constitute the majority of primary malignant cardiac neoplasms and the second most common primary cardiac tumor.[4] Primary cardiac sarcomas, by definition, are confined to the heart or pericardium at the time of diagnosis with no evidence of extracardiac primary neoplasm. Although all types of sarcomas affect the heart, the most common cell types are angiosarcoma (37% of cases), unclassified or undifferentiated sarcoma (24%), malignant fibrous histiocytoma (MFH) (11%-24%), leiomyosarcoma (8%-9%), and osteosarcoma (3%-9%).[5]

Patients affected with cardiac or pericardial neoplasms often present with cardiovascular compromise or embolic phenomena and exhibit cardiomegaly on chest radiography. Dyspnea is the most common presenting complaint. Primary cardiac sarcomas most commonly metastasize to the lungs but also to lymph nodes, bone, liver, brain, bowel, spleen, adrenal .[1,4,7] As in this case, she presented with dyspnea and at the time of presentation, she had lung metastases.

Approximately 80% of cardiac angiosarcomas occur in the right atrium and involve the pericardium. Cardiac sarcomas that typically affect the left atrium are MFH, osteosarcoma, and leiomyosarcoma.[5] In this case tumor affected right atrium, right ventricle and involve pericardium and mediastinum.

The pathologic features of cardiac sarcoma are extremely varied. The vast majority of cardiac sarcomas are large, invasive masses at the time of diagnosis. The most common cell types are angiosarcoma , unclassified or undifferentiated sarcoma and malignant fibrous histiocytoma (MFH)[5,6] Unclassified and undifferentiated sarcomas are lack of specific histologic, ultrastructural ,or immunohistochemical features.[1,4] In this case histologic type was unclassified sarcoma.

The most common radiographic abnormality in patients with cardiac sarcoma is cardiomegaly. Other findings include heart failure, pleural effusion, focal cardiac mass, pulmonary consolidation, and pericardial effusion.[4,5]

Echocardiography remains the initial imaging modality of choice for evaluating cardiac masses. It accurately delineates cardiac anatomy in multiple aspects. However, echocardiography has limited capability to demonstrate tumor infiltration and cannot delineate mediastinal and extracardiac involvement.[8] In this case, echocardiogram showed large inhomogeneous mass attach to the right atrium without obstruction during cardiac cycle, suggestive of cardiac tumor.

Because CT is beneficial in the evaluation of cardiac sarcomas as it demonstrates the broad-based tumor attachment; myocardial, pericardial, and mediastinal invasion; as well as extension into the great vessels and pulmonary metastases. In this case, CT scan revealed heterogeneous enhancing mass involving right atrium, right ventricle, pericardium and mediastinum, which may be pericardial tumor with myocardial and mediastinal involvement or myocardial tumor with pericardial and mediastinal involvement. Multiple nodular lesions were suggestive of pulmonary metastases.

MR imaging typically demonstrate large, heterogeneous, broad-based masses that frequently occupy most of the affected cardiac chamber or multiple chambers. Pericardial and extracardiac invasion, valvular destruction, tumor necrosis, and metastases are frequently seen and are all characteristic features of malignant lesions. Pericardial invasion is characterized by disruption, thickening, or nodularity. In this case MRI was not performed.[9,10]

Primary cardiac sarcomas are highly aggressive lesions that are uniformly fatal. The mean survival of affected patients is from 3 months to 1 year.[1,4] The patient outcome is almost invariably poor due to unfavorable location, their rapid growth and early metastasis. However, the mainstay of treatment is surgical resection because the surgical resection can substantially alleviate symptoms and yield a modest improvement in survival.[2,8] Even after complete tumor excision, however, local recurrence and metastatic disease occur frequently and early, usually within 1 year.[4] Chemotherapy and radiation therapy have not proved to be beneficial for the treatment of affected patients.[11,12] Death in these patients usually results from postoperative complications, cardiopulmonary failure from progressive tumor growth, and metastatic disease.[4] Heart transplantation has been performed in some patients with unresectable cardiac sarcoma with satisfactory results.[11,13] Success of molecular targeted therapy in gastrointestinal stromal tumor, Kapposi's sarcoma and angiosarcoma, has given an exciting new prospect for treatment of cardiac sarcoma. However, in this case palliative approach was preferred.

CONCLUSION

Primary cardiac sarcoma is a rare tumor and has a very poor prognosis due to very aggressive behavior, most often presents with advanced disease and early metastasis. The initial diagnosis is usually suggestive at echocardiogram, but identification of mediastinal invasion and extracardiac metastasis is best achieved with CT and MRI. The mainstay of treatment is surgical resection. However, local recurrence and metastatic disease occur frequently and early. Chemotherapy and radiation therapy have not proved beneficial for the treatment of affected patients. So the mean survival of affected patients is from 3 months to 1 year.

ACKNOWLEDGEMENT

The author would like to thanks Professor Benjaporn Chaiwun, MD, Department of pathology, Faculty of Medicine, Chaingmai University for pathological report and pictures. Thanks also to Apichart Chanthra, MD, Department of pediatric, Buddhachinnaraj Hospital for echocardiogram report and pictures.

The author acknowledges Associated

Professor Nisa Muangman, MD, Department of radiology, Siriraj Hospital for revision of the manuscript.

REFERENCE

1. Burke A, Virmani R. Atlas of tumor pathology. 3rd ed. Washington, DC: Armed Forces Institute of Pathology; 1996.
2. Vander Salm TJ. Unusual primary tumors of the heart. Semin Thorac Cardiovasc Surg 2000; 12(2): 89-100.
3. De Zwaab C, Bekkers SCAM, Van Garsse L, Jansen R, Van Suylen RJ. Primary monophasic mediastinal, cardiac and pericardial synovial sarcoma: a young man in distress. Neth Heart J 2007; 15(6): 226-8.
4. Burke AP, Cowan D, Virmani R. Primary sarcomas of the heart. Cancer 1992; 69 (2): 387-95.
5. Grebenc ML, Christenson ML, Burke AP, Green CE, Galvin ER. Primary Cardiac and Pericardial Neoplasms: Radiologic-Pathologic Correlation. RadioGraphics 2000; 20 (4): 1073-103.
6. Bishnoi SK, Bardia A, Meena VYGL, Jakhar S, Jain S. Case report -I; Primary cardiac sarcoma. Indian Journal of Medical & Peadiatric Oncology 2007; 28(2): 40-3.
7. Burke AP, Virmani R. Osteosarcomas of the heart. Am J Surg Pathol 1991; 15(3): 289-95.
8. Best AK, Dobson RL, Ahmad AR. Best Cases from the AFIP Cardiac Angiosarcoma. RadioGraphics 2003; 23 Suppl 1: S141-5.
9. Araoz PA, Eklund HE, Welch TJ, Breen JF. CT and MR imaging of primary cardiac malignancies. RadioGraphics 1999; 19(6): 1421-34.
10. Siripornpitak S, Higgins CB. MRI of primary malignant cardiovascular tumors. J Comput Assist Tomogr 1997; 21(3): 462-6.
11. Putnam JB, Sweeney MS, Colon R, Lanza LA, Frazier OH, Cooley DA. Primary cardiac sarcomas. Ann Thorac Surg 1991; 51(6): 906-10.
12. Butany J, Yu W. Cardiac angiosarcoma; two cases and a review of the literature. Can J Cardiol 2000; 16(2): 197-205
13. Gowdamarajan A, Michler RE. Therapy for primary cardiac tumors: is there a role for heart transplantation? Curr Opin Cardiol 2000; 15(2): 121-5.

SPATIAL RESOLUTION PERFORMANCE OF WHOLE-BODY LSO PET/CT SCANNER

Chatchai NAVIKHACHEEVIN, M.Sc.[1]

ABSTRACT

Spatial resolution of Biograph 16 HI-REZ PET/CT system has been performed following the NEMA NU 2-2001 protocols. Three types of point source made with capillary tube, tiny foam bead, and ion exchanged resin were used for this purpose. ImageJ software was used to analyze the reconstruction image on PC. The results from three types of point source were in acceptance limit. In this study, point source made with resin was easy to be prepared and small size for spatial resolution performance.

Key Words: LSO, PET/CT, Biograph 16 HI-REZ

INTRODUCTION

Spatial resolution is one of the performance parameter for PET/CT scanner. This represents its ability to distinguish between two points of radioactivity in an image. The full description of spatial resolution requires two components; a transaxial component in the planes perpendicular to the scanner axis, and an axial component parallel to the axis (slice thickness). In addition, for off-center positions, transaxial resolution is usually given in terms of a radial (along the radius) and a tangential (perpendicularly to the radius) components. Common methods to measure this in emission tomography are to image a point source giving a point spread function (PSF), or a line spread function (LSF). Usually, the resolution is expressed as the full width at half maximum (FWHM) of the profile. Good approximation used frequently to this profile is Gaussian function. There are many factors that influence the resolution in a PET reconstruction. These include non-zero positron range after radionuclide decay, non-colinearity of the annihilation photons due to residual momentum of the positron, distance between the detectors, width of the detectors, stopping power of the scintillation detector, incident angle of the photon on the detector, the depth of the interaction of the photon in the detector, number of angular samples, and reconstruction parameter (matrix size, windowing of the reconstruction filter, etc.).[1,2] The detector array of current clinical scanners may consist of many rings of detectors, which are aligned axially. A volumetric PET data set is commonly reconstructed by collection a stack of two-dimensional (2D) transaxial image perpendicular to the axial (bed) direction. Thus, images along the axial direction, i.e., in the coronal or sagittal planes, are generated by re-sampling the volume voxel matrix along these plane.[3] Accordingly, while in the transaxial plane, the spatial resolution is partly limited by the width of the detectors, the resolution along the axial direction is affected by the spacing of the detector rings.

The National Electrical Manufacturers Association (NEMA) has recommendation for standard PET performance measurement, NU 2-2001.[4] The measurement is performed by imaging point sources in air, and then reconstructing images with no

[1] Division of Nuclear medicine, Department of Radiology, King Chulalongkorn Memorial Hospital, Thai Red Cross Society, Bangkok, Thailand 10330

smoothing. Although this does not represent the condition of imaging a subject in which tissue scatter and a limited number of acquired events require the use of a smooth reconstruction filter, the measured spatial resolution provides a best case comparison among scanners, indicating the highest achievable performance.

NU 2-2001 specifies that the activity be contained in a glass capillary tube with an inside diameter of 1 mm or less and outside diameter of less than 2 mm. The axial extent of activity in the capillary shall be less than 1 mm. The purpose of this study is to used another type of point sources such as foam bead and ion resin to perform spatial resolution compare to capillary tube method.

MATERIAL AND METHODS

The LSO-based whole body PET/CT scanner, Siemens Biograph 16 HI-REZ, combines a sixteen slices helical CT, Somatom Sensation 16,. This CT scanner can acquire slice thickness range 0.6 to 10 mm. The tube current can be varied between 28 and 500 mA and tube voltage can be set to 80, 120 and 140 KVp. The anode heat storage capacity was 5.3 MHU. The PET/CT 16 HI-REZ includes the Pico-3D electronics to improve count rate performance. PET component of the tomography has no septa, thus allowing 3D-only acquisitions. The main PET specification was summarized in Table 1.

Table 1 Specification of Siemens Biograph 16 HI-REZ PET/CT scanner

Parameter	Value
Detector material	LSO
Crystal dimensions (mm^3)	4.0 x 4.0 x 20
Crystal array	13 x 13
Crystal per detector block	169
Number of detector blocks	144
Photomultiplier tubes (PMTs)	4 per block
Detector ring diameter (mm)	830
Detector per ring	624
Number of detector rings	39
Total number of detectors	24,336
Transaxial FOV (mm)	585
Axial FOV (mm)	162
Number of image planes	81
Plane spacing (mm)	2
Coincidence time window (nsec)	4.5
Upper level energy discriminator (KeV)	650
Lower level energy discriminator (KeV)	425
Patient port (mm)	700

Point source preparation

Glass capillary tubes of 1 mm inner diameter (ID), 1.4 mm outer diameter (OD), and 75 mm length were filled with ^{18}F-FDG solution of approximately 0.5 GBq/ml for 1 mm in length and well sealed to form point source.

Soaking the beads of tiny foam and resin in 18F-FDG solution of approximately 0.5 GBq/ml for 1-2 min to form point source. Three beads of foam and resin will had total activity less than 10 MBq. The ratio of random to total evens would be less than 5% in the FOV. These three beads of point sources were placed on a piece of tape which was then suspended from a needle.

Point source positioning

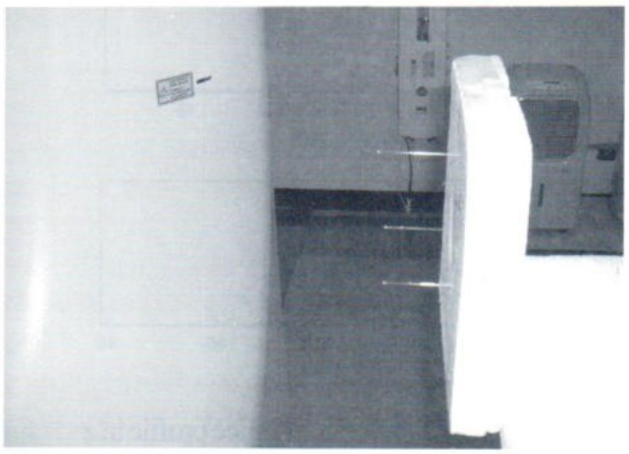

Fig.1 Capillary point sources were suspended by a fixture.

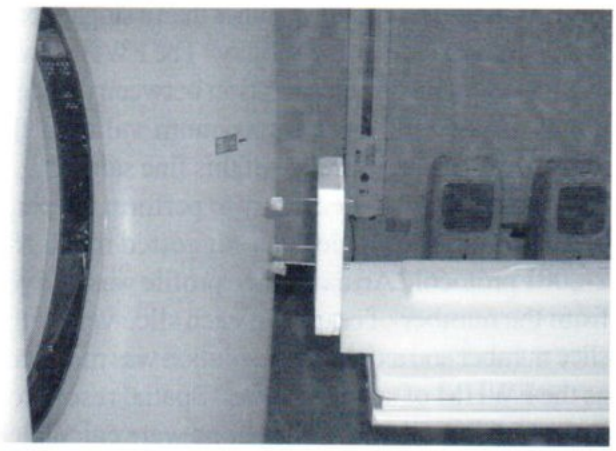

Fig.2 The needle with foam point sources were suspended by a fixture

Source holder made of foam plate was used as a fixture to position the point source (Fig.1, 2). The point source was positioned at three different locations (x,y) defined by (0,1) cm, (10,0) cm, and 0,10) cm. The point source is not to be placed at the center of the FOV, (0,0), where inconsistent results may arise from the high density of lines of response (LOR).[5] Once in place, the 3 point sources were aligned (axially) in the scanner FOV by use of laser lights. Two sets of emission measurements were obtained with the sources centered at 2 axial positions in the scanner FOV, as shown in Figure 3, in the center and at one quarter of the axial FOV (4.05 cm). Two millions net true counts were acquired for each position to ensure adequate statistic.

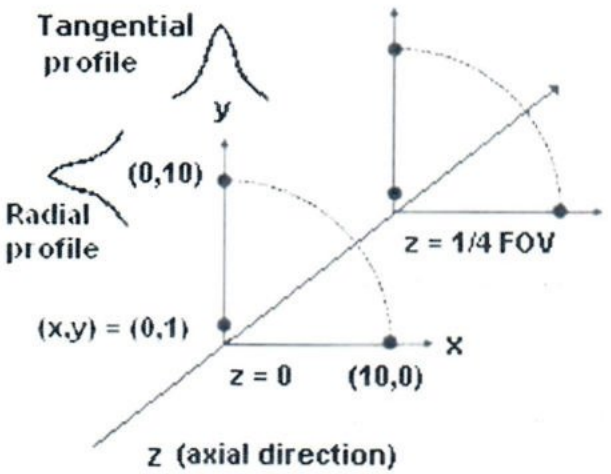

Fig.3 Position of the point sources in FOV for resolution measurement

To measure the pixel size and slice width of image plane, two resin point sources were fixed on linear graph paper 10 cm apart with a piece of tape, and placed on center of the transaxial FOV aligned with the axis of tomograph by using laser alignment device. Two millions net true counts were acquired.

Reconstruction and data analysis

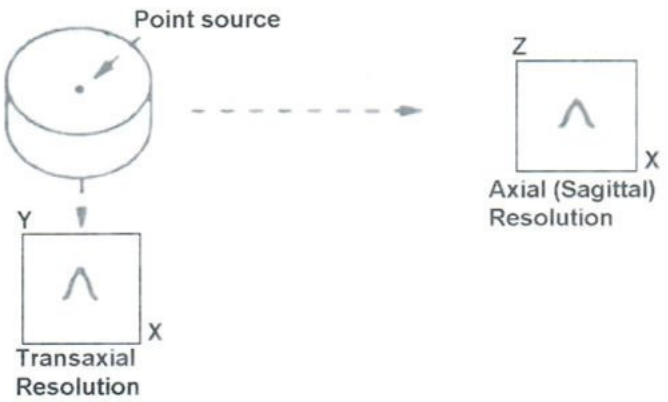

Fig.4 For 3D acquisition, a point source can be used to simultaneously measure both transverse and axial resolution[6]

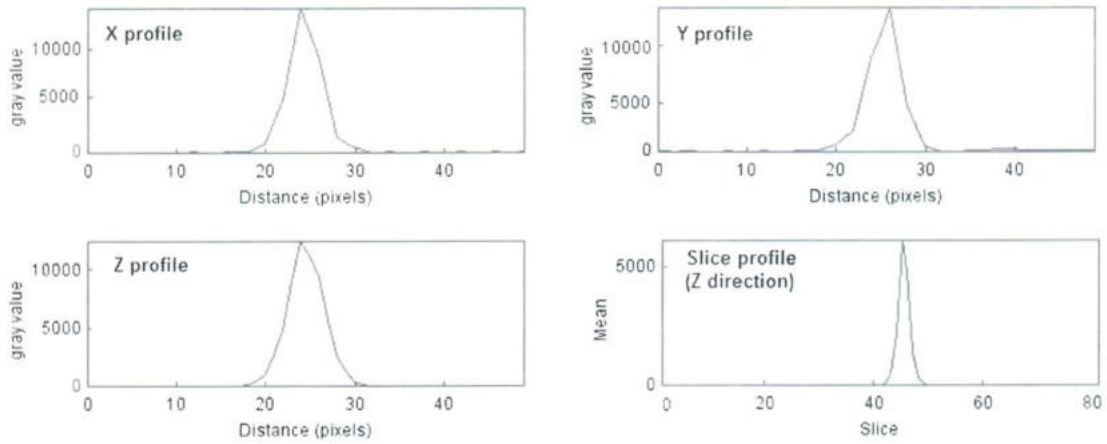

Fig.5 Example of profile curves of resin at point (0,1) in all three directions and slice profile in z direction

All corrections were applied to data. For each position, the images were reconstructed using the FBP algorithm onto a 336x336 matrix with all pass filter and reconstruction zoom was set to 2. Due to limitation of the system, the reconstruction images were transferred to CD in DICOM format and used ImageJ version 1.38 to analysis in personal computer (PC). As x and y define the transaxial plane and z defines the axial direction as show in Figure 4. The FWHM were determined in all three directions by forming one-dimensional (1D) response functions (as show in figure 5) through the peak of the distribution in three orthogonal directions. The width of profile curve was approximately 2 times of the expected FWHM in those directions, rather than a single pixel, to reduce measurement variability.[7] The FWHM were calculated by linear interpolation between adjacent pixels at one half on the maximum value of the response function. Because of this fine sampling, it was not regarded as necessary to perform the parabolic fit of the curve peak as suggested in the NU 2-2001 protocol.[8] An axial slice profile was derived from the number of counts in each slice versus the slice number and axial slice resolution was measured as the FWHM of such a profile.[9] Spatial resolution measured in x, y, and z-directions were calculated by formula as shown in table 2, and reported as values of system resolution.

Table 2 Formulas for computing spatial resolution report values (RESx, RESy, and RESz refer to the spatial resolution measured in the x, y, and z-directions)

	Formula
At 1 cm radius	
Transverse	$RES = \{RESx_{x=0,y=1,z=center} + RESy_{x=0,y=1,z=center} + RESx_{x=0,y=1,z=1/4FOV} + RESy_{x=0,y=1,z=¼FOV}\}/4$
Axial	$RES = \{RESz_{x=0,y=1,z=center} + RESy_{x=0,y=1,z=1/4FOV}\}/2$
At 10 cm radius	
Transverse radial	$RES = \{RESx_{x=10,y=0,z=center} + RESy_{x=0,y=10,z=center} + RESx_{x=10,y=0,z=1/4FOV} + RESy_{x=0,y=10,z=1/4FOV}\}/4$
Transverse tangential	$RES = \{RESy_{x=10,y=0,z=center} + RESx_{x=0,y=10,z=center} + RESy_{x=10,y=0,z=1/4FOV} + RESx_{x=0,y=10,z=1/4FOV}\}/4$
Axial resolution	$RES = \{RESz_{x=10,y=0,z=center} + RESz_{x=0,y=10,z=center} + RESz_{x=10,y=0,z=1/4FOV} + RESz_{x=0,y=10,z=1/4FOV}\}/4$

RESULTS

The reconstructed imaged for pixel size determination of 336x336 matrixes with zoom 2 was 1.015 mm in x, y, and z direction, and slice thickness was 2 mm. The results of the FWHM measurement on each plane were given in Table 3. By using formula in table 2 to calculate spatial resolution of the system and compared the result with performed by Bercier et al,[10] which these values were used as Siemens typical specification of Biograph 16 HI-REZ PET/CT system, as show in table 4.

Table 3 The reconstructed image resolution expressed as FWHM (mm)

Position	Axis	Capillary		Foam		Resin	
		Center	Off center	Center	Off center	Center	Off center
(0,1)	x	4.350	4.366	4.430	4.311	4.431	4.196
	y	4.519	4.383	4.737	4.725	4.397	3.989
	z	4.853	4.925	4.631	5.216	4.484	4.606
	slice	4.952	5.017	4.993	5.093	4.693	4.387
(10,0)	x	5.144	4.919	5.085	4.769	5.101	5.082
	y	4.951	5.066	5.112	5.455	5.088	5.221
	z	6.070	6.345	6.260	6.365	5.941	6.407
	slice	6.633	7.015	6.833	6.996	6.674	7.259
(0,10)	x	4.667	4.874	4.960	5.034	4.938	4.829
	y	5.149	4.915	5.445	5.268	5.207	5.179
	z	5.393	5.655	5.740	5.716	5.319	5.683
	slice	5.855	5.882	5.891	5.824	5.793	5.700

Table 4 NEMA NU 2-2001 Spatial resolution (mm)

Radial position and parameter	Capillary	Foam	Resin	Bercier
1 cm offset				
Transverse	4.4	4.5	4.2	4.2
Axial	4.8	4.9	4.5	4.5
Slice	4.9	5.0	4.5	-
10 cm offset				
Transverse tangential	4.8	5.1	5.0	4.6
Transverse radial	5.0	5.1	5.1	5.0
Axial	5.8	6.0	5.8	5.5
Slice	6.3	6.3	6.3	-

DISCUSSION

For capillary point source, the small volume of the source (~1 mm in length) necessitates a very high specific activity to get a reasonable counting rate. It is difficult to accurately draw up this amount of fluid without wetting the walls of the capillary beyond the desired region as pointed out by Erdi et al.[11] Figure 6 show an example of small excess activity at middle source due to the problem of source preparation. This will make its not real point source as we need. Tiny foam bead was used to perform point source. We perform size screening first. Foam bead that can insert to 1 mm ID of capillary tube was selected. We found that, its very light and easy to blow away. Ion exchange resin was the third choice because of very small size. Both foam and resin can be soaked in ^{18}FDG solution to make the point source.

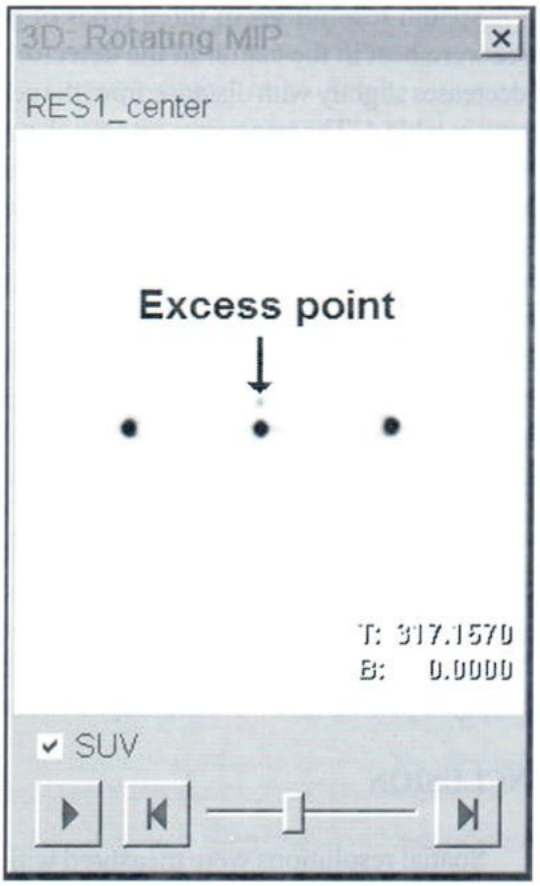

Fig.6 Maximum Intensity Projection (MIP) image of Capillary point source, middle source have excess activity due to contamination of inner wall.

Table 5 Summary results of spatial resolution (mm)

Parameter	Capillary	Foam	Resin	Acceptance Test	Acceptance Limit[12]
Transaxial Resolution					
FWHM @ 1 cm	4.4	4.5	4.2	4.5	≤ 4.6
FWHM @ 10 cm	4.9	5.1	5.0	4.8	≤ 5.3
Axial Resolution					
FWHM @ 1 cm	4.8	4.9	4.5	4.5	≤ 4.9
Slice @ 1 cm	4.9	5.0	4.5	-	-
FWHM @ 10 cm	5.8	6.0	5.8	5.4	≤ 6.1
Slice @ 10 cm	6.3	6.3	6.3	-	-

Spatial resolutions of three types of point source were best in the center of the detector ring and decreases slightly with distance from the center, as show in table 4. The transverse resolution across the FOV of the scanner is fairly good. This is an importance feature since lesions at any location within the body could be identified with the same resolution. Slice thickness resolution is greater than z resolution due to larger multiplication factor, 2 mm in thickness and 1.015 mm thickness in z pixel size, but reflects exactly the clinical situation. So, image with fine pixel would have better spatial resolution. This PET/CT system was installation more than 1 year, and replaced some block of detector for two times. So, this will make the worse resolution than we perform at acceptance test, as show in table 5. Resin point source had good result at central point (0,1) same as Bercier study, but worsen at 10 cm radius. However, these three types of point source were in acceptance limit.[12]

CONCLUSION

Spatial resolutions were measured with the point source made with thin capillary tube, foam bead, and ion exchange resin. The results were in acceptance limit. Ion exchanged resin was most easy to perform point source. ImageJ is free software and can be used to analyze the image on PC. So, we can check resolution and other performance parameters at any time such as post system service or periodical check.

REFERENCES

1. Pasawang P, Sontrapornpol T, Navikhacheevin C, Krisanachinda A. Performance Evaluation of a Biograph 16 Hi-Rez PET Scanner at King Chulalongkorn Memorial Hospital. Thai JRT 2006; 31: 9-14.
2. Turkington TG. Introduction to PET Instrumenttation. J Nucl Med Technol 2001; 29: 1-8
3. Kennedy JA, Israel O, Frenkel A, Bar -Shalom, Azhari H. Super-Resolution in PET Imaging. IEEE Trans Med Imaging 2006; 25: 137-147
4. Martinez MJ, Bercier Y, Schwaiger M, Ziegler SI. PET/CT Biograph Sensation 16: Performance improvement using faster electronics. Nuklearmedizin 2006; 45: 126-133
5. National Electrical Manufactures Association. NEMA Standards Publication NU 2-2001: Performance Measurements of Positron Emission Tomographs, Rosslyn, VA: National Electrical Manufactures Association; 2001
6. Karp JS, Daube-Witherspoon ME, Hoffman E, et al. Performance Standard in Positron Emission Tomography. J Nucl Med 1991; 32: 2342-2350
7. Daube-Witherspoon ME, Karp JS, Casey ME., et al. PET Performance Measurements Using the NEMA NU 2-2001 Standard. J Nucl Med 2002; 43: 1398-1409
8. Herzog H, Tellmann L, Hocke C, et al. NEMA NU 2-2001 Guided Performance Evaluation of Four Siemens ECAT PET Scanners. IEEE Trans Nucl Sci 2004; 51: 2662-2669
9. Brambilla M, Secco C, Dominietto M, et al. Performance Characteristics Obtained for a New 3-Dimensional Lutetium Oxyorthosilicate -Based Whole-Body PET/CT Scanner with the National Electrical Manufacturers Association NU 2-2001 Standard. J Nucl Med 2005; 46: 2083-2091
10. Bercier Y, Casey M, Young J, Wheelock J, Gremillion T. LSO PET/CT Pico performance improvements with ultra Hi-Rez option, IEEE Nuclear Science Symposium Conference Record, Rome, Institute of Electrical and Electronics Engineers,Inc. 2004; 7: 4038-4042
11. Erdi YE, Nehmeh SA, Mulnix T, Humm JL, Watson CC. PET Performance Measurements for an LSO-Based Combined PET/CT Scanner Using the National Electrical Manufacturers Association NU 2-2001 Standard. J Nucl Med 2004; 45: 813-821
12. CPS Innovation: Product Specification LSO PET/CT HI-REZ 16, Knoxville, TN: CPS Inc.; 2004

COMPUTED TOMOGRAPHIC SCANS OF BRAINS IN ACCIDENTAL AND EMERGENCY PATIENTS AT SAPPASITTHIPRASONG HOSPITAL; A RETROSPECTIVE STUDY OF THE INDICATIONS AND FINDINGS.

Sittiporn SASIWANAPONG, MD.,[1] Nitaya SNITWONGSE NA AYUDHYA, M.Sc.,[1] Somrak LOWANITCHAI, MD.[1]

ABSTRACT

The requisition for computed tomographic (CT) scan of brain had been increasing continually each year at Sappasitthiprasong Hospital. In 2006, 80% of them were sent from Accident-Emergency Division, most of them were in a condition of Glasgow Coma Scale (GCS) score, of 15. (table 1) The retrospective studied were performed by reviewing the medical records and the CT brain scans of both the traumatic and the non-traumatic groups. (table 2) The demographic data, GCS score and clinical symptoms or indications were collected to observe the prevalence of negative and positive CT findings in order to determine the indications that are favorable correlated with positive CT findings in acute traumatic head injuries with GCS 15. There were totally 454 patients, included with an average of 43.08 ± 13.30 years, male 69.16%. The numbers of positive findings were more than that of the negative ones in the non-traumatic cases and traumatic cases with GCS less than 14. Where as in the 243 traumatic cases, only 84 had positive CT brain scan findings, of which 14 cases or 10.7% were the cases with GCS score of 15. In this group the indications that significantly constituted positive CT findings were headache, sign of basal skull fracture, skull crown fracture, nausea, vomiting, drowsiness and amnesia, respectively. This study agreed with particular indications that could limit the use of CT scan without underestimating the lesions at particular setting.

Keywords: computed tomography, Glasgow coma scale (GCS), indications and findings.

BACKGROUND AND RATIONALE

Sappasitthiprasong Hospital was a central hospital in Northeast of Thailand that had faced the crisis of increasing numbers of computed tomographic (CT) scans each year. In 2006, there were 12,126 patients underwent CT scans, of which 10,370 were CT scan brains (85.52%). Of all the CT scan brains, 80% were requested by the physicians in charge at Division of Accidents and Emergency. The decisions to perform CT scans partly depended on individuals, clinical signs and symptoms, and Glasgow coma scale (GCS) scores of patients at those moments. In patients with acute traumatic head injuries, CT scan brains were reasonably highly recommended for those with GCS score of less than 14, which referred to the moderate and severe head injuries. In cases with GCS 14-15 or mild head injuries, the every-case- CT scanning was being in controversial concerning the appropriate indications.[1]

[1] Division of Radio-Diagnosis, Department of Radiology, Sappasitthiprasong Hospital, Ubon Ratchatani, 34000 Thailand

Many settings and institutes had designed some guidelines of CT scan brain indications in patients with mild head injuries based upon the researches and consensus such as Canadian CT head rules, NICE (the National Institute of Clinical Excellence) guidelines and NCWFNS guidelines (The Neurotraumatology Committee of the World Federation of Neurosurgical Societies).[2,3,4] The details were varied since the patients of interest were different from setting to setting, which determined the characteristics and severity of accidents,[5] the risk factors, and the restriction of resources, such as CT scan machines, human resources i.e. physicians, radiologists, radio-technologists, nurses, etc. The improper guideline could result in either the underestimation of diseases or unnecessary over utilization of the apparatus. Because CT scan brain was an expensive tool that needed high maintenance cost yearly, the risk of radiation to patients and personnels (once CT scan brain radiation dose equivalent to 100 times of chest radiography),[6] the particular indications that related with the positive findings would reduce the requirements of CT scan brain in some cases without the pitfalls to patients and treatments.

This retrospective study observed the prevalence of negative and positive CT findings in patients referred from Division of Accidents and Emergency at Sappasitthiprasong Hospital, Ubon Ratchatani in order to determine the indications that favorably correlated with positive CT findings in acute traumatic head injuries with GCS 15.

MATERIALS AND METHOD

The CT scan brains were performed by Toshiba Asteion Super 4, multi-four slices. The requisition papers of the patients aged 4 years old and more from Division of Accidents and Emergency, Sappasitthiprasong Hospital, Ubon Ratchatani underwent CT scan of brain at Department of Radiology, Sappasitthiprasong Hospital from August to October 2006 were obtained. These papers had to contain the GCS score of the patients or they would be excluded. For data collection, the radiologists reviewed the CT scan of brain images of these patients through the workstation monitors and reported the CT scan findings. The results were positive if there were abnormalities of any intracranial lesions including hematoma, tumor, infarction, infection, atrophy, or calcification. By reviewing the patients' medical records, demographic data and the clinical symptoms and indication for CT scan brain were carried out. The frequency of positive CT scans was determined for each group and then entered in two-by-two table. Chi square test was used to calculate with 95 percent confidence intervals.

RESULTS

All eligible patients underwent CT scan brains during August to October 2006 were 454, ranging from 4 to 95 years old (mean age, 43.08 ± 23.30 years), male percentage of 69.16. They were separated into two groups of 243 traumatic patients (mean age, 31.65 ± 17.53 years; male, 77.05%; alcoholic intoxication, 39.09%) and 211 non- traumatic patients (mean age, 56.23 ± 22.17 years; male, 60%). In traumatic group, there was no significant difference in mean ages of the patients with negative CT findings and with positive CT findings. In contrast with those in non- traumatic group, the patients with positive CT findings had more average age than the ones with negative CT findings. The details were shown in table 1.

Table 1 The mean age and gender of patients and the CT findings.

Subjects (cases)	Trauma (243)			Non- trauma (211)		
	Negative CT (159)	Positive CT (84)	P-value 0	Negative CT (93)	Positive CT (118)	P- value 0.07
Mean age, years (SD)	31.61 (17.77)	31.74 (17.18)	0.94	50.99 (24.14)	60.37 (19.61)	<0.01
Male (%)	118 (73.75)	70 (83.33)	0.08	56 (60.9)	70 (59.32)	0.82

Because of no significant difference in CT findings of the positive and negative groups in non -traumatic group (P= 0.07), we continued the analysis in traumatic group. The traumatic patients were divided into 3 subgroups according to GCS score; GCS 14-15 (mild head injury), GCS 9-13 (moderate head injury), and GCS 8 or less (severe head injury). It was found that the patients with GCS 14-15 had the results of negative CT findings significantly more than of positive CT findings. The ratio of positive to negative CT findings increased while the GCS score decreased as shown in Table 2.

Table 2 The frequency of negative and positive CT findings in traumatic patients with different GCS scores.

Details (cases)	Negative CT	Positive CT	P-value
GCS 14-15 (147)	127	20	<0.01
GCS 9-13(38)	18	20	0.02
GCS 8 or less(58)	14	44	<0.01

In the traumatic group, there were 131 patients with GCS 15, which had 14 positive CT results or 10.7% (P =0), whereas there were 16 cases with GCS 14, which had 6 positive CT results (37.5%, P=0.82). The results of positive and negative findings were comparable and indifferent in the traumatic patients with GCS 14, therefore the analysis of indications were conducted only in the traumatic patients with GCS 15.

The indications reviewed from medical records of the traumatic patients with GCS 15 were demonstrated in Table 3. One patient could have more than one indication depending on what physicians had recorded on patients' presentation at the time of arrival at the Division of Accidents and Emergency.

Table 3 the indications and CT findings in patients with GCS 15.

Symptoms/ indications	Total (Cases) N=131	Negative CT (Cases) N=117	Positive CT (Cases) N=14	P value	Likelihood ratio*
Headache	27	17	10	<0.001	9.63
Signs of basal skull fracture	8	3	5	<0.001	8.54
Skull Fracture	14	8	6	<0.001	6.27
Nausea/Vomiting	9	5	4	<0.001	5.42
Drowsiness	4	2	2	<0.01	5.29
Amnesia	10	6	4	<0.01	4.84
Loss of consciousness	78	68	10	0.4	1.70
Laceration, abrasive wound (head)	13	11	2	0.63	1.51
Seizure	3	3	0	1.0	0.00
Fracture of facial bones	6	6	0	1.0	0.00

*Likelihood ratio defined as the probability of getting the positive finding if the patient really had the indication of interest with the corresponding probability if they had not.

DISCUSSION

CT scan brains were performed to screen for intracranial abnormality because of their high efficiency, accuracy, fast and easy practice. Besides the radiation dose, there was neither side effect nor invasive process to the patients that resulted in the increasing numbers of CT scan brains every year. There would be no debate if CT scan brain was not the expensive medical apparatus that needed yearly high cost of maintenance depending on workload. Moreover the patients had to spend 30-60 minutes more time at the emergency room to confirm that they were really free of the suspected disease.

In non traumatic patients from Division of Accidents and Emergency, the CT brain scans were found to have positive findings significantly more than the ones in the traumatic group ($P<0.0025$). The diseases were detected in more than half of the patients and the indications were recorded properly in the same direction such as hypertension, focal neurological deficits, paralyses, seizure, etc. (data not shown). The patients with positive results had more

average ages than the patients with negative results. In other words, there were more chances to detect abnormality by CT brain scan in elderly patients from the Division of Accidents and Emergency, and non- traumatic elderly patients could get more risks than the youngs.

The traumatic patients in this study were not only the accidental patients but also the abused ones. There were no significant differences in the mean age of patients with positive and negative CT findings. The traumatic patients were, in average, not as old as the non traumatic ones (32 VS 60 years), ranging from 7 to 55 years old. The Canadian CT head rules had considered that the patients with mild head injuries aged 64 years old and more or more than 60 years old indicated by NCWSNF[7] needed to undergo CT brain scan. In this study, there were no positive CT finding found in traumatic patients ages more than 64 years (N= 7), which might be the consequence of the eligible subjects concerned this aspect were too small.

The CT scan brains in traumatic patients from Division of Accidents and Emergency significantly yielded negative results more than positive results (P=0). However according to GCS score grouping, only the patients with GCS 14-15, which was 60 % of all, statistically had the negative findings more than the positive ones. The decreasing GCS score, the increasing number of positive finding, possibly by itself, the GCS score of less than 14 could be the proper indication for CT scan brain in acute traumatic patients at Sappasitthiprasong Hospital.

Consequently, besides the GCS score, the traumatic patients with GCS 14-15 still needed other indications to be included to have increasing numbers of positive findings. In patients with GCS 14 the positive findings were not significantly different from the negative findings (37.5%, P = 0.82). The patients with GCS 15 had 10.7% of positive finding, which corresponded with other studies that ranging from 3-13%.[8] The indications that correlated with positive CT findings more than with negative CT findings were headache, sign of basal skull fracture, skull fracture, nausea vomiting, drowsiness and amnesia. There were four indications from our results that were similar to Canadian CT Head Rule and NICE Guidelines including sign of basal skull fracture, skull fracture, vomiting and amnesia. The indication of headache was corresponding to NCWFNS guidelines. This study did not agree with NCWFNS guidelines for the indication of loss of consciousness (LOC) that was considered as an indication for CT scan brain. LOC was a symptom that highly relied on the patients because it gained from the patients' interview not by directly observing the patients. M Sosbi et al. had found that headache in combination with reduction in consciousness such as LOC increased the chance of positive CT finding.[9] This study confirmed his study that headache together with LOC had likelihood ratio more than headache alone ($P< 0.001$, LLR =12.10). Our result disagreed with indications of alcohol or drug intoxication and the wound from upper level of clavicle ($P> 0.05$), which they were recommended in some study.[1] In fact these two indications could be counted on the characteristics of individuals or people at certain settings not the symptoms of trauma. It could be classified as risk factors that might be varied from ethnicities, customs, or geography. Risk factors from one place could not be the same in others.

This retrospective study had collected data from medical files recorded by the physicians at the times. It was up to individuals to count the importance to the details they had written. There was no statistical differences of CT scan findings among the physicians referring (data not shown). However 65% of CT brains scans in this study were requested by junior medical staffs, whose experience might be not as strong as senior staffs and influenced the increasing number of decision in performing the CT to avoid underestimation.[10]

CONCLUSION

The CT brain scan referred from Division of Accidents and Emergency, Sappasitthiprasong Hospital revealed the reasonable outcome of positive CT finding numbers in non traumatic patients and

traumatic patients with GCS less than 14. The positive CT brain scan finding in traumatic patients with GCS 15 was 10.7%. The indications that favorably correlated with positive CT findings in acute traumatic head injuries with GCS 15 were headache, sign of basal skull fracture, skull fracture, nausea vomiting, drowsiness and amnesia. These indications should be co-considered in traumatic patients with GCS 15 to perform a CT brain scan. The results of this study both agreed and disagreed with the studies in the literatures. Eventually the decision to use guideline should be testified at other settings.

REFERENCES

1. Haydel MJ, Preston CA; Indications for computed tomography in patients with minor head injury. *N Engl J Med.* 2000 Jul 13; 343 (2): 100-5
2. Stiell IG, Wells GA, Vandemheen K, Clement C, Lesiuk H, Laupacis A, McKnight RD, Verbeek R, Brison R, Cass D, Eisenhauer ME, Greenberg G, Worthington J; The Canadian CT Head Rule for patients with minor head injury. *Lancet.* 2001 May 5; 357 (9266): 1391-6
3. National Institute for Clinical Excellence. Head injury triage, assessment, investigation and early management of head injury in infants, children and adults. Clinical guideline 4. London: NICE, 2003: 96-7.
4. Fabri A, Servadei F, Marchesini G, Morselli-Labate AM, Dente M, Ievese T, Spada T, Vandelli A; Prospective validation of proposal for diagnosis and management of patients attending the emergency department for mild head injury; *J Neurol Neurosurg Psychiatry.* 2004; 75: 410-6
5. Swann I J, Kelliher T, Kerr J; Are we ready for NICE head injury guidelines in Scotland? The major challenge for A&E is implementation of realistic Guidelines. *Emerg. Med. J.* 2004; 21;401
6. National Radiological Protection Board. http://www.nrpb.org/radiation_topics/medical/ted_equivalent.htm.
7. Servadei F, Teasdale G, Merry G; Defining acute mild head injury in adults: A proposal based on prognostic factor, diagnosis and management. *J Neurotrauma.* 2001; 18(7): 657-64
8. Jagoda AS, Cantrill SV, Wears RL, Valadka A, Gallagher EJ, Gottesfeld SH, Pietrzak MP, Bolden J, Bruns JJ Jr, Zimmerman R. Clinical policy: neuroimaging and decisionmaking in adult mild traumatic brain injury in the acute setting. *Ann Emerg Med.* 2002; 40: 231-249.
9. Sobri M, Lamont A C, Alias N A, WIN M N. Red flags in patients presenting with headache: clinical indications for neuroimaging. *B JR; 76* (2003), 532-535
10. Mukerji N, Wallace D, Mitra D. Audit of the change in the on-call practices in neuroradiology and factors affecting it. *BMC Medical Imaging;* 2006, 6: 13

PROPTOSIS; CAUSES AND DIAGNOSTIC ROLE OF CT

Chanya CHAISIRIRAT M.D.[1]

ABSTRACT

Proptosis of the eye is an important clinical manifestation of orbital diseases. Proptosis due to any cause can compromise visual function and the integrity of the eye. Delayed diagnosis and improper treatment can lead to unintended sequelae.

The aim of this study was to retrospectively analyze the causes of adult proptosis and was to present the diagnostic role of CT in evaluation of proptosis.

We reviewed 39 adult patients, over 15 years of age. They presented to out-patient of Kamphaengphet Hospital with clinical proptosis. The period of collections extended from January, 2006 to February, 2008.

There are numerous causes of proptosis. In order of frequency, the causes of proptosis is trauma[15] following by tumors[9] and inflammatory diseases including thyroid opthalmopathy and orbital pseudotumor.[7] The most common cause of adult proptosis in Kamphaenphet hospital is trauma, which is different from those reported in other literatures.

In conclusion, with recent improvements in scanning techniques along with the wider availability of the current CT scanner, it has been proven to be excellent in identifying orbital pathology responsible for proptosis especially in places where MRI is not available.

Key words: CT, proptosis

INTRODUCTION

Proptosis is forward projection or protrusion of one or both eyeballs. Oweing to the rigid bony structure of the orbit with only anterior opening for expansion and seeing the objects by the eye, any increase in orbital contents taking place from the sides or from behind will displace the eyeball forward.

The definition of exophthalmos and proptosis are similar but in common usage, the latter tends to be more severe and gross. Some authors reserve the term exophthalmos as protrusion secondary to endocrine dysfunction and proptosis as any non -endocrine-mediated protrusion.[2,3,5]

Proptosis can be the sign of myriad disease processes including tumor, infection, inflammation, trauma, metastasis, endocrine dysfunction and vascular diseases.[1,2,3,5]

Whatever the underlying pathology, the orbit is basically conical in shape and so if something increases the volume within the orbit, the eye will be pushed outward.

[1] Department of Radiology, Kamphaengphet Hospital, Kamphaengphet 62000, Thailand

The patient who presents with proptosis must be evaluated. Imaging studies and corresponding laboratory investigations to ascertain the causes of the diseases must be obtained. The failure to address these findings can lead to unexpected sequelae. Certain symptoms, such as pain or a sudden diminution of vision, indicate a more rapid course and impose a more rapid investigation to obtain the diagnosis and treatment. Preservation of vision and function of the globe and orbit is of paramount importance.

We describe the variety of causes of proptosis and present the diagnostic role of CT in evaluation of the precise location and extent of the lesions.

MATERIALS AND METHODS

In clinical, the definition of proptosis is anterior displacement of one or both globes. The usual amount of ocular protrusion as measured from the lateral orbital rim to the corneal apex is 14 to 21 mm in adults. Protrusion greater than 21 mm or a 2 mm difference between the two sides is generally abnormal.[2,3,5]

Pseudoproptosis is either the simulation of abnormal prominence or a true asymmetry that is not the result of increased orbital contents.[5]

All of our patients, clinical proptosis were determined by ophthalmologist. On CT scans, proptosis is defined as globe protrusion > 21 mm anterior to the inter-zygomatic line on axial scans at the level of the lens.[5]

We retrospectively reviewed all 39 patients who came to out patient department of Kamphaengphet Hospital with proptosis, from January, 2006 to February, 2008. All of them underwent to perform CT by double slices spiral CT, (HiSpeed CT/e Dual CT scanner system, GE). Before commencing for CT examination, the evaluation including all the preceding history, complete ocular examination and laboratory investigation were recorded.

Various techniques of CT were applied to solve the different problems. The CT technique was to obtain a lateral scannogram with supine position and contiguous axial sections with slice thickness of 3-5 mm. Coronal CT with 3 mm. thickness in prone position were obtained in selected cases when required. The scans were obtained both prior to and after administration of intravenous contrast media, except in cases of trauma that were obtained only in plain study.

Final diagnosis of our patients was made by the CT findings correlated with clinical details, laboratory data, response to treatment and histopathological findings.

RESULT

39 patients with various age groups from over 15 to 68 years years, both sexes, (male 23 and female 16) with unilateral (36) and bilateral (3) proptosis were recorded.

39 patients were studied with proptosis, apparently resulting from multiple etiologies. In order of frequency, the causes of proptosis were: 15 orbital and facial trauma, 9 tumors including orbital tumors (metastasis and lymphoma) and paraorbital tumors (meningioma, sella mass, local spread of nasopharyngeal and paranasal sinus CA), 4 thyroid eye disease, 3 orbital pseudotumor, 3 orbital cellulitis, 1 ethmoidal mucocele, 1 fibrous dysplasia, 1 post traumatic carotid-cavernous sinus fistula, 1 cavernous sinus thrombosis, 1 sphenoid dysplasia in neurofibromatosis type I.

Various lesions causing proptosis are grouped in the table 1.

TRAUMA (15 patients)

Trauma is the most common cause. Most of them were young men with motorcycle accident. All 15 patients of traumatic proptosis have various degrees of intraorbital hemorrhage and soft tissue injury including preseptal and retro-bulbar regions (Figure 1). One or more fractures of orbital osseous wall and periorbital soft tissue contusion were seen

in all cases. 7 patients had orbital soft tissue emphysema. Associated facial bony fractures are seen for 5 cases. There were 8 patients who had evidence of directed or indirected sign of skull base fracture. 6 patients had intracranial injury, 2 of 6 were acute subdural hematoma and the rest 4 patients were localized frontal and or temporal brain contusions. One patient developed orbital cellulitis.

TABLE 1

CAUSES OF PROPTOSIS OF 39 PATIENTS

CAUSES OF PROPTOSIS	NO. OF PATIENTS	PERCENTAGE
TRAUMA	**15**	**39%**
TUMORS	**9**	**23%**
1. Orbital tumor		
- Metastasis	1	
- Lymphoma	1	
2. Paraorbital tumors		
- Meningioma	2	
- Maxillary CA	2	
- Nasopharyngeal CA	2	
- Sella mass	1	
INFLAMATION	**7**	**18%**
1. Thyroid ophthalmopathy	4	
2. Pseudotumor	3	
INFECTION	**4**	**10%**
1. Orbital cellulitis	3	
2. Ethmoidal mucocele	1	
VASCULAR	**2**	**5%**
1. Post traumatic CCF	1	
2. Cavernous sinus thrombosis	1	
OTHERS	**2**	**5%**
1. Fibrous dysplasia	1	
2. Sphenoidal, NF type1	1	

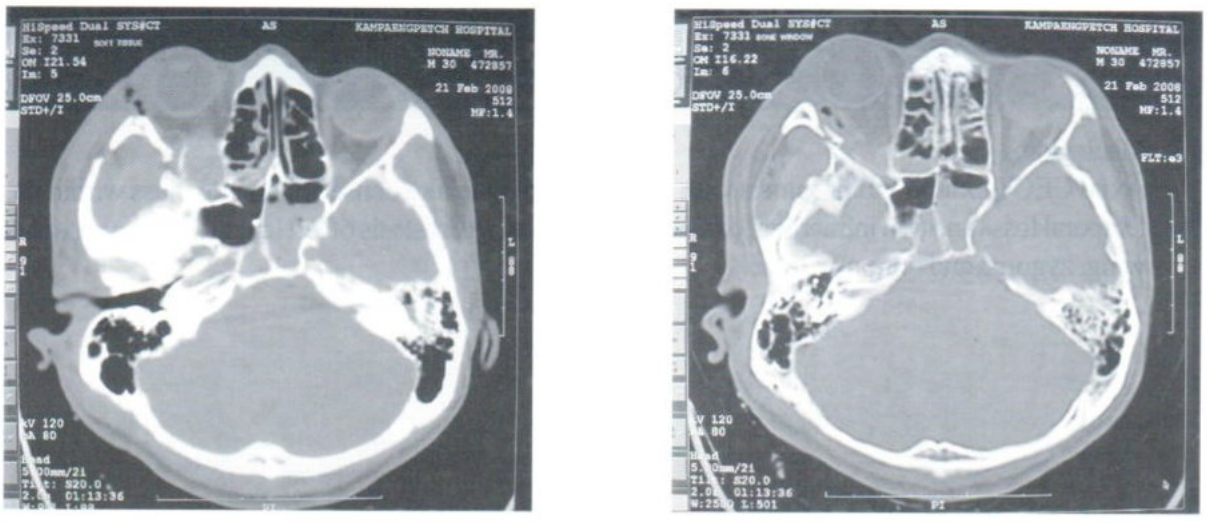

Fig.1 Axial CT with bone window setting shows right proptosis, comminuted fractures of right lateral orbital wall, retrobulbar hemorrhage, soft tissue swelling and emphysema. Skull base fracture with blood within the sphenoid and ethmoid sinuses are observed.

TUMOR (9 patients)

Second most common causes is tumor, there are 9 cases, including orbital and paraorbital tumors, as described.

Two patients were meningioma, CT reveal dense enhancing enplaque mass and dural enhancement within the temporal fossa and bony hyperostosis of sphenoid wing, zygoma, lateral orbital wall and temporal bone resulting in proptosis (Figure 2).

Four patients were primary paranasal sinus CA[2] and nasopharyngeal CA.[2] CT showed aggressive inhomogeneous enhancing primary soft tissue mass, adjacent bony destruction with orbital and or cavernous sinus invasion.

One patient was found to have a huge sella mass with gross cavernous sinus and orbital cone involvement. It was not known the exact pathology. This patient was referred.

One patient was probably orbital lymphoma; the CT shows homogeneous enhancing mass with extraconal and intraconal components. The tumor involved adjacent lacrimal gland and outward displacement of the globe. No bony destruction or optic nerve invasion is seen.

Orbital metastasis was presumed for one case, she had underlying primary CA of the breast. She developed unilateral proptosis. CT of orbit was performed. It reveals large soft tissue mass at the lateral extraconal retrobulbar space with blastic and lytic destruction of sphenoid bone (Figure 3).

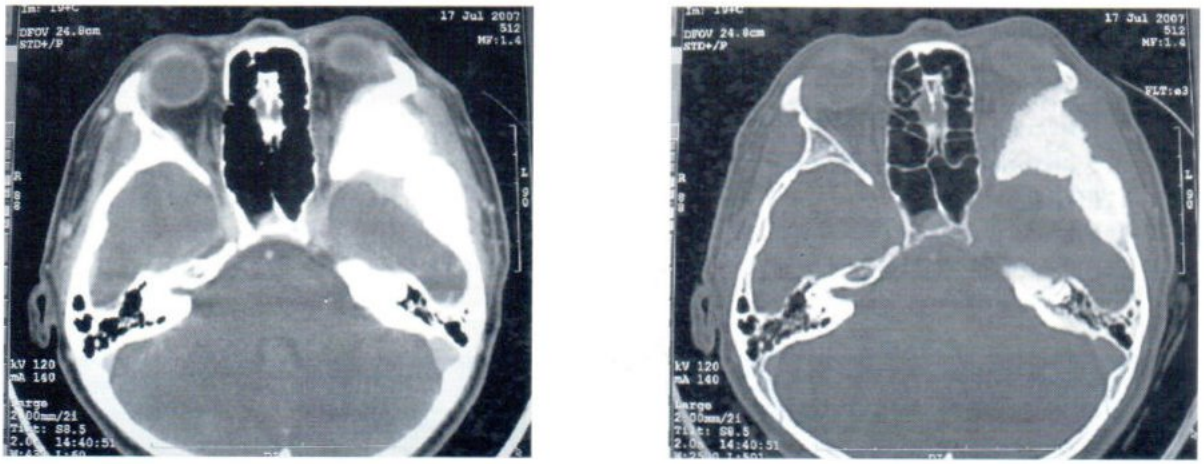

Fig. 2 Meningioma
Axial CECT exhibit left proptosis with extra-axial plaque like dense enhancing mass within the left temporal fossa and thin intraorbital component. There is hyperostosis of left lateral orbital wall, sphenoid wing, zygoma and temporal bone.

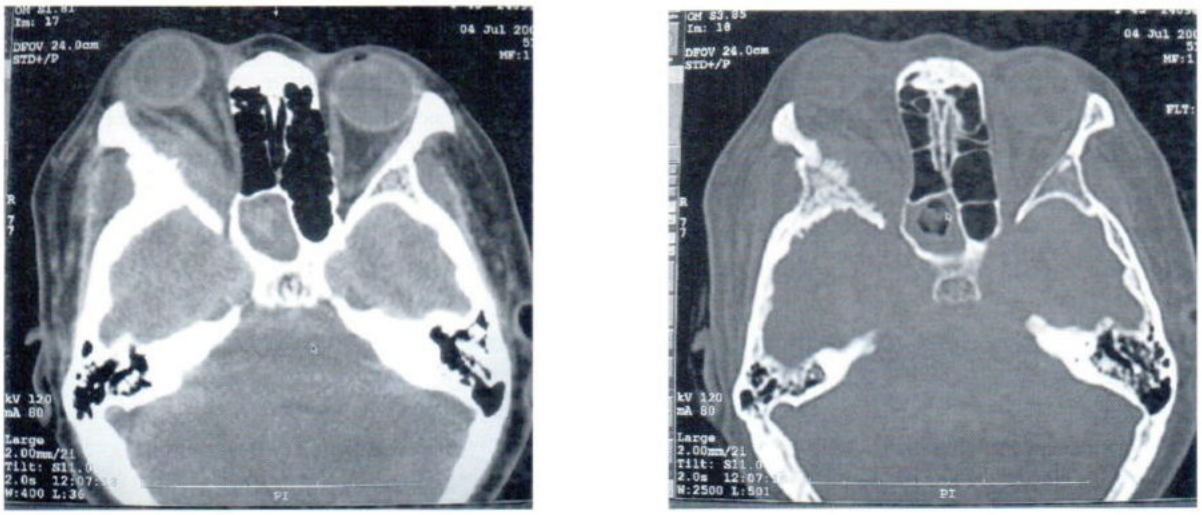

Fig. 3 Metastasis
Axial plain CT demonstrate right proptosis with large right lateral extraconal retrobular mass extending into sphenoid sinus. There is mixed sclerotic and lytic destruction of the right sphenoid wing, mimic meningioma.

INFLAMMATION (7 patients)

Thyroid ophthalmopathy with proptosis were found in 4 patients. All cases have history of hyperthyroid. 3 of them have abnormal thyroid function test. Bilateral multiple extraoccular muscles involvement were seen in 3 cases, one of them was not symmetry. Unilateral involvement was seen in one case. CT were reviewed, the contents of the orbits swelling due to inflammation that affects primarily the muscles. Various degrees of enlarged extraoccular muscles with almost tapering insertions were observed (Figure 4). The optic nerve at the orbital apex did not be grossly affected in all cases.

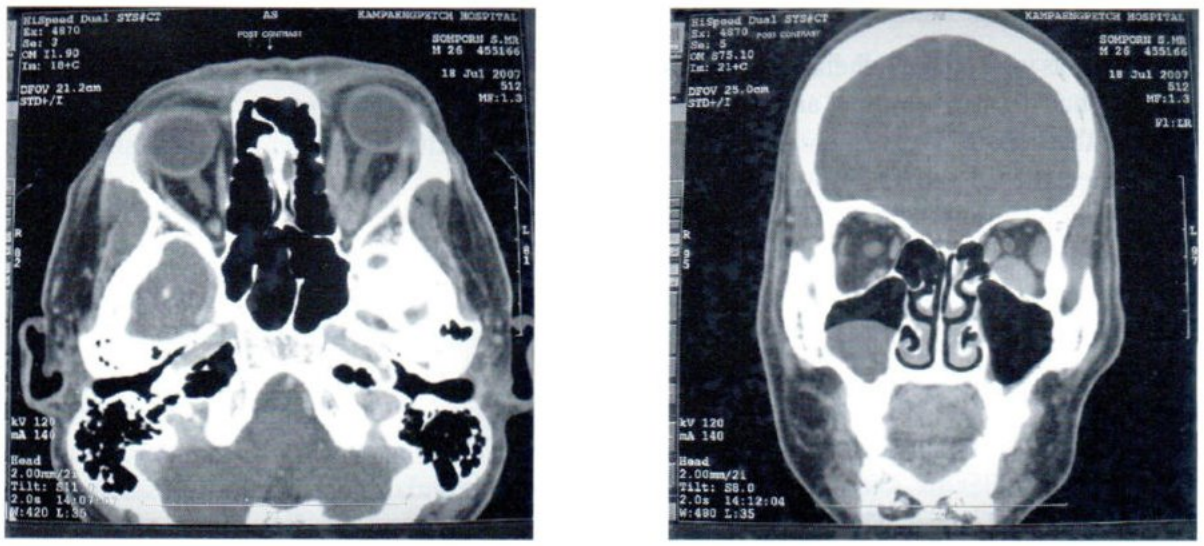

Fig.4 Thyroid Ophthalmopathy
Axial and coronal CT demonstrate unilateral left proptosis, enlarged left extraoccular muscles, maximally in the mid part with typical tapering at the insertions, involving inferior, lateral and medial rectus muscles.

There were 3 cases of pseudotumors, all of them are unilateral involvement. CT showed inflamed intraorbital structures including globe, lacrimal gland, extraocular muscle and orbital fat. There was no optic nerve involvement of our collected cases. One of them was a myositic type with isolated enlarged inferior rectus muscle and tendon insertion, it may be named pseudotumor variant (Figure 5). The rest two patients are diffuse lesions, their CT show diffuse enhancing uveal-scleral thickening, slight enlarged rectus muscles, retrobulbar fat infiltration and preseptal soft tissue swelling. Lacrimal gland involvement is seen in one case. Clinical details, CT features, prompt clinical response to steroid treatment and dramatic improvement on CT support the diagnosis of pseudotumor.

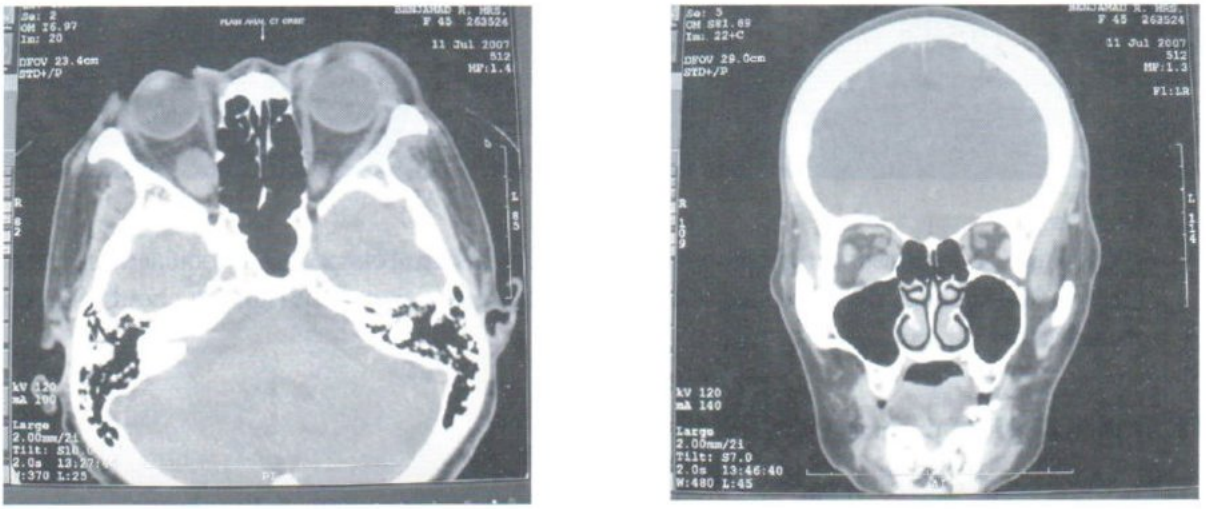

Fig.5 Pseudotumors
Axial and coronal CT reveal myositic type of pseudotumor, there is isolated enlarged right inferior rectus muscle belly and tendon insertion

INFECTION (4 patients)

3 patients were orbital cellulitis with proptosis. First patient had diffuse preseptal and retrobulbar cellulitis with eyeball involvement secondary to foreign bodies; the CT shows proptosis, preseptal soft tissue swelling, uveoscleral thickening and some increase enhancing retrobulbar fat. The second patient developed small subperiosteal involvement secondary to head and facial trauma. Formation of small subperiosteal abscess with medial enhancing rim along the lateral orbital wall, swollen enlarged preseptal soft tissue, retrobulbar fat infiltration, some enlarged rectus muscles and loss of soft tissue plain in the infratemporal fossa. The last patient was diffuse orbital cellulitis secondary to sinusitis, the CT features reveal increase density of soft tissue and inhomogeneous contrast enhancement in all compartments including preseptal and retrobular spaces.

One patient was diagnosed as ethmoidal mucocele. CT showed a large nonenhancing cystic mass arising from right ethmoid air cell. Expansion and remodeling of the bony wall, some erosion of medial wall of the right orbit were found. It was situated along the posteromedial aspect of right globe. Proptosis and optic nerve compression were seen (Figure 6).

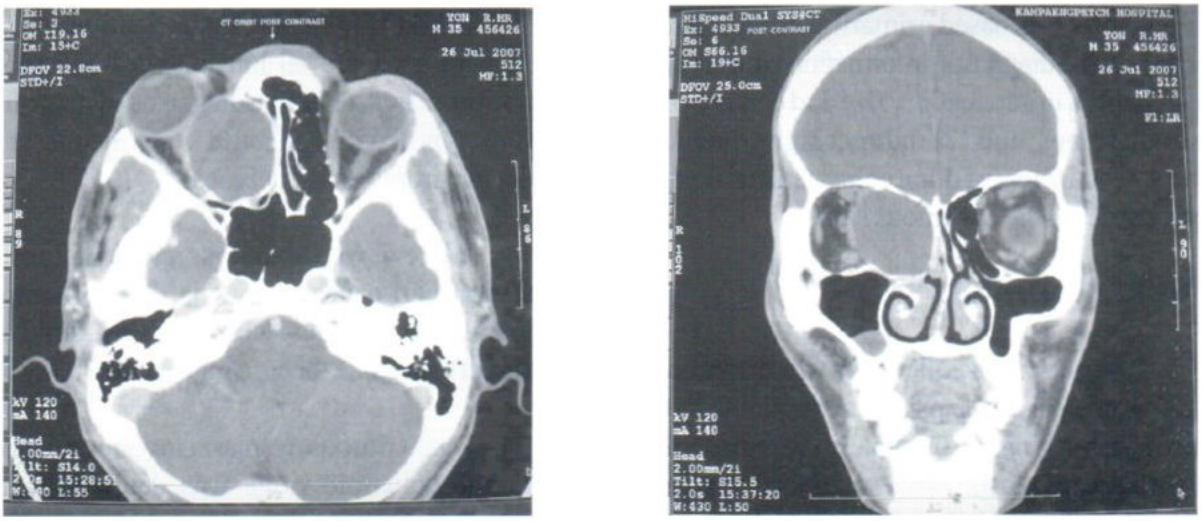

Fig.6 Ethmoidal Mucocele
Axial and coronal CT demonstrate right proptosis with a large expansile nonenhancing cystic mass arising from right ethmoid sinus with bony remodeling and some erosion of right medial orbital wall.

VASCULAR (2 patients)

In our result, there was one patient who was diagnostic as carotid cavernous fistula after head trauma. He presented as palsatile proptosis. CT reveal unilateral proptosis, associated enlargement and tortuous of the superior ophthalmic vein, swollen dense enhancing cavernous sinus with enlarged contour, some thickened extraocular muscles and notable ipsilateral dilated intracranial cortical venous drainage (Figure 7).

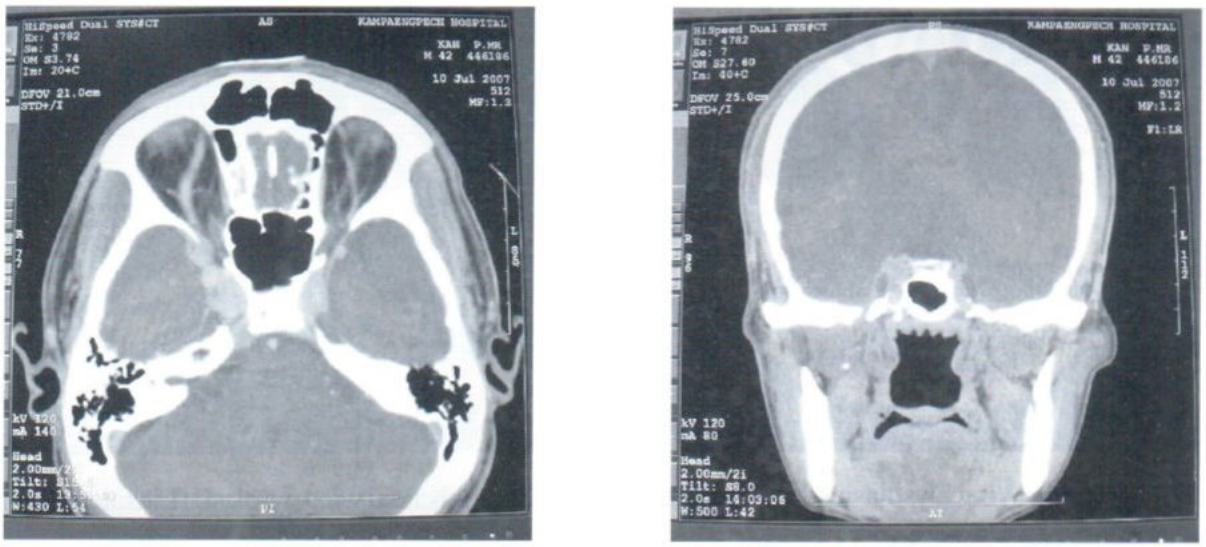

Fig.7 Carotid Cavernous Fistula
Axial and coronal contrast enhanced CT images show right proptosis with enlargement and tortuous of the right superior ophthalmic vein, swollen enhancing right cavernous sinus.

Another patient had cavernous sinus thrombophlebitis caused by paranasal sinusitis in 58-year-old woman, underlying poor controlled DM. She presented with right ocular pain and diplopia.

The diagnosis was based primarily on clinical data. CT can provide diagnostic information with (1) direct signs, changes in attenuation, size and contour of the cavernous sinus, and (2) indirect signs, including proptosis and increased dural enhancement along the lateral border of the cavernous sinus

OTHERS (2 patients)

The one of our collections was diagnosed as neurofibromatosis, proptosis was complained by the owner. Eye examination by clinician was made, there is no definite proptosis. However, she underwent an outpatient CT. CT demonstrate significant right sphenoid wing abnormality. Much of greater wing was absent. Slight herniation of the temporal lobe into the orbit and a convex bulging temporal fossa were found. Direct contact of the temporal lobe with the orbital soft tissue was noticed (Figure 8). Proptosis was measured on CT; there is no definite proptosis, too.

In addition general examination revealed more than six Café au lait macules and several neurofibromas. A tentative diagnosis of neurofibromatosis type1 with sphenoid wing dysplasia was made, but proptosis is equivocal.

We reviewed textbooks and literatures, this condition can cause proptosis due to herniated temporal lobe and bulgy temporal fossa, simulating an intraorbital space-occupying lesion (Figure 9).

Facial fibrous dysplasia involving temporal bone and sphenoid ridge was detected for one patient, the CT show some proptosis with enlarged expansion of involved bones.

Pseudoproptosis was not found in our series, it means that there was no negative CT finding in patients coming with proptosis whom CT were taken.

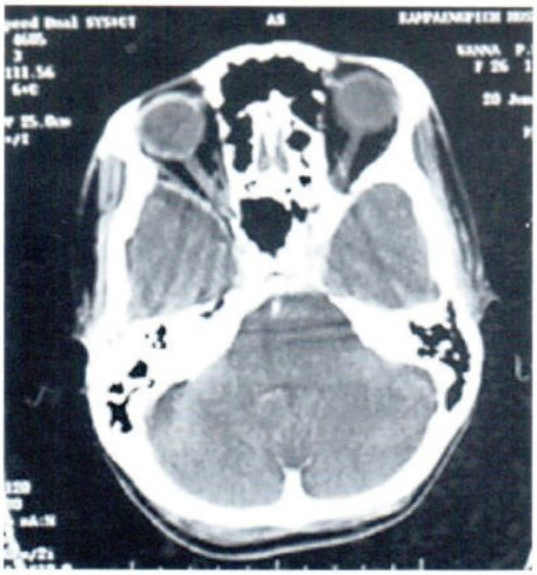

Fig.8 Sphenoid Wing Dysplasia (Case Study)

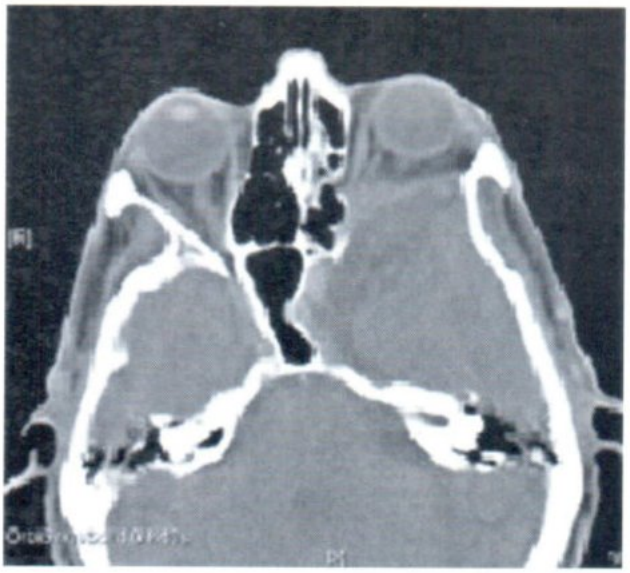

Fig.9 Sphenoid wing dysplasia (Literature Review)

Fig.8 An axial CT scan demonstrates dysplasia and absence of the right sphenoid bone and slight bulging of right temporal lobe, no definite proptosis.

Fig.9 An axial CT shows much absence of left sphenoid, enlarged middle cranial fossa, herniated temporal lobe and accompanying CSF sleeve anteriorly, simulating and intraorbital space occupying lesion, resulting in proptosis.[9]

DISCUSSION

Proptosis is a sign of an underlying disorder, and not a diagnosis itself. There are numerous causes. Due to the lack of direct visualization of the pathology in orbital disease, a thorough history and radiographic investigations are extremely helpful in arriving at a differential diagnosis and appropriate treatment. Actually, the diagnosis of proptosis can be made by multiple radiographic studies including ultrasonography (US), Magnetic Resonance Imaging (MRI) and computed tomography (CT).

Plain radiograph; there are a variety of views of the orbit that can be requested such as Caldwell, Water's, Rhese, lateral and axial basal views, however the findings are not pathognomonic of most of the proptosis.[1,2,5]

US has the advantage of ease to use, no ionizing radiation, excellent tissue differentiation and cost effectiveness. Additionally its safety, noninvasive nature and low cost makes it an attractive first line imaging modality and as a screening method before undertaken CT and MRI in some places. However, US is inferior to CT and MRI in depicting the bony wall and orbital apex, and of limited value in assessing lesions in the sinus and intracranial spaces. Other disadvantages of US are that, one can not take image of both orbits simultaneously and it is difficult for a nonspecialist to interpret. For these reason, US remains unpopular.[1,2,5]

MRI with its superb soft tissue contrast and multiplanar ability provides excellent rendering of orbital anatomy and pathology but is limited by lack of wider availability and high cost.[1,2,3,5]

CT is the most useful initial investigation, due to easy availability and operability, good maintenance and high speed. CT is currently the most valuable technique for delineating the shape, location, extent and character of lesion of the orbit. Furthermore, current CT scanner administers a very low dose of radiation.[2,3,5]

In our work up of proptosis, we found that plain CT was usually sufficient and most lesions were already well visualized especially in cases of orbital trauma, foreign body, orbital lesion associated with paranasal sinus diseases and thyroid ophthalmopathy. While contrast CT was generally used to assess tumor, vascular disorder and inflammation.

The common causes of proptosis in adult and children are different. A retrospective analysis by Sindhu et al examined 57 children with proptosis. Orbital cellulitis was the most common cause (22 cases), followed by thyroid eye disease (8 cases), optic nerve glioma (8 cases), orbital rhabdomyosarcoma (7 cases).[1] KK. Sabharwal et al reported 50 patients, the most common cause is tumor (23 cases) and infection (14 cases), followed by inflammatory disease (9 cases), and trauma (3 cases).[2]

Of our report, 39 cases of adult proptosis can be the result of a myriad of diseases. The most common cause is trauma (15 cases), following by tumor (9 cases), inflammatory disease (7 cases), infection (3 cases). The most common condition causing proptosis of our study was trauma that does not correlate with prior literatures. The explanation is that motorcycle accident without wearing helmet has been a big problem in our province. With the exception of traumatic cause, our result correlates well with the findings of KK. Sabharwal et al and Masud MZ et al. Both of them also described tumors as the most common causes in their studies.[1,2]

CONCLUSION

The most common cause of proptosis in adult presenting to Kamphaengphet Hospital was trauma, following by tumors and thyroid ophthalmopathy. Our result is not comprehensive but can help in forming a differential diagnosis of proptosis.

Proptosis is just a sign, it is usually necessary to undertaken specific radiographic investigation to further narrow down the different causes of proptosis.

We thought that CT is the main tool and most useful investigation. It is useful to characterize the precise location and extension. Furthermore, CT is more precise in demonstrating the bony changes.

CT features, in relation with age, clinical pictures, laboratory investigation, and response to treatment are able to give the correct diagnosis in almost cases. Once the etiology of proptosis is established, the appropriate treatment was done, the undesirable sequelae is diminished.

Although, MRI is the most excellent modality, we presumed that, CT scan can be considered as a cost effective, non invasive and reliable diagnostic modality for evaluation of proptosis. This is particularly true in the places where MRI and specialist for orbital US are unavailable.

ACKNOWLEDGEMENT

I am indebted to Dr. Kamchai Rungsimunpaiboon, M.D. Director of Kamphaengphet Hospital. I am grateful to ophthalmologists, Department of ophthalmology. I would like to thank Mrs. Jiraporn Maneeprai for her help about manuscript preparation.

REFERENCES

1. SINDHU K, DOWNIE J, GHABRIAL R, MARTIN F. Aeitiology of chilhood proptosis. Journal of Peadiatrics and Child Health 1998; 38(4): 374-376
2. KK SABHARWAL, AL CHOUCHAN, S JAIN. CT Evaluation of proptosis. Ind J Radiol Imag 2006; 16(4): 683-688.
3. Micheal Mercandetti. Exophthalmos. http://www.emedicine.com/oph/topic616.htm
4. Masud MZ, Babar TF, Iqbal A et al. Proptosis -eitiology and demographic pattern. J. Coll. Physicians Surg. Pak. 2006; 16(1): 38-41
5. I. Munshi. Investigation of proptosis. Department of Ophthalmology University of The Witwatersrand, Johannesberg, August 2000.
6. S. Haward Lee, Krishna C.V.G. Rao, Robert A, Zimmerman. The orbitCranial MR and CT, third Edn. 1992:128-186.
7. Poonyathalang A, Preechaweat P, Laothammatat j, Charuratana O. Four recti enlargement at orbital apex and thyroid associated optic neuropathy. J Med Assoc Thai 2006; 89(4): 468-472
8. George RA, Godara SC, Som PP. Cranio -orbital -temporal neurofibromatosis : A case report and review of literature. Neuroradiology Ind J. Radiol Imag 2004; 14(3): 217-219
9. Debendra Sahu, Nick Maycock, Adam Booth. A case report of pulsating exophthalmos. British Journal of Ophthalmology 2006; 90: 1-126
10. Jacquemin C, Bosley TM, Liu D, Svedberg H, Buhaliqa A. Reassessment of sphenoid dysplasia associated with neurofibromatosis type 1. AJNR Am J Neuroradiol. 2002 Apr; 23(4):644-8.
11. Andy de Oliveira, Adriana Gonzaga Chaves, Ernesto Narutoma Takahashi Fernanda Akaki, Antonio Augusto Sampaio Cicero Matsuyama. Frontoethmoidal mucocele: acase report and litherature review. Rev Bras Otorrhinolaringol. 2004; 70 (6): 550-4.

CT CORRELATION WITH SEVERITY AND OUTCOME IN TRAUMATIC HEAD INJURY PATIENTS IN SAKONNAKHON HOSPITAL, THAILAND.

Sudaphan PRAMUALCHAROENKIJ, M.D.[1]

ABSTRACT

OBJECTIVE: To evaluate which features on the admission CT scan might add significantly to the neurologic status for predicting the outcome in patients with head injury.

MATERIALS AND METHODS: 95 CT scans of patients with all grades of traumatic head injuries were retrospectively reviewed for roentgen findings on admission. Details from the CT scan on hemorrhage (type, number and size) and midline shift were correlated with neurologic status (assessed with Glasgow Coma Scale [GCS]) and patient outcome at discharge time (assessed with the Glasgow Outcome Scale [GOS]).

RESULTS: GCS score was significantly lower in patients with subarachnoid hemorrhage, subdural, intracerebral hemorrhage, midline shift and associated primary brain injury. GCS changed as a function of hematoma size ($P<.001$) in the patient with focal hemorrhage. The presence of subarachnoid hemorrhage, subdural, intracerebral hematoma and midline shift were also significantly associated with poor outcome. Patients with normal CT scan were significantly more likely to have no or mild neurologic dysfunction and good outcome than those with intracranial hemorrhage ($P<.001$).

CONCLUSION: CT findings, including type and number of intracranial hemorrhage, location, bleeding size, associated brain injury and midline shift have been the essential factors to predict the clinical outcome.

INTRODUCTION

Craniocerebral injuries are a common cause of Sakonnakhon hospital admission following trauma. CT remains to be essential for detecting lesions that require immediate neurosurgical intervention as well as those that require in-hospital observation and medical management. In patients with traumatic head injury, previous studies suggested that factors predictive of patient's outcomes included age, Glasgow Coma Score (GCS), pupil score, injury severity score and the results of CT scan of brain.[1,2] There have been interests in the correlation between the results of the CT scan of brain and the severity of injury and the outcome of patients.

This study aims to investigate the association between abnormalities seen on CT scan of brain and the severity and outcome of injury. Specific CT abnormalities of interest are the type, number and amount of bleeding, together with the magnitude of midline shift. Severity of injury is represented by the Glasgow Coma Scale, and patient's outcome are assessed in correlation with the Glasgow Outcome Scale.

[1] Department of radiology, Sakonnakhon hospital, Sakonnakhon, 47000, Thailand.

MATERIALS AND METHODS

95 patients with all grades of traumatic head injury, admitted to Sakonnakhon Hospital during 1 December 2007 to 1 January 2008, comprised for the head injury data base. These patients, aged range from 2 to 77 years (median age, 31 years), had minimal systemic injury (ie, they had no intraabdominal or intrathoracic injury, although some had bone fractures).

CT scans were obtained with the available scanner (Philips SR7000) shortly after admission to the hospital. All scans were contiguous, 10 mm.-thick sections from external auditory meatus to the vertex. No contrast medium was administered. The scanner was operated at 120 kvp and 150 mA for 2 seconds. All CT scans were read blindly by one radiologist and were categorized according to whether the scan revealed lesions or appeared normal. The abnormalities were recorded for the number and type of any hemorrhage (table 1): epidural hematoma (EDH), subdural hematoma (SDH), subarachnoid hemorrhage (SAH), intracerebral hemorrhage (ICH); and the presence of midline shift. The severity of the head injury and the patient's outcome were determined with standard methods: The Glasgow Coma Scale (GCS), which incorporates measures of the best motor and verbal responses and eye opening, was used to assess the neurologic function. Neurologic abnormalities were scored as follows: 8 or less, severe; 9-12, moderate; and 13-15, mild. The patient's outcome was used to classify the patient's status at the time of discharge into two main groups as good (good recovery and moderately disabled) and poor outcome (severely disabled, persistent vegetative state and death).

Table 1 Summary of key abnormalities sought on CT Scans

Variable	All 95 patients
EDH	
YES	7 (7.36)
NO	88 (92.64)
SDH	
YES	18 (18.95)
NO	77 (81.05)
SAH	
YES	14 (14.74)
NO	81 (85.26)
ICH	
YES	23 (24.21)
NO	72 (75.79)
Midline shift	
YES	12 (12.63)
NO	83 (87.37)
location	
0 location	45 (47.37)
1 location	12 (12.63)
2 locations	38 (40.00)
CT finding	
YES (normal)	45 (47.37)
NO (hemorrhage)	50 (52.63)

Values in parentheses are percentage.
EDH = Epidural hematoma
SDH = Subdural hematoma
SAH = Subarachnoid hemorrhage
ICH = Intracerebral hemorrhage

The volume of each hemorrhage was calculated in several steps. First, the CT section on which the hemorrhage appeared to be the largest was chosen. The largest diameter was measured and considered to be the length (Fig1). Second, the width was measured perpendicular to the length where the width appeared to be the greatest. Third, the height was calculated by adding together the number of sections on which the hemorrhage appeared. The thickness of the top and the bottom sections was assigned at a value of 8 mm. (because it was not clear whether the lesion extended through the entire section), while the ones in between were assigned at a value of 10 mm. Whenever a lesion was seen on only one section, its height was estimated to be 6 mm. Fourth, the length, width, and height were used to estimate the volume of the lesion, which was modeled as an ellipsoid. Patients with diffuse bleeding (SAH, SDH along tentorium and falx) were excluded from blood volume analysis.

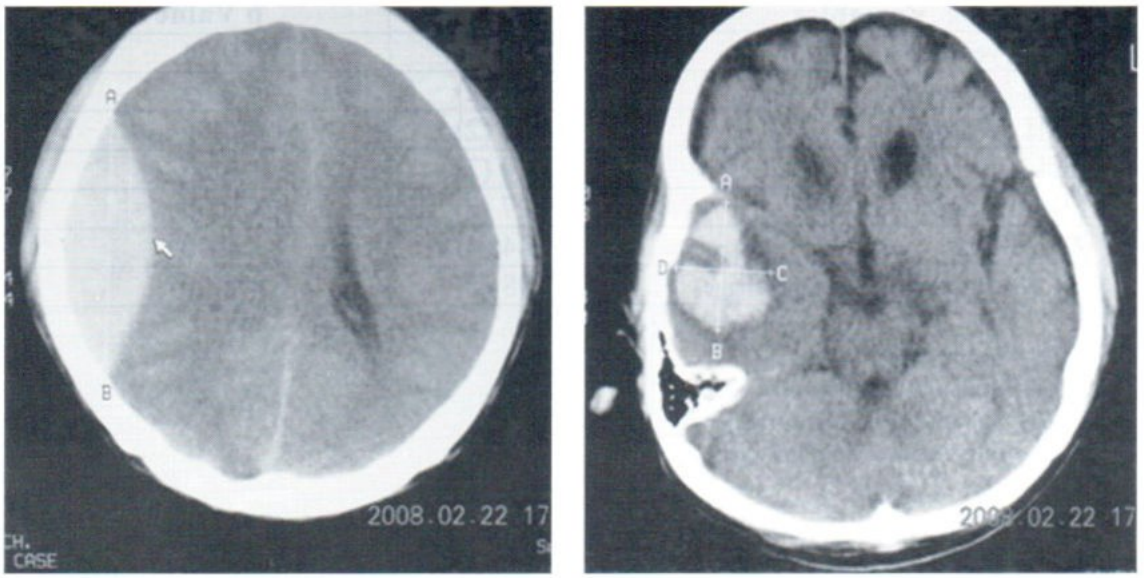

(a) (b)

Fig. 1 Measurement of intracranial hemorrhages. (a) Single intracraniocerebral hematoma, (b) Single EDH. A-B distance indicates length; C-D distance indicates the width

Data analyses

$\chi 2$ tests were used to investigate any associations between GCS total score on admission with each of the features on the CT scans. The relationships between hematoma size and GCS was studied with regression methods. A linear regression model was used for analysis of GCS scores. Patients in whom CT scans appeared normal were assigned a nominal lesion size (0.3 of a voxel), so that their scores could be represented in figure 2. Statistical significance was assessed with $\chi 2$ tests on the basis of the Pearson distribution.

Logistic regression modeling was used to assessed the prognostic significance of the features on CT scans and the two groups of patient outcome.

RESULTS

Fifty of the 95 patients with head injury had intracranial hemorrhages. Motor vehicle accidents comprised 41 of the injuries (82%); the 9 other injuries were caused by accidentaly fall (n=4 [8%]), assaults (n=5[10%]). The median age of the 45 patients with normal CT scans was 30 years. 6% of the patients with normal CT scans was older than 60 years, whereas, 12% of the 50 patients with intracranial hemorrhage were older than 60 years.

Relationship between the appearance of the CT scans and GCS.

Table1, summarises the features visible on all 95 CT scans. The association between the CT features and GCS was very similar to the association of CT features with grade of the injury and therefore the detailed results are reported for GCS only (table2). Patients with subarachnoid hemorrhage, subdural hematoma, intracerebral hemorrhage and midline shift had significantly lower GCS scores ($P<.05$). The presence of epidural was not associated with GCS total.

Table 2 Association between Glasgow Coma Scale and abnormalities sought on CT Scans

Variables	χ^2 Test (df)	p Value
EDH (yes/no)	2.14 (2)	0.34
SDH (yes/no)	7.36 (2)	< 0.05
SAH (yes/no)	8.33 (2)	< 0.05
ICH (yes/no)	2.70 (2)	< 0.05
Midline shift (yes/no)	9.27 (2)	< 0.05
2 locations	21.44 (4)	< 0.001
CT finding (normal /hemorrhage)	17.98 (2)	< 0.001

EDH = Epidural hematoma
SDH = Subdural hematoma
SAH = Subarachnoid hemorrhage
ICH = Intracerebral hemorrhage

In the 40 with focal intracranial hemorrhage (subarachnoid hemorrhage, interhemispheric and tentorial subdural hematomas were excluded) and the 45 with normal CT scans, the results of a regression analysis of GCS and the lesion size revealed that the GCS scores changed as a function of lesion size. The slope coefficien of this scatter diagram was statistically significant. ($P<.001$), (Fig 2).

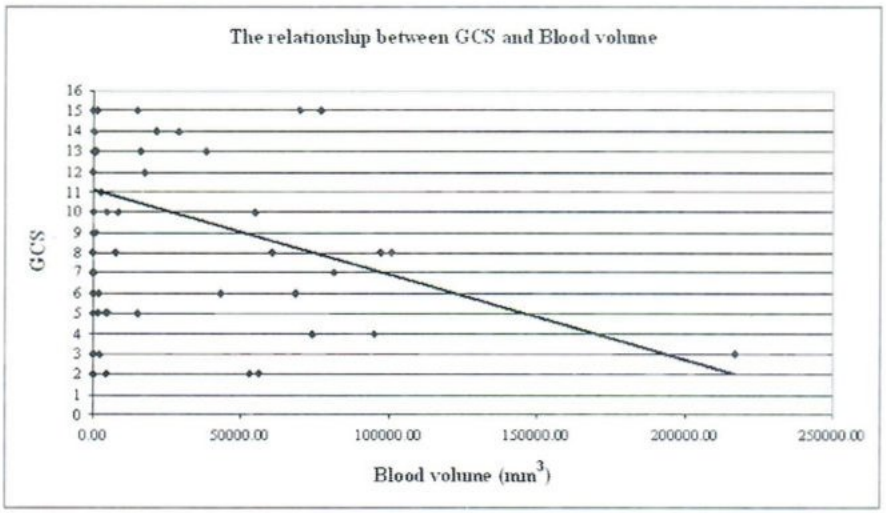

Fig. 2 Scatter diagram show the relationship between GCS and hematoma size (expressed in cubic millimeters (Blood volume))

Patients with normal CT scans at the time of admission were significantly more likely to have no or mild neurologic dysfunction (GCS scores of 13-15) than those with intracranial hemorrhage ($\chi 2 = 16.31$, $df = 2$, $P < .001$).

The difference between patients with normal CT and those with intracranial hemorrhage was also present in their outcomes. Ninety-eight percent of the group with normal CT scans (n = 44/45) had either good recoveries or moderate disabilities versus 54% of those who had intracranial hemorrhage (n = 27/50), ($\chi 2 = 24.04$, $df = 1$, $P < .001$). However, a normal CT scan did not necessarily imply that the patient recovered fully; nine of these patients (20%) remained moderately or severely disabled. Nevertheless, no patient in the group with normal CT scans become persistently vegetative or died compared with 21 patients (42%) with intracranial hemorrhage.

Relationship between the appearance of CT scan and clinical outcome at discharge time were studied. Logistic regression modelling was used to investigate the associations between the two main groups of the patient's outcome (good or poor outcome) at the time of discharge with the features on CT scans (table3). Significant positive associations were found between poor outcome and subarachnoid hemorrhage, subdural hematoma, intracerebral hemorrhage, midline shift and associated intracranial hemorrhage. Negative association was found between poor outcome and the presence of epidural hematoma.

Table 3 Logistic regression model with P values for sequential tests. Odds ratios (ORs) and 95 % confidence intervals (95 % CIs) for predicting outcome for 95 patient on CT Scans. Estimated OR > 1 indicates a poor outcome, estimated OR < 1 indicates improved outcome.

Variables	P Value	OR	95% CI
EDH (yes/no)	0.78	0.68	0.04 – 10.60
SDH (yes/no)	< 0.01	11.04	2.52 – 48.30
SAH (yes/no)	< 0.05	8.67	1.67 – 45.07
ICH (yes/no)	< 0.001	6.54	1.59 – 26.96
Midline shift (yes/no)	< 0.001	1.10	0.32 – 1.44
2 locations (yes/no)	< 0.001	10.35	3.66 – 29.23
CT finding (normal / hemorrhage)	< 0.001	28.69	3.56-231.10

EDH = Epidural hematoma
SDH = Subdural hematoma
SAH = Subarachnoid hemorrhage
ICH = Intracerebral hemorrhage

Among the 50 patients with intracranial hemorrhage, 11 patients who had more than one bleeding site, such as subarachnoid hemorrhage and intracerebral hemorrhage (Fig3), significantly had lower GCS ($P < .001$) and poor outcome ($P < .001$).

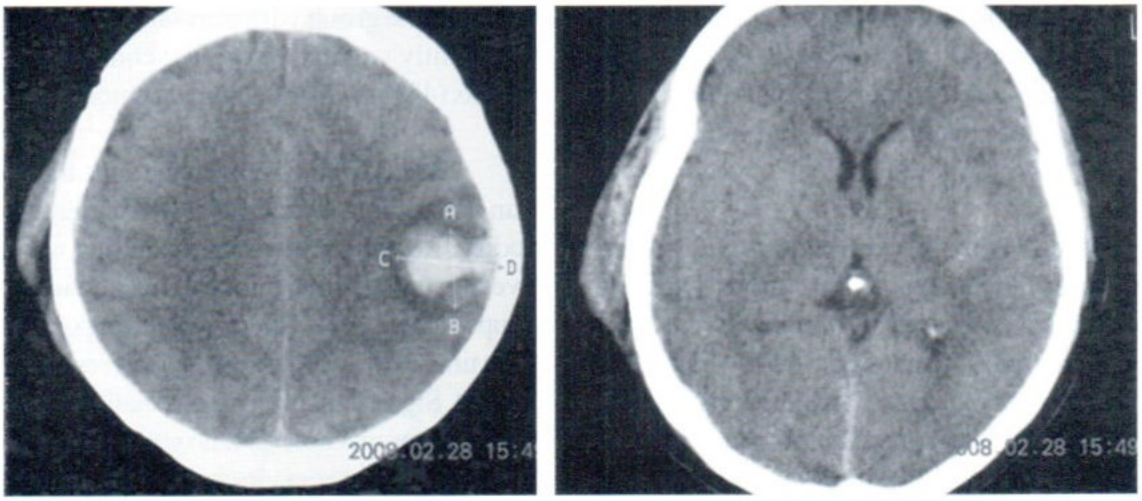

(a) (b)

Fig 3 CT scans of a 41-year-old woman with admission GCS score=10. Axial non- enhanced CT revealed an intracerebral hematoma of cortical left frontoparietal lobe (a). Associated minimal subarachnoid hemorrhage was also detected as increase attenuation of sylvian fissures (b).

GCS = Glassgow Coma Scale **GOS** = Glassgow Outcome Scale

DISCUSSION

CT was paramount important as one of the influential factors to determine neurological status and patient outcome. In regard to this study, SAH, SDH, ICH, midline shift and associated intracranial hemorrhages were associated with GCS and poor outcome in which they were concordant with prior study.[1] Thus it would be possible to identify these more severely injured patients with worse prognosis by noting these easy to identify features on the CT, and target their management accordingly. The presence of EDH was not significantly associated with severity of injury and poor outcome, however.[1]

Acute SDH remains one of the most lethal of all head injury and the extent of primary underlying brain injury is more important than the SDH itself in dictating the outcome. Many patients with SDH showed immediate post-traumatic coma, and mortality among them was greater when compared to those that did not have immediate coma.[3] In this study, 12 of 18 patients with SDH account for severe head injury (GCS of 8 or less), and 10 of these 12 patients developed poor outcome. SDH is commonly associa ted with extensive primary brain injury (brain contusion, diffuse axonal injury, SAH).[4,5]

SAH was frequently diagnosed in patients with head injury and became significance in order to assess severity and outcome. Interestingly, diffuse axonal injury and diffuse cerebral swelling were found in patients with SAH more than those without SAH.[6] The SAH appeared on CT scan in this study was categorized as minimal and larger extent, which the latter had lower GCS and poorer outcome.[7] Half of the patients who died in this study had SAH on CT scan (8 of 16 patients).

Intracerebral hematomas were collections of blood within the brain itself. In the traumatic setting, they result from coalescence of contusions. Increased intracranial pressure, herniation and brain stem failure can subsequently develop, particularly with contusions in the temporal lobes.

Factors affecting prognosis of intracerebral hematoma that had been previously studied, were the presence of associated lesion, actual midline shifted of 4.5 mm or more on initial CT scan, obliteration of suprasellar cistern.[8] In this study, intracerebral hemorrhage had low GCS and poor outcome in particular if associated with other types of primary brain injury. In addition, those having coexisted midline shift, the mortality rate was greatly increased (6 of 7 patients died in this study).

For EDH, it has not associated with GCS and poor outcome.[1,9,10] As 6 of 7 patients diagnosed EDH yet had good outcome, only one patient with the age of 62, with GCS at 8, had a large EDH and midline shift was deceased. Parameters influenced poor prognosis in patients with EDH were age more than 55, low GCS, larger bleeding site, associated primary brain injury and midline shift. Motality rates are essentially nil for patient not in coma preoperatively and approximately 20% for patients in deep coma.[9]

About the size of focal hematomas, the CT scan was used to evaluate the amount of volume of bleeding. The lower GCS has been significantly correlated with larger extent of hematoma ($P<.001$), similar to previous study.[11] This may not surprising because increasing lesion size should compress and distort vital structures in the diencephalons and upper brain stem and increase degree of cerebral swelling. However, the severity of head injury and the patient's outcome may arise from other factors rather than bleeding site and size. Therefore, it is necessary that we have to consider other various important factors such as associated brain contusion, diffuse axonal injury, brain swelling or brain herniation.

Twelve percents of patients in this study with intracranial hemorrhage still had full GCS, a bit higher than that of overseas studies.[12,13] Haydey, et al identified patients with mild head injury who should undergo CT scan based on clinical findings (headache, vomiting, age over 60 years, drug or alcoholic intoxication, deficits in short-term memory, physical trauma above the clavicles and seizure) and , thus, did not recommend CT scan in all patients with mild head injury.[12]

EDH = Epidural Hematoma
SDH = Subdural Hematoma
SAH = Subarachnoid Hematoma
ICH = Intracerebral Hematoma

There were a few limitations of this study. First, it was a small sample sizes, the second was some factors that occasionally missed in the GSC evaluation for instances, alcoholic drinkers, third, how GOS was assessed (Grading of GOS was categorized at the time patients have left the hospital instead of the standard at 6 or 12 months interval after injury), and fourth, the size of hematomas in this study may not exactly accurate, due to the amount of SAH, at the tentorial and interhemispheric SDH were not calculated.

CONCLUSION

CT features in patients with head injury have been associated with severity and treatment outcome. Hence, radiologists should pay special attention to such CT findings including type and number of intracranial hemorrhage, location, bleeding extent, associated primary and secondary brain injury and midline shift because any of those findings have been contemplated as the essential factors to determine the clinical results.

ACKNOWLEDGEMENT

I would like to thank Dr.Thana Tongkon, Department of neurosurgery, Sakonnakhon hospital for useful clinical knowledge.

REFERENCES

1. Wardlaw JM, Easton VJ, Statham P, et al. Which CT features help predict outcome after head injury?. J Neurol. Neurosurg. Psychiatry 2002; 72: 188-192

2. Signorini DF, Andrews FJD, Jones PA, et al. Predicting survival using simple clinical variables: a case study in traumatic brain injury. J Neurology Neurosurg Psychiatry 1999; 66:20-5.
3. Meagher RJ, Young WF. Subdural hematoma: **http://www.emedicine.com/Neuro/topic 575.htm** 2006 Nov.
4. Servadei F, Nasi MT, Giuliani G, et al. CT prognostic factors in acute subdural hematomas: the value of the 'worst' CT scan. Br J Neurosurg 2000; 14(2): 110-6
5. Kotwica Z, Brzezinski J. Acute subdural haematoma in adults: an analysis of outcome in comatose patients. Acta Neurochi (Wien) 1993; 121(3-4): 95-9
6. Tokutomi T. Traumatic SAH on the computerized tomography scan in patients with severe traumatic brain injury; a report from the Japan Neurotrauma Data Bank. Neurotraumatology 2004; 27(2): 161-4
7. Yoshihiro T, Takuya K, Yoshihiro N, et al. CT for acute stage of closed head injury. Radiation Medicine 2005; 23(5): 309-16
8. Hack Gun Bae. Traumatic intracerebral hematoma. Journal of Korean Neurosurgical Soceity 1989; 18(4): 571-9
9. Price DD, Wilson SR. Epidural Hematoma: **http://www.emedicine.com/emerg/topic 167.html** 2008 Jan.
10. Bricolo AP, Pasut LM. Extradural hematoma: toward zero mortality. A prospective study. J Neurosurg 1984;14(1):8-12
11. Kido DK, Cox C, Hamill RW, et al. Traumatic brain injuries: predictive usefulness of CT. Radiology 1992; 182: 777-81
12. Haydel MJ, Preston CA, Mill T, et al. Indications for computed tomography in patients with minor head injury. N Engl J Med 2000; 343: 100-05
13. Jeret JJ, Mandell M, Anziska B, et al. Clinical predictors of abnormality disclosed by computed tomography after mild head trauma. Neurosurgery 1993; 32: 9-15

THE DETERMINATION OF THE AVERAGE PATIENT SKIN DOSE AND ITS FACTORS AFFECTING IN CARDIAC CATHETERIZATION PROCEDURES

Phattanapong SAENCHON, M.Sc.,[1] Anchali KRISANACHINDA, PhD.,[1] Somjai WANGSUPHACHART, M.D.[1]

ABSTRACT

The patient dosimetry for cardiac catheterization and its factors affecting in this study were determined using Dose Area Product (DAP) method. The skin dose was calculated from DAP meter readout and information from portal film determination. Factors affecting patient dose are fluoroscopy time, patient body mass index (BMI), kVp, mAs, experience of the cardiologists, number of frames and etc. The measurement was carried out from 73 patients who underwent the cardiac catheterization procedures examination such as Diagnostic Coronary Angiography (DCA), Cardiac intervention; Percutaneous Transluminal Coronary Angioplasty (PTCA)/stent and cardiac radiofrequency ablation at King Chulalongkorn Memorial Hospital. The result of the average patient skin dose from DCA was 9.52 cGy in tube A (Postero-Anterior) and 18.67 cGy in tube B (Lateral), PTCA/stent 35.95 cGy in tube A and 85.42 cGy in tube B and cardiac radiofrequency ablation 64.82 cGy for single plane. The patient skin dose is more dependent on the fluoroscopy time than other factors. The patient skin dose and the fluoroscopy time was well correlated for RF ablation ($r = 0.90$), PTCA/stent ($r = 0.83$) and DCA ($r = 0.60$). The average patient skin doses in this study were less than threshold dose of skin injury (2Gy). Only two patients received the dose higher than the threshold dose (2.12, 4.51Gy) from cardiac radiofrequency ablation and cardiac interventional studies respectively. The benefit of this study are reported and established the patient skin dose in order to protect the patient from skin injury and increase the cardiologists, awareness for cardiac catheterization procedure.

Keywords: Patient skin dose, Cardiac catheterization procedures

BMI = Body Mass Index, **DAP** = Dose Area Product
DCA = Diagnostic Coronary Angiography
PTCA = Percutaneous Transluminal Coronary Angioplasty

INTRODUCTION

Cardiac catheterization procedures such as Diagnostic Coronary Angiography (DCA), Cardiac Intervention; Percutaneous Transluminal Coronary Angioplasty (PTCA)/Stent and Cardiac Radiofrequency Ablation have lower risks than surgical procedures and their wide acceptance has led to an increasing number being performed.[1] The extensive use of this procedure increases risk of radiation induced effects in patients. The highest entrance skin dose may be harmful as skin injuries. Two types of radiation effect may occur are deterministic and stochastic effects. The risk for long-term stochastic effects may be

[1] Department of Radiology, Faculty of Medicine, Chulalongkorn University, Bangkok Thailand

assessed by effective dose.[2] The majority of instances reported by the United States Food and Drug Administration (FDA) results from cardiac radio frequency ablation and coronary angioplasty.[3-4] The FDA, the World Health Organization (WHO), the International Commission on Radiological Protection (ICRP) and the International Atomic Energy Agency (IAEA) published documents[5-6] to avoid deterministic effects in cardiology procedures. There is now general agreement that the patient skin dose should be determined if there is a risk that doses approach or exceed the threshold levels for deterministic effects. A threshold level of concern is 2 Gray (Gy) for the onset of transient erythema and 3 Gy for hair loss.[5,7] Cardiologists should be aware of potential for serious radiation induced skin injury caused by long periods of fluoroscopy occurring with some of these procedures. Further from patient skin dose, the procedure complexity and factors affecting patient skin dose are very important factors for evaluation during procedures. In September 1995, FDA of the United States issued a public health advisory entitled *Avoidance of Serious X-rays Induced Skin Injuries to Patients during Fluoroscopy-Guided Procedure*.[8] The advisory recommended, among several items, that information be recorded in the patient's record which permits estimation of absorbed dose to the skin. The purpose of the recommendation is to encourage identification of those areas of the skin which are irradiated at levels of absorbed dose that approach or exceed a threshold for injury.[9] In this study, the patient skin dose is measured using Dose Area Product (DAP) dosemeter, where the detector is placed on the collimator of the X-ray tube. The readout data from the meter is in the unit of cGy.cm^2. The patient skin dose (cGy) is determined from the calculation when the radiation area in cm^2 is obtained. The radiation area is determined from the verification films used in the radiation therapy. Film is placed on the couch under the patient and exposed for the whole examination.

The objective of this study is to evaluate the average patient skin dose in each procedures and factors (kV, mAs, fluoroscopy time, patient body mass index (BMI), number of frames, number of procedures and etc.) affecting patient skin dose during cardiac catheterization procedures.

FDA = United States Food and Drugs Administration
WHO = World Health Organization
ICRP = International Commission on Radiological Protection
IAEA = International Atomic Energy Agency
GY = Gray
DAP = Dose Area Product
EAP = Exposure Area Product

MATERIALS AND METHODS

MATERIALS

A. Radiographic-Fluoroscopic system

Table1 The x-ray machines used for cardiac catheterization.

Procedures	Manufacturer	Model / Year
Diagnostic Coronary Angiography (DCA), Cardiac intervention; Percutaneous Transluminal Coronary Angioplasty (PTCA) / stent	Siemens	AXIOM-Artis/2004
Cardiac radiofrequency ablation	GE	Advantx L/C/1994

B. Radiation dosimeters

- **Ionization chamber and electrometer.** Victoreen 4000 M^+ ionization chamber was used for the determination of the table attenuation coefficient, the beam quality half value layer (HVL) and the equipment quality control.
- **Portal film (Verification film).** The non screen ready packed film used for the radiation area verification.
- **Dose Area Product (DAP) meter (Model PTW-Diamentor E).** DAP meter is used to measure the absorbed dose in air (mGy), times the area of the x-ray field (cm^2), on patient skin. The relationship between DAP and exposure-area product (EAP) is essentially a single conversion factor that relates dose to exposure. EAP is expressed in roentgen -cm (R-cm2) and DAP is expressed in gray-cm^2 (Gy-cm^2, usually read in cGy-cm^2).

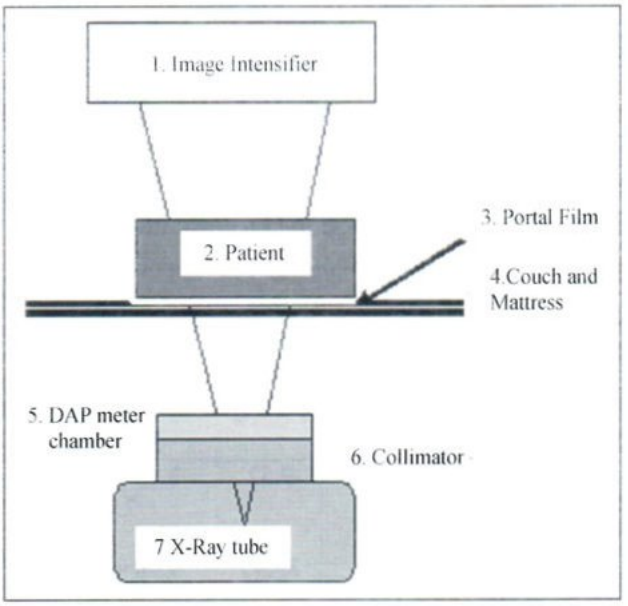

Fig. 1 Setting of the devices for patient skin dose determination

METHODS

The study was carrying out into 5 steps.

1. Quality control of Radiographic/ Fluoroscopic system.

The performance of the Radiographic/ Fluoros- copic system was evaluated with the following studies.[10]

- Dose assessment
- Automatic brightness control test
- Maximum dose rate assessment
- Table attenuation
- Image size assessment
- Half value layer assessment
- Image quality assessment

2. Recorded the patient data collection. The setting of the device for data collection is shown by the followings.

2.1 DAP chamber was placed on the collimator of the x-ray tube.

2.2 Portal film was placed on the couch under the patient around the patient's back at heart portion.

3. Analysis of the data.

3.1 Develop the portal film to determine the radiation area (cm2), calculate the absorbed dose (cGy) from the DAP meter reading (cGy.cm2).

3.2 Determine the absorbed dose in cGy using the data from the DAP meter readout in cGy.cm2 divided by the area from portal film in cm2

3.3 Apply the correction factors from table transmission and DAP Meter calibration and DAP correction factor.

4. Evaluation of the factors affecting the patient skin dose in cardiac catheterization procedure.

5. Evaluation of the correlation between the patient skin dose and the potential related factors such as fluoroscopic time, mAs, kVp, experience of the cardiologists, number of cine frames and patient BMI for cardiac catheterization procedures.

RESULTS

Patient skin dose in cardiac catheterization procedure

The result of patient skin dose for 73 cases are presented in Table 2 and Figure 1. The average patient skin dose from DCA was 9.52 cGy in tube A (Postero-Anterior) and 18.67 cGy in tube B (Lateral), PTCA/stent was 35.95 cGy in tube A and 85.42 cGy in tube B and cardiac radiofrequency ablation was 64.82 cGy for single plane.

Table 2 Patient skin dose in cardiac catheterization procedures.

Procedures	Patient skin dose (cGy)					
	Tube A		Tube B		Single plane	
	Average	Range, Median	Average	Range, Median	Average	Range, Median
DCA (32 cases)	9.52	2.13 - 23.94, 7.75	18.67	2.47 – 77, 16.36	-	
PTCA/ stent (21 cases)	35.95	3.58 - 97.72, 23.86	85.42	20.4 – 451, 53.42	-	
RF ablation (20 cases)			-		64.82	11.9 – 212, 50.78

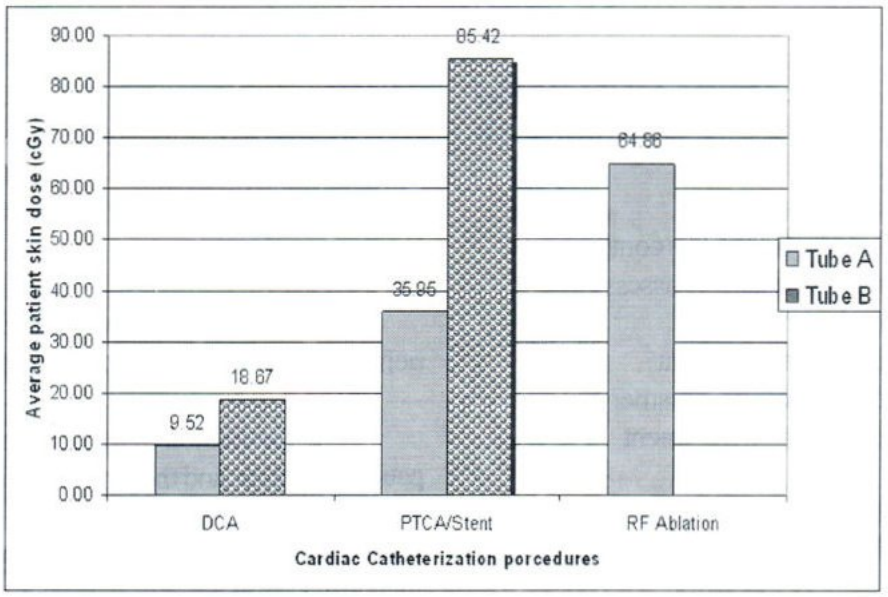

Fig. 2 The average patient skin dose (cGy) in cardiac catheterization procedures.

DAP meter readout in cardiac catheterization procedures

The DAP meter readout (cGy.cm2) for 73 cases is presented in Table 2. The average DAP meter readout from DCA was 861.06 cGy.cm^2 in tube A (Postero-Anterior) and 1,653.59 cGy.cm^2 in tube B (Lateral), PTCA/stent was 3,478.43 cGy.cm^2 in tube A and 7,595.67 cGy.cm^2 in tube B and cardiac radiofrequency ablation was 10,652.70 cGy.cm^2 for single plane

Table 3 DAP meter readout in cardiac catheterization procedures

Procedures	DAP meter readout (cGy.cm^2)					
	Tube A		Tube B		Single plane	
	Average	Range, Median	Average	Range, Median	Average	Range, Median
DCA (32 case)	861.06	171-2287, 843.50	1,653.59	166-7902, 1,510.50		-
PTCA/stent (21 case)	3,478.43	263-9,263, 3023	7,595.67	1,507-36,044, 5,041		-
RF ablation (20 case)			-		10,652.70	1,775-44,702, 7,874

Factors affecting patient skin dose in cardiac catheterization procedures

Factors affecting patient skin dose such as fluoroscopic time, patient body mass index (BMI), the number of cine frames, kVp and mAs are shown in Table 4 and 5 from 32 DCA and 21 PTCA/stent patients.

Table 4 The result of factors affecting patient skin dose in DCA.

Parameter	Tube A		Tube B	
	Average	Range, Median	Average	Range, Median
Fluoroscopic time (min)	2.08	0.50 - 6, 1.50	1.51	0.30 - 7.10, 0.80
Patients Body Mass Index (BMI: kg/m^2)	24.29	15.43 - 38.09, 24.34	24.29	15.43 - 38.09, 24.34
Number of cine frames	495	216 – 1141, 480	480	216 – 1144, 468
kVp for DA and DF	66.50	56.50 - 90.40, 66.50	74.73	64.50 - 101.90, 71.85
mAs for DA and DF	143.82	102.8 - 172.8, 141.80	156.65	109.7 - 179.8, 161.50
kVp for DSA	74.11	62.20 - 99.60, 70	79.28	63.50 - 110.8, 77.95
mAs for DSA	781.37	602.70 - 814.70, 799.80	786.77	649.50-816.60, 801.25

BMI = Body Mass Index **DF** = Diagnostic Fluroscopy
DA = Diagnostic Angiography **DSA** = Diagnostic Systomic Angiography

Table 5 The result of factors affecting patient skin dose in PTCA/stent

Parameter	Tube A		Tube B	
	Average	Range, Median	Average	Range, Median
Fluoroscopic time (min)	7.76	0.80 - 22.50, 6.60	13.64	0.70 - 61.50, 5.70
Patients Body Mass Index (BMI: kg/m^2)	24.42	18.82 - 30.85,23.94	24.42	18.82 - 30.85,23.94
Number of cine frames	941	334 – 1927, 836	936	336 – 1854, 836
kVp for DA and DF	69.15	60.70 - 87.70, 68.00	76.83	67.60 - 92.90, 76.70
mAs for DA and DF	160.85	122.50 - 180.90, 162.70	165.86	141.40 - 182.10, 170
kVp for DSA	72.69	64 - 95.90, 69.50	80.58	67.40-92.10, 81.50
mAs for DSA	774.95	549 – 845.30, 799	801.70	718.70 - 820, 803

The results of the study shows as the data in Table 6 performed on 20 patients of cardiac radiofrequency ablation, show factors affecting patient skin dose such as fluoroscopic time, patient body mass index (BMI), kVp and mAs.

Table 6 The result of Factors affecting patient skin dose in cardiac radiofrequency ablation

Parameter	Cardiac radiofrequency ablation Single plane	
	Average	Range, Median
Fluoroscopic time (min)	24.64	7.00 - 96.70, 16.70
Patients Body Mass Index (BMI: kg/m^2)	23.21	18.37 - 29.38, 22.13
kVp for DA and DF	76.60	75.00 - 92.00, 75.00
mAs for DA and DF	2.58	1.00 - 6.20, 3.00

Table 7 Experience of the cardiologists in cardiac catheterization procedures

Procedures	Experience of the cardiologists (Years)	
	Average	Range, Median
DCA	11	8-14, 13
PTCA/stent	10	8-14, 9
RF ablation	7	5-9, 7

DISCUSSION

The average patient skin dose and its affecting factors were carefully studied in cardiac catheterization procedures during the year 2004-2006 at King Chulalongkorn Memmorial Hospital. Among 73 patients who underwent cardiac catheterization procedures there are 32 cases of diagnostic cardiac angiography (DCA), 21 cases of cardiac intervention and 20 cases of cardiac radiofrequency ablation. The average patient skin dose from DCA was 9.52 cGy (range, median, 2.13 - 23.94, 7.75) in tube A (Postero -Anterior) and 18.67 cGy (range, median, 2.47 - 77, 16.36) in tube B (Lateral), PTCA/Stent was 35.95

cGy (range, median, 3.58 - 97.72, 23.86) in tube A and 85.42 cGy (range, median, 20.4 - 451, 53.42) in tube B and cardiac radiofrequency ablation was 64.82 cGy (range, median,11.9 - 212, 50.78) for single plane. Two patients received higher than threshold erythema dose of PTCA/Stent (4.51 Gy) and cardiac radiofrequency ablation (2.12 Gy).

DAP meter readout (cGy.cm2) were recorded for all patients who underwent cardiac catheterization procedures. The average from DCA was 861.06 cGy.cm^2 (range, median, 171-2,287, 843.50) in tube A (Postero-Anterior) and 1,653.59 cGy.cm^2 (range, median, 166-7,902, 1,510.50) in tube B (Lateral), PTCA/stent was 3,478.43 cGy.cm^2 (range, median, 263-9,263, 3,023) in tube A and 7,595.67 cGy.cm^2 (range, median, 1,507-36,044, 5,041) in tube B and cardiac radiofrequency ablation was 10,652.70 cGy.cm^2 (range, median, 1,775-44,702, 7,874) for single plane.

Table 8 The correlation coeficient (r) between the average patient skin dose and factors affecting patient skin dose in cardiac catheterization procedures.

Parameters	The correlation coeficient (r)				
	DCA		PTCA/stent		Cardiac RF ablation
	Tube A	Tube B	Tube A	Tube B	Single plane
Fluoroscopic time (min)	0.30	**0.60**	0.47	**0.83**	**0.90**
Patient Body Mass Index (BMI: kg/m^2)	0.28	0.30	0.04	0.13	0.35
number of cine frames	0.30	0.10	**0.64**	**0.70**	-
kVp for DA and DF	0.20	**0.80**	0.34	0.39	0.14
mAs for DA and DF	**0.60**	0.004	0.008	0.12	0.04
kVp for DSA	**0.65**	**0.80**	0.001	0.34	-
mAs for DSA	0.31	0.50	0.41	0.15	-
Experience of cardiologists	0.32	0.16	0.16	0.15	0.30

DSA = Diagnostic Systomic Angiography
DA = Diagnostic Angiography
DF = Diagnostic Fluroscopy

The results were compared with other studies as shown in Table 9 for the number of patients and DAP meter readouts.

Table 9 Comparison DAP readouts with other studies from cardiac catheterization procedures.

Procedures	Study	Number of Patients	DAP meter readout ($Gy.cm^2$) Average	Range or Maximum	Median
DCA	De Putte, S., 2000	62	60.6	144	56.82
	Clark, A. L., 2000	117	14.2	1.1-11.3	-
	Neofotistou, V., 1998	198	72	27-79	-
	Vano, E., 1995	288	66.5	11.6 – 482	45.75
	This study	**32**	**12.57**	**1.66-79.02**	**9.52**
PTCA/stent	Karambatsakidou et al, 2005	10	35.0	16-115	-
	Bazli et al, 2004	32	111	22.4-477	111
	Delichas, M. G., 2003	47	63	13-122	-
	Zorzetto, M., 1997	31	91.8	-	-
	Padovani, R., 1997	54	102	-	-
	Vano et al, 1995	45	66.8	12.8-345	66.8
	This study	**21**	**55.37**	**2.63-360.44**	**35.93**
RF ablation	McFadden, S. L., 2002	50	123	21-430	-
	Webster, C. M., 2001	23	105	14-341	-
	Neofotistou, V., 1998	21	-	2.9-134	-
	Broadhead, D. A., 1997	81	95	-	-
	This study	**20**	**106.52**	**17.75-447.02**	**78.74**

CONCLUSION

Two patients from PTCA/stent and cardiac radiofrequency ablation procedures received skin dose over threshold level for erythema (2 Gy) of 4.51 Gy (fluoroscopic time 96.70 min: 04/05/06) and 2.12 Gy (fluoroscopic time 61.50 min: 16/04/06) respectively.

Fluoroscopic time is a factor showing high correlation with dose to the patient especially in the cardiac ablation of single plane procedures and in DCA, PTCA/stent on tube B of lateral projection of Bi-plane procedures (Table 8). As DAP meter was recorded dose when the exposure was on, the readouts show the amount at different position on skin as the tube moved most of the time. The calculated dose does not account for single position. Furthermore different beam geometries and output modes of operation had been selected. Therefore, the dose determined was average skin dose rather than the maximum skin dose.

The body mass index of a patient is also weakly related to the risk for high skin dose in the cardiac catheterization procedures of this study. This means that the size of a patient is far less an important predictor of the dose to be delivered than are other factors, such as the complexity of a procedure. A large patient will contribute to the elevation of a high dose delivery during a complicated procedure.

The number of cine frames in this study is poor correlation for DCA but better correlation for PTCA/stent. The number of cine frames has little effects in DCA because of a short time procedure and small number of cine frames, while PTCA/stent took longer time and more number of cine frames during

procedure. One of the important factor affecting the patient skin dose is the use of frame rate, for this study is fixed at 15 frames/sec, which was not influence in this study. Nevertheless, it is necesssary to optimize the patient skin dose from low number of cine frames to avoid radiation induced skin injuries in patients who underwent cardiac catheterization procedures. Nowaday the cine frame is dependent on the cardiologists to manage the procedures.

The kVp for DA and DF was poor correlation with the average patient skin dose for cardiac radiofrequency ablation and PTCA/stent at both tubes. For DCA the correlation was good in tube A but poor correlation in tube B. Tube B is at lateral position therefore the kVp is higher than tube A (PA; Postero Anterior position). The correlation between the average patient skin dose and the kVp for DSA was good in tube B and fair in tube A. In PTCA/ Stent, no correlation in tube A and very poor in tube B, as high kVp was used in tube B for in lateral position. The mAs for DA and DF and DSA was poor correlation with the average patient skin dose for DCA and PTCA/stent. Only tube A in DCA the correlation was good. As the equipment is automatic brightness control system, the quality control (QC) program is nescessory for the fluoroscopic x-ray output measurement. The calibration of the equipment, condition of the x-ray tube and any potential changes of the filtration were evaluated. A low radiation output could mean either the kVp or mAs was too low, it's also optimized the average patient skin dose for cardiac catheterization procedures.

The experience of cardiologists is a major factor in dose management but showing poor correlation with the patient skin dose. Fellows training in diagnostic cardiac procedures could causes a significant increase in patient exposure during fluoroscopy. Exposure can be further reduced by limiting the number of diagnostic procedures performed with, or by cardiology fellows. It would be important to decide if a cardiology fellow or only who will eventually become cardiologist should receive enough practical training.

The average patient skin dose from DAP meter is more significantly. It may be estimated from DAP meter readout but determination of the dose was depended on the procedure, the direction of the tubes and the experience of the cardiologist. The calibration of DAP meter is necessary as the routine quality control.

The patient skin dose is an important factor during the cardiac catheterization procedures. Cardiologists and staff should be aware of several parameters influencing the dose, therefore the record of concerned factors should be conducted. In case of the over exposure leading to the skin injury, the cardiologists should inform the clinician to follow up and proper treatment for such the late effects.

The correlation factors should be posted for the staff awareness such as fluoroscopic time on tube B. DAP meter threshold value as mentioned in this study.

DAP = Dose Area Product

REFERENCES

1. Grossman W.Historical perspective and present practice of cardiac catheterization. In: Baim DS, Grossman W, eds. **Grpssman's cardiac catheterization, angiography and intervention,** 6th ed. Philadelphia. PA: Lippincott Williams &Wilkins, 2000: 3-14.
2. International Commission on Radiological Protection. Recommendations of the International Commission on Radiological Protection, **ICRP publication 60.** Oxford: Pergamon,1991.
3. Shope TB. Radiation - induced skin injuries from fluoroscopy. **Radiographics.** 1996; 16: 1195-1199.
4. Koeing TR, Mettler FA, Wagner LK. Skin injuries from fluoroscopically guided procedures: part 2, review of 73 cases and recommendations for minimizing dose delivered to the patient. **Am J Roentgenol.** 2001; 177: 13-20.

5. US Food & Drug Administration (FDA), Avoidance of serious x-ray induced skin injuries to patents during fluoroscopically-guided procedures. **Medical Bulletin.**1994; 24(2):7-17.
6. Joint WHO/ISH/CE workshop on efficacy and radiation safety in interventional radiology; 1995 October9-13; Minich Neuremberg, Germany. Germany: **Bundesamt fur Strahlenschutz,** Bfs-ISH-178/97, 1997.
7. Koeing TR, Wolff D,Mettler FA, Wagner LK. Skin injuries from fluoroscopically guided procedures:part 1. Characteristics of radiation injury. **Am J Roentgenol.** 2001;177: 3-11.
8. Food and Drug Administration, "**Important Information for Physicians and Other Health Care Professionals"** Recording Information in the patient's Medical Record that Identifies the Potential for Serious X-Ray Induced Skin Injuries Following Fluoroscopically Guided Procedures (September 15th 1995).
9. Shope TB. "Regulations and recommendations relevant to interventional radiology" in Syllabus: categorical course in physics:physical and technical aspects of angiography and interventional radiology Oak Brook, **Radiological Society of North America.** 1995; 195-205.
10. Kumkrua C. **The patient skin dose determined by radiochromic film and DAP meter method in cardiac catheterization and interventional radiology.** Thesis for the Degree of Master of Science in Medical Imaging, Department of Radiology Faculty of Medicine Chulalongkorn University. Thailand. ISBN : 974-17-6527-4.2004; 1-3.

FETAL DOSE ASSESSMENT FOR BREAST CANCER RADIATION THERAPY WITH COBALT-60 QUADRATE TECHNIQUE

Lalida TUNTIPUMIAMORN,[1] MSc., Chumpot KAKANAPORN,[1] MSc., Yaowalak CHANSILPA,[1] MD., Porntip IAMPONGPAIBOON,[1] Kuakoon CERSAKUL[2]

ABSTRACT

Objective There is no current information about the estimated fetal dose from an extensive breast cancer radiation treatment which include internal mammary chain (IMC), supraclavicular (SPC) and tangential chest wall. The aim of this work was to determine an appropriate irradiation technique and to build a fetal dose data set for the management of pregnant women needing breast irradiation.

Methods Measurements with thermoluminescent (TLD-100) dosimeters were performed in an anthromorphic phantom which was modified to simulate a pregnant patient at first month to sixth month of pregnancy: i.e., 4, 12 and 24 weeks of gestation. Two similar treatment plans, quadrate technique with the open and wedge tangential field, were delivered with a total dose of 50 Gy using Cobalt-60 gamma-ray. Abdominal shielding was constructed and its efficacy was verified. Results of the measured doses were analyzed and plotted as a function of depth and distance from the tangential field edge.

Results Minimum fetal doses in all three gestational periods were detected by the open tangential field quadrate technique with the shielding. With the total prescription dose of 50 Gy, the corresponding average measured doses at 4, 12 and 24 weeks gestation were found to be 5.4 ± 1.19, 11.0 ± 5.18 and 19.6 ± 17.3 cGy or 0.11%, 0.22% and 0.39 % of the total dose, respectively. The modification device, a wedge filter, was found out to yield more external scattered radiation dose to the fetus, about 17-27%, in comparison with the open tangential field technique. The measured dose in the shielding technique, both the open and wedge tangential field technique, was lower than the non-shielding technique approximately 50-60%. For all three periods in a simulated pregnant phantom, the fetal doses showed a small change with depth. But the fetal doses were likely to decrease exponentially with the distance from the primary beam edge. This observation was seen both in the second and third trimesters with correlation coefficients, $R^2 = 0.93$ and 0.94 respectively.

Conclusion A reliable and accurate data set to assess the doses to fetus for breast cancer pregnant patient receiving Cobalt-60 gamma ray with quadrate technique irradiation was obtained. Fetal doses presented in a graph, plotted as the function of depth and distances were found to be useful in the risk management for any individual pregnant patient requiring cobalt-60 quadrate technique radiation therapy at our institution.

[1] Division of Radiation Oncology, Department of Radiology, Faculty of Medicine, Siriraj Hospital, Mahidol University, Bangkok-10700, Thailand

[2] Maharaj Nakornrajchasima Hospital, Nakornrajchasima, Thailand

INTRODUCTION

Recently, recorded in our tumor registry, the most common malignancy in Thai women has been noted to have changed from carcinoma of the cervix to carcinoma of the breast.[1] There are some conditions for which radiation therapy may be required for pregnant woman with malignancy. However, irradiation may increase the risk of malformations in the conceptus with the threshold for this effect reported to be 10 cGy.[2] Ensuring that the radiation dose to the fetus over the treatment course will be kept below the threshold, is very crucial for the planning and management of the treatment. Several studies have been reported on the radiation therapy of breast cancer during pregnancy.[3-7] But the measurements were restricted to a limited number of techniques, e.g., photon energy, gestation periods and also the shielding designs. In our institution, Cobalt-60 gamma-ray with the quadrate irradiation technique is still used as the standard treatment for breast cancer. Since the anatomic site of the breast is quite near the fetus, dose reception is a key factor for a treatment decision. For a busy department, estimated fetal dose for any individual patient was occasionally performed with a one point measurement using an ionization chamber and square phantom. However, the accuracy for these simple measurements may not be adequate for the treatment management of that particular patient. Investigation of the fetal doses received from radiation therapy of the breast using an anthromorphic phantom, and numerous measuring points combined with the routine techniques used in the clinic will provide a much more confident assessment and prediction. In this study, the fetal dose at different gestation periods (4^{th},12^{th}, and 24^{th} week) with Cobalt-60 quadrate techniques irradiation were assessed. To determine which technique will be suitable for giving to the pregnant patients, two similar treatment plans, the open and the wedge tangential field, were compared. Shielding equipments were constructed and verified for their efficacy. Measurement doses from TLD were analyzed and plotted as graph information in correlation with depths and distances from the tangential field edges in all three gestational periods.

MATERIAL & METHODS

All treatment fields in the quadrate technique were defined on the left side of an anthromorphic phantom with 80 cm SSD under the simulator. According to the planning, the tangential field width in most patients were actually found to be 6-9 cm; the maximum field width 9 cm was selected to be used in the study. In the technique of wedge tangential field, a 30 degree wedge angle was used in the planning. Detail of the treatment fields and calculation is presented in Table 1.

The Alderson Rando phantom was modified to simulate pregnant women at different gestational ages. A slice corresponding to the position of the fetus was replaced by a slice made from molded paraffin wax, according to the report of conceptus size for Thai women.[8] Accuracy in the dose determination (within $\pm$ 5%) using paraffin wax was determined prior to use in the study.

To reduce the dose delivered to the fetus, a shielding device was designed and constructed. It was modified from a bridge over patient as described in AAPM report no. 50.[2] Each side and the top of the device were able to support a 2.5 cm thick lead sheet as shown in Fig 2.

Table 1 Quadrate treatment fields and calculation depth

Treatment field	Field size in cm (width x length)	Calculation depth (cm)
Internal Mammary Chain	6 x15	4
Supraclavicular	16 x 9	6.8
Medial & Lateral Tangential	9 x 18	4.3

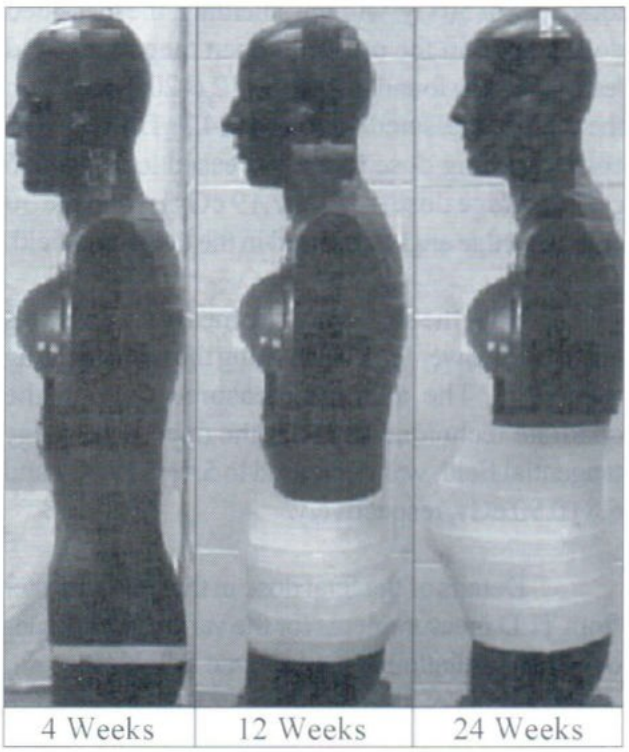

Fig.1 Three gestational age pregnant phantoms.

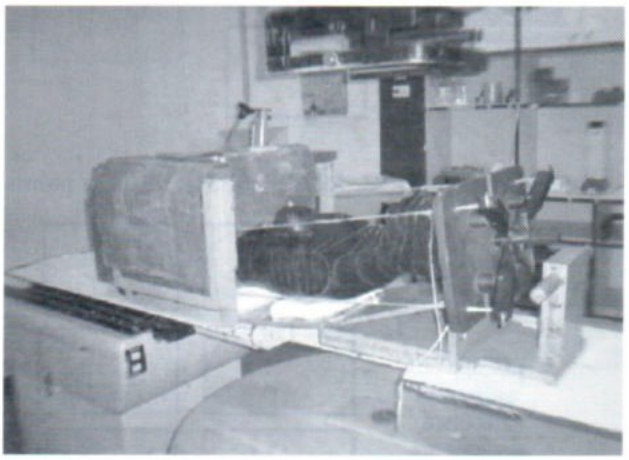

Fig.2 An abdominal shielding device design for a pregnant patient.

All TLD -100 dosimeters (1x1x6 mm. rod shaped) were then calibrated with the Cobalt-60 source. Points of measurement were determined based on the data of the fetal position and size from the past studies.[9-10] The phantom was irradiated with Cobalt-60 gamma-ray for each technique three times. To increase TLD reading sensitivity, we exposed the phantom with a radiation dose of 10 Gy. In anticipation, the linearity tests between the TLD scattered doses reading and the different amount of primary doses were performed and a 10 Gy primary doses was found to be practical for using in the study.

4 weeks (slice 31: 20 TLD points

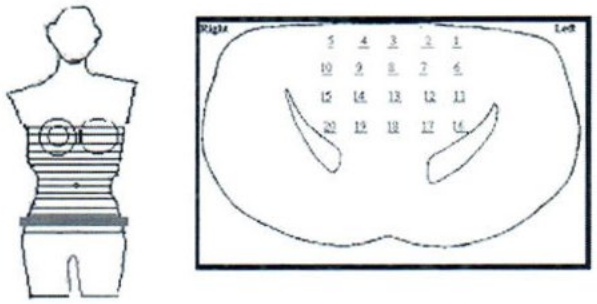

12 weeks (slice 25, 27, 28, 31): 75 TLD points

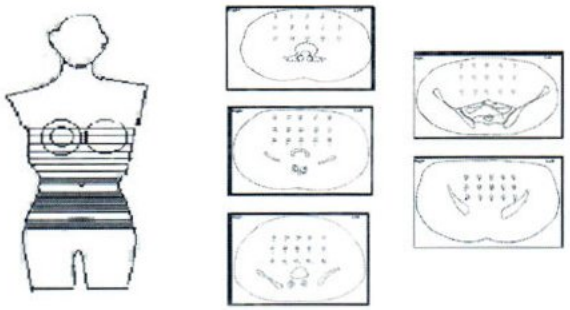

24 weeks (slice 22, 23, 26, 27, 30, 31): 79 TLD points

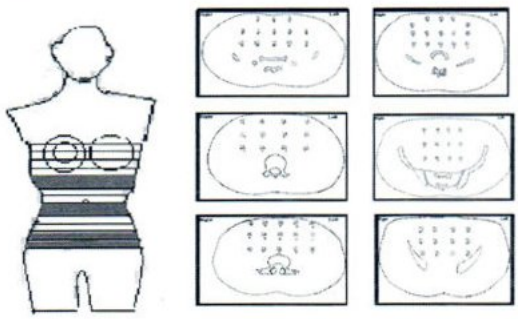

Fig.3 TLD measurement points in the slices representing fetus at different gestational phantom.

RESULTS

Fetal Doses at 4th Week Gestation

For the first trimester, the fetus was estimated to be located in slice 31. To measure the doses, 20 TLD points were distributed at the different depths from 5 to 12 cm below the skin. Distances between the estimated fetus and the primary beam (lower border of the tangential field) was 27.5 cm. With a total dose of 50 Gy, without shielding, the measured doses range in the quadrate open tangential field technique was found to be from 12.6-20.2 cGy, with the average measured dose being 14.3±1.70cGy. The corresponding dose range increased to 13.0-22.6 cGy (average dose = 16.7±2.19 cGy) when the 30 degree wedge angle was used in the tangential field.

With the shielding , the measured dose was about 60% lower than when using the non-shielding technique. The average measured dose in the quadrate technique for both the open and wedge tangential field, was decreased to 5.4±1.19 cGy and 6.8±0.90 cGy, respectively.

Details of the fetal dose in the first trimester from TLD measurements for the various techniques of breast irradiation is summarized in Table 2.

Table 2 Estimated fetal dose at a 4th week gestation period for various techniques of breast irradiation.

Technique	Dose range (cGy)	Avg ±SD (cGy)	% of Prescription dose	% Dose increase from wedge	% Dose decrease from shielding
Non- shielding					
Open Tangential	12.6-20.2	14.3±1.70	0.286	-	-
Wedge Tangential	13.0-22.6	16.7±2.19	0.334	16.8	-
Shielding					
Open Tangential	3.5-7.9	5.4±1.19	0.106	-	62.9
Wedge Tangential	5.2-8.2	6.8±0.90	0.134	26.5	59.9

Fetal Dose at 12th Week Gestation

For the second trimester, the pregnant phantom was inserted with 75 TLD positions at 5 distances: 12.5, 17.5, 20, 22.5, and 27.5 cm from the primary beam (slice no. 25-31). The average measured doses at each slice depended on the distance from the fetus to the primary field edge, as shown in Table 3.

Table 3 Measured dose range and average measured dose (in parenthesis) in cGy at a 12th week gestation period at different slice levels for various techniques of breast irradiation (15 TLD positions per slice)

Technique	Slice 31 (27.5cm)	Slice 29 (22.5cm)	Slice 28 (20 cm)	Slice 27 (17.5cm)	Slice 25 (12.5cm)
Non-shielding					
Open Tangential	15.2-22.0 (18.8±2.10)	21.1-38.0 (29.5±4.75)	25.0-41.8 (30.6±8.90)	25.4-44.5 (35.0±5.55)	33.7-64.1 (46.1±8.66)
Wedge Tangential	19.0-23.1 (20.5±1.37)	22.3-46.3 (34.7±6.14)	27.9-52.5 (39.0±7.50)	30.0-49.2 (39.9±6.32)	43.4-77.5 (58.5±10.26)
Shielding					
Open Tangential	5.1-8.0 (6.3±0.85)	4.7-12.6 (7.7±2.25)	6.7-13.4 (10.2±1.99)	7.1-14.9 (11.2±2.19)	14.6-23.7 (19.8±2.94)
Wedge Tangential	6.2-10.7 (8.3±1.18)	6.0-14.2 (9.7±2.41)	8.9-16.9 (12.5±2.33)	10.8-22.0 (16.5±3.08)	17.4-28.7 (23.3±3.48)

Fetal Dose at 24th Week Gestation

79 positions of TLD were distributed at 6 slice levels (slice no.22-31)to predict the peripheral doses for the third trimester. In the technique of open tangential field with shielding, the maximum measured dose of 61.2 cGy, was found at the slice nearest the field edge at the left corner of the abdomen and the average dose was 49.9±7.25 cGy. Table 4 presented the measured dose range together with the average dose at each slice level for the 24th week gestation period.

Table 4 Measured doses range and average measured doses (in parenthesis)in cGy for a 24th week gestation at different slice levels for various techniques of breast irradiation.

Technique	Slice 31 (27.5cm)	Slice30 (25 cm)	Slice27 (17.5cm)	Slice26 (15 cm)	Slice23 (7.5cm)	Slice22 (5 cm)
Non-shielding						
Open	10.6-22.4	13.9-22.1	20.6-45.3	28.7-58.9	48.0-86.2	58.4-107.3
Tangential	(16.6±3.52)	(18.2±2.64)	(33.7±7.45)	(41.2±8.74)	(69.7±13.56)	(83.0±17.27)
Wedge	13.1-25.6	18.7-23.4	26.3-55.7	37.6-74.8	64.6-109.5	78.4-134.4
Tangential	(19.3±3.83)	(20.9±1.59)	(42.0±8.59)	(52.9±11.01)	(90.7±15.72)	(108.7±18.3)
Shielding						
Open	4.2-6.8	4.0-8.5	6.3-15.7	7.7-18.2	24.7-45.2	35.5-61.2
Tangential	(5.1±0.83)	(6.1±1.51)	(9.8±2.89)	(12.7±3.25)	(35.7±6.58)	(49.9±7.25)
Wedge	5.6-10.1	4.9-12.3	9.3-23.0	11.1-26.7	42.7-60.8	51.1-77.2
Tangential	(7.3±1.39)	(9.0±2.43)	(14.3±4.19)	(18.6±4.84)	(50.8±6.41)	(62.3±8.22)

DISCUSSION

Optimal irradiation technique for breast cancer pregnant patients

Radiation-related risks throughout pregnancy vary according to gestational ages. For a given radiation dose, the risk to the fetus is most significant during the first trimester, less in the second and least in the third trimester. Malformation of organs (3-8 week after conception) appears to have a threshold of 10 cGy. The fetal dose is considered to be negligible at less than 5 cGy. The risk of organ malformation will be significantly increased at dose level above 15 cGy.[11]

In this study, the results showed that the quadrate, open tangential fields, with shielding technique yielded the minimum peripheral doses in all three gestational ages as shown in Fig 4. However, in the first trimester the measured doses both in the open and wedge tangential fields were found to be lower than the threshold doses. This data ensured that the efficacy of our shielding was sufficient enough to be used in a clinic.

For the second and third trimester, the maximum doses found in using this technique were seen at the slice nearest to the primary beam. They were 23.7 cGy and 61.2 cGy respectively. From the T65DR dosimetry system, a significant excess in the risk of SHS (small head size) occurred between 0.1-0.19 Gy.[12] But this risk is evidently greatest during the embryonic period, smaller during the second

trimester and even smaller during the third trimester of pregnancy. Also the risk of severe mental retardation (SMR) was observed at the threshold about 0.65 Gy at the gestational age of 16 to 25 weeks post conception.[13] These results clearly indicated that the quadrate open tangential field technique with shielding was the optimal radiation treatment for pregnant breast cancer patient undergoing Cobalt-60 radiation therapy.

Fetal dose as a function of depth

When depth of the measurement points perpendicular with the body surface were determined. Average TLD measured dose at a given depth in the open tangential field and shielding technique were plotted as presented in Fig.5. It was notably seen that at all gestational ages, changes of the fetal dose with depth were quite small. This finding agreed with previous studies performed with the megavoltage beams.[14-15] Graph information in Fig.5 will help in predicting the fetal doses at any given depth for the quadrate open tangential field technique used for the pregnant breast cancer patients during the entire pregnancy.

In addition, it was notable that at the first trimester, when the results in all techniques were analyzed as shown in Fig.6, fetal doses in the shielding technique ,in both the open and wedge tangential field, increased linearly with depth, while with the non -shielding condition, the results were shown to be in contrast. This evidence suggested that, at the shallow depth, the fetal dose was mostly influenced by the contribution of external scattered dose, such as from the collimator, head leakage and modification devices more than the internal scattered dose. The appropriate shielding thickness will play an important role in attenuating these unwanted external scattered doses.

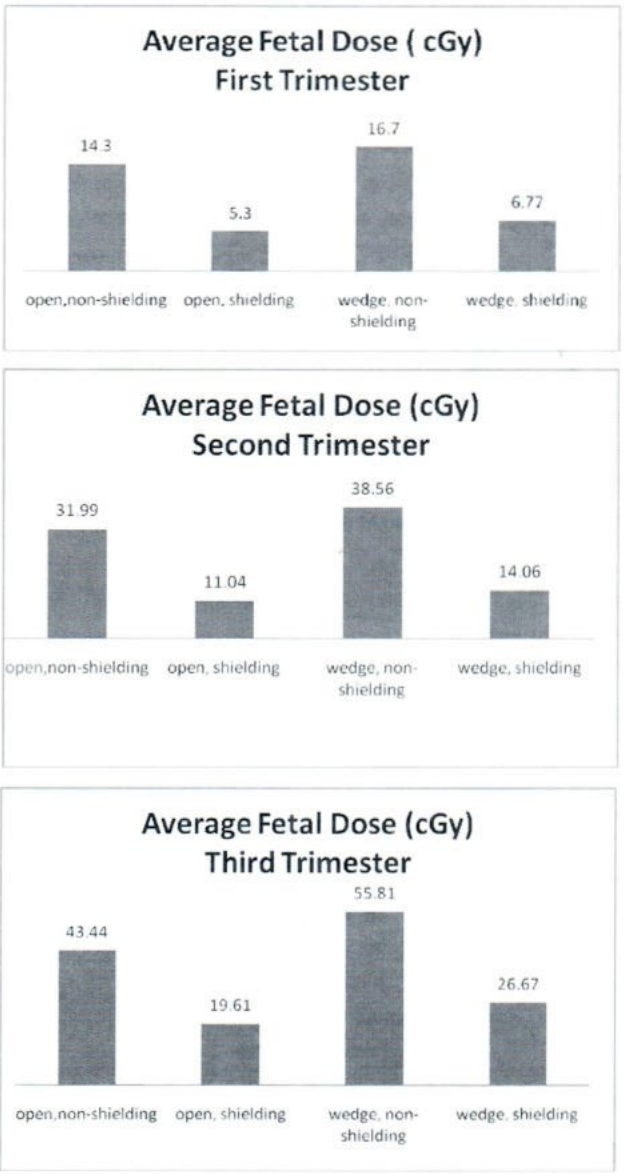

Fig.4 Average fetal doses in different techniques in all three gestational age.

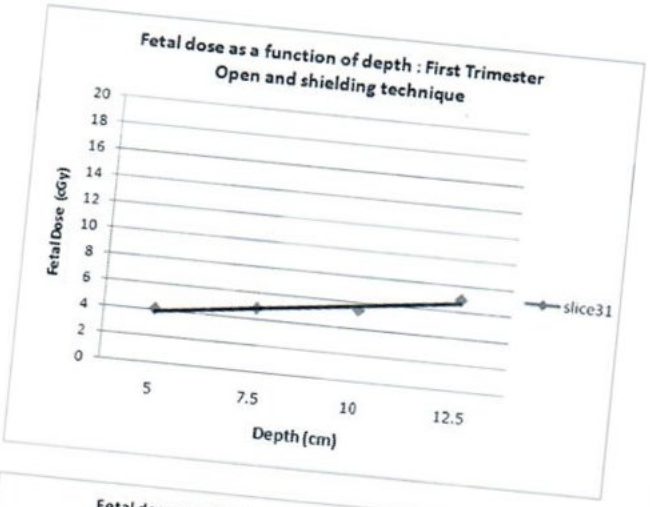

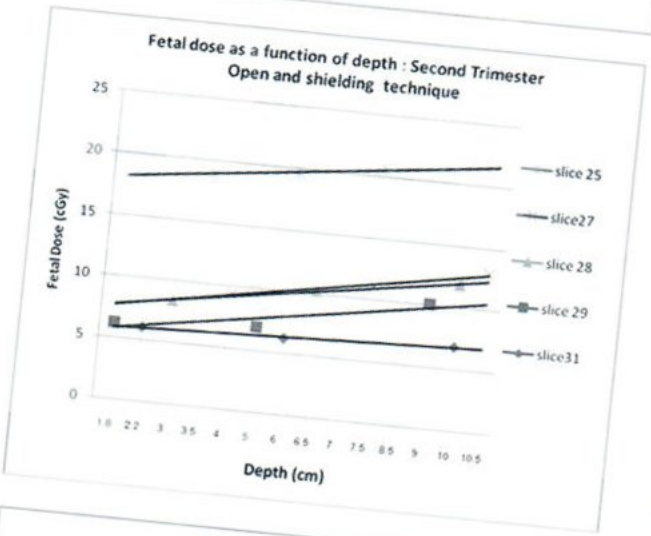

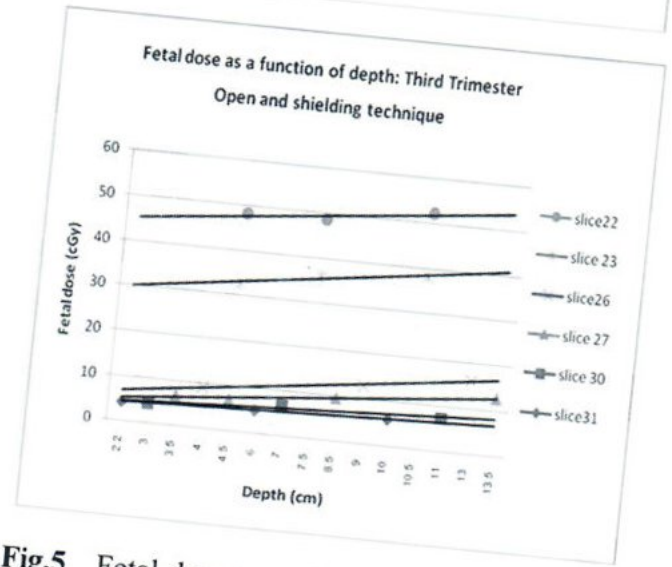

Fig.5 Fetal doses as a function of depth in the different gestational periods pregnancy

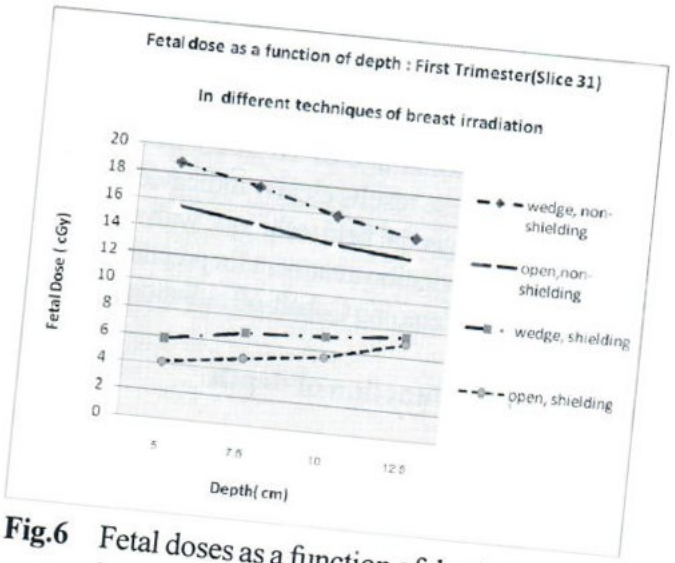

Fig.6 Fetal doses as a function of depth at slice 31 in the first trimester phantom with the different techniques of breast irradiation.

Fetal doses as a function of distances.

The most important factor for judging the magnitude of the peripheral dose was the distance from the field edge. Our data in the second and third trimester in Fig.7 showed that the fetal doses were decreased nearly exponentially in accordance with the distance from the field edge. In the open tangential field with shielding, this relationship was found with correlation coefficients (R^2) equal to 0.931 and 0.946 in the second and third trimester, respectively.

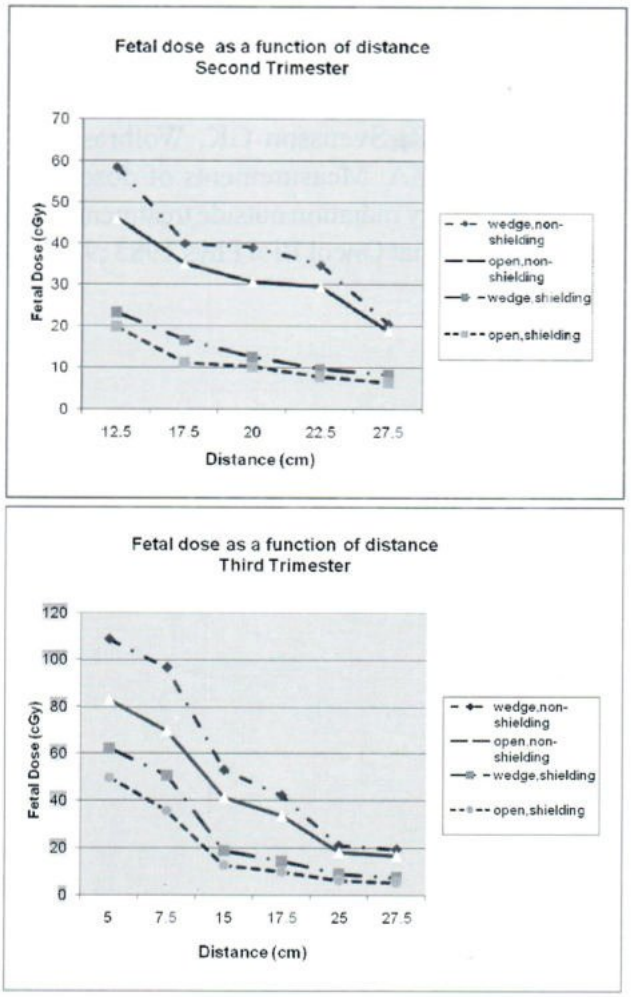

Fig.7 Fetal doses as a function of the distance from the field edge at the second and third trimester.

CONCLUSION

Anticipated fetal dose reception from Cobalt-60 gamma-ray quadrate technique irradiation with abdominal shielding by phantom dosimetry was obtained. Estimated fetal doses for any individual patient whose anatomy was similar to the measurement geometry can be easily predicted from this data set. Risk evaluation and optimal treatment management can be performed with no time delay, as opposed to the cumbersome measurement conditions usually used for each pregnant patient.

REFERENCE

1. Siriraj cancer center. Tumor registry. Statistical report. Faculty of Medicine Siriraj Hospital 2006: 18
2. Stovall M, Blackwell CR, Cundiff J , Novack DH, Palta JR, Wagner LK, et al. Fetal dose from radiotherapy with photon beam. Report of AAPM Radiation Therapy Committee Task Group no. 36. Med Phys 1995; 22(1): 63-82
3. Ngu SLC, Duval P, Collins C. Fetal radiation dose in radiotherapy for breast cancer. Aust Radiol 1992; 36: 321-2
4. Antepas CE, Sandilos PH, Kouvaris J, Balafouta E, Kalinou E, Kollaros N, et al. Fetal dose variation during breast cancer radiotherapy. Int J Radiat Oncol Biol Phys, 1998 ; 40: 995-8
5. Antolak JA, Strom EA. Fetal dose estimates for electron beam treatment to the chest wall of a pregnant patient. Med Phys 1998; 25 (12): 2388-91
6. Kouvaris JR, Antepas CE, Sandilos PH, Plataniotis GA, Tympanides CN, Vlahos LJ. Postoperative tailored radiotherapy for locally advanced breast carcinoma during pregnancy : a therapeutic dilemma. Am J Obste Gynaecol, 2000; 183: 498-9
7. Van der Geissen PH. Measurement of the peripheral dose for the tangential breast treatment technique with Cobalt-60 gamma radiation and high energy x-rays. Radiother Oncol 1997; 42: 257-64
8. Linasmita V and Sugkraroek P. Normal uterine growth curve by measurement of symphysial -fundal height in pregnant women seen at Ramathibodi Hospital. J Med Ass Thailand 1984: 67(suppl 2): 22-6
9. Osei EK, Faulkner K. Fetal position and size data for dose estimation. Br J Radiol 1999; 72: 363-70
10. Rogozzino MW, Breckte BS, Hill LM, Gray JL. Average fetal depth in utero: data for estimation of fetal absorbed radiation dose. Radiology 1986; 158(2): 513-5

11. National council on radiation protection. Medical radiation exposure of pregnant and potentially pregnant women. Report number 54. Washington, DC: NCRP ; 1977
12. Miller RW, Mulvihill JJ. Small head size after atomic irradiation. Teratology, 1976: 14; 355 -357
13. Otake M, Yoshimaru H, Schull WJ. Severe mental retardation among the prenatally exposed survivors of the atomic bombing of Hiroshima and Nagasaki: A comparison of TD65 and DS86 dosimetry system. Tech Rep. 16-87 Radiation Effects Research Foundation, Hiroshima, 1987
14. Fraass BA and Geien J . Peripheral dose from megavoltage beams. Med Phys,1983; 10: 809-818
15. Kase KR, Svensson GK, Wolbrast AB, Marks MA. Measurements of dose from secondary radiation outside treatment field. Int J Radiat Oncol Biol Phys,1983 ;9: 1177 -1183-

ULTRASOUND FINDINGS OF ACUTE AND CHRONIC CHOLECYSTITIS

Daranee PITANUPONGSA, M.D.[1]

ABSTRACT

A retrospective study of ultrasound findings of patients who underwent cholecystectomy with histopathologically proven to be acute or chronic cholecystitis in Trang Hospital were studied from January 2005 to February 2008. There were 26 patients; acute cholecystitis 14 cases and chronic cholecystitis 12 cases. Gallstone were the most frequent sonographic findings of acute and chronic cholecystitis (93% and 83% respectively). Gallbladder distention and diffuse gallbladder wall thickening with anechoic zone were seen more frequent in acute cholecystitis but contracted gallbladder and diffuse gallbladder wall thickening without anechoic zone were seen more frequent in chronic cholecystitis. Complications of acute cholecystitis were found in 50% of cases. Localized thickening of the gallbladder wall that mimicked gallbladder carcinoma were found in 3 cases (25%) of chronic cholecystitis and additional CT scan of upper abdomen were performed in 2 cases. All of the patients with acute cholecystitis were diagnosed by ultrasonography and only 2 cases of the patient with chronic cholecystitis need CT for further investigation.

INTRODUCTION

The role of computed tomography (CT) in the evaluation of abdominal pain continue to be spreading. Acute cholecystitis is the most common cause of acute right upper quadrant abdominal pain. Ultrasound should be used as the initial imaging method to be employed. It is a relatively inexpensive, non-invasive, rapidly performable at the bedside without radiation hazard. The present study aimed to describe ultrasound findings of patients with acute or chronic cholecystitis diagnosed and treated at my hospital.

MATERIAL AND METHOD

The ultrasound findings of 26 patients who underwent cholecystectomy with histopathologically proven to be acute or chronic cholecystitis at Trang Hospital from January 2005 to February 2008, were reviewed, retrospectively.

Ultrasonographic examinations were performed with a realtime scanners (SSD 2200, Aloka), using 3.5 MHz convex transducer.

Ultrasond features, operative and histopathologic findings were analyzed.

RESULTS

I found acute cholecystitis (14 cases, 54%) more than chronic cholecystitis (12 cases, 46%). Two cases of chronic cholecystitis had subsegnently acute exacerbation.

Acute cholecystitis were divided into two groups, with or without complications. Seven patients had acute uncomplicated cholecystitis and the other seven cases had complications; gangrenous cholecystitis 4 cases, emphysematous cholecystitis 2 cases and gallbladder perforation 1 case.

[1] Department of Radiology, Trang Hospital, Trang, Thailand.

All of the acute uncomplicated cholecystitis had gallstones and diffuse gallbladder wall thickening. Anechoic zone in the gallbladder wall thickening were shown in 6 cases. Gallbladder distention were identified in 3 cases and with pericholecystic fluid in 2 cases respectively (Fig.1, 2).

In acute cholecystitis with complications, gallstones were found in 6 cases. Five cases had gallbladder distention. Gangrenous cholecystitis had anechoic zone in the thickened gallbladder wall in 1 case, sloughing of gallbladder wall in 2 cases and intraluminal membrane in 1 case (Fig.3). Diffuse echogenicity in gallbladder lumen was seen in one case of gangrenous cholecystitis (Fig.4). Air collections within the lumen of gallbladder were detected in both cases of emphysematous cholecystitis (Fig.5A). These findings were confirmed at abdominal radiographs (Fig.5B). Only one case had gallbladder perforation by evidence of ill-defined gallbladder wall with complex pericholecystic fluid collection (Fig.6). Pericholecystic fluid were seen in 2 cases of acute complicated cholecystitis. Ultrasound findings of acute cholecystitis were summarized in table 1.

Most of chronic cholecystitis (10 cases, 83%) had gallstones. The contracted gallbladder were seen in 9 cases. Diffuse gallbladder wall thickening were found in 7 cases but anechoic zone in the thickened gallbladder wall were found in only 2 cases of chronic cholecystitis with acute exacerbation (Fig.7, 8). One case had gallbladder distention. The localized thickening of gallbladder wall were identified in 3 cases. Additional CT scans of upper abdomen were performed in 2 cases. Focally ulcerated mucosa were demonstrated in both cases and muddy gallstone was found in one case (Fig.9, 10). The third case, no further investigation was performed. Mucus cyst was identified, histopathologically (Fig.11). Diffuse echoge- nicity in gallbladder lumen was seen in one case of chronic cholecystitis with acute exacerbation. Ultrasound findings of chronic cholecystitis were summarized in table 2.

Table 1 Ultrasound findings in acute cholecystitis (14 cases)

Findings	Number (%)	Acute uncomplicated cholecystitis case (n = 7)	Acute cholecystitis with complications case (n = 7)
1. Gallstones	13 (93%)	7	6
2. Gallbladder distention	8 (57%)	3	5
3. Diffuse gallbladder wall thickening (> 3 mm.)	8 (57%)	7	1
- Anechoic zone in the gallbladder wall		6	1
4. Pericholecystic fluid	4 (28.5%)	2	2
5. Sloughing of gallbladder wall	2 (14%)	0	2
6. Intraluminal membrane	1 (7%)	0	1
7. Ill-defined gallbladder wall with complex pericholecystic fluid collection	1 (7%)	0	1
8. Reflective echoes in the gallbladder fossa with associated reverberation artifact	2 (14%)	0	2
9. Diffuse echogenicity in gallbladder lumen	1 (7%)	0	1

Table 2 Ultrasound findings in chronic cholecystitis (12 cases)

Findings	Number (%)	Chronic Cholecystitis case (n = 10)	Chronic cholecystitis with acute exacerbation case (n = 2)
1. Gallstones	10 (83%)	8	2
2. Contracted gallbladder	9 (75%)	8	1
3. Gallbladder distention	1 (8%)	1	0
4. Diffuse gallbladder wall thickening (> 3 mm)	7 (58%)	5	2
-Anechoic zone in the gallbladder wall		0	2
5. Localized thickening of gallbladder wall	3 (25%)	3	0
6. Diffuse echogenicity in gallbladder lumen	1 (8%)	0	1

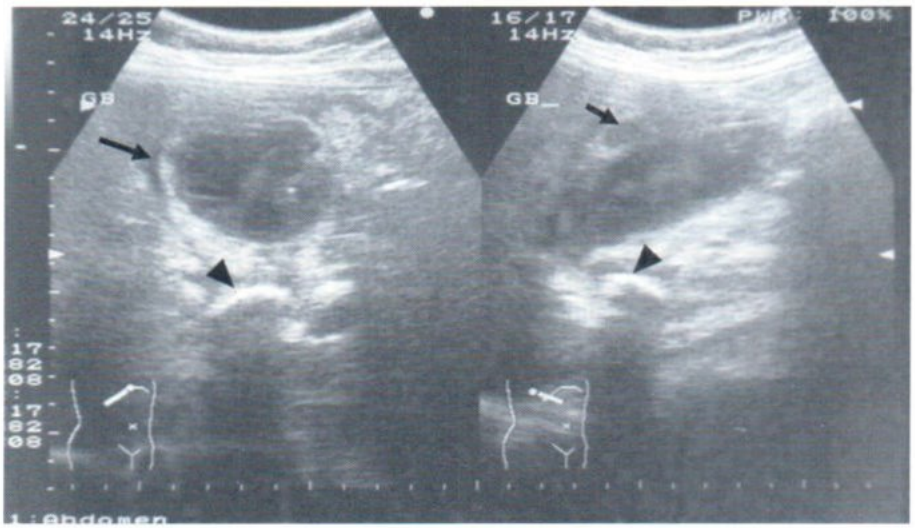

Fig.1 Acute uncomplicated cholecystitis. Ultrasound demonstrates a shadowing stone (arrowheads) impacted in the gallbladder neck. The gallbladder wall is thickened with anechoic zone in the wall (short arrow). Pericholecystic fluid (long arrow) is seen.

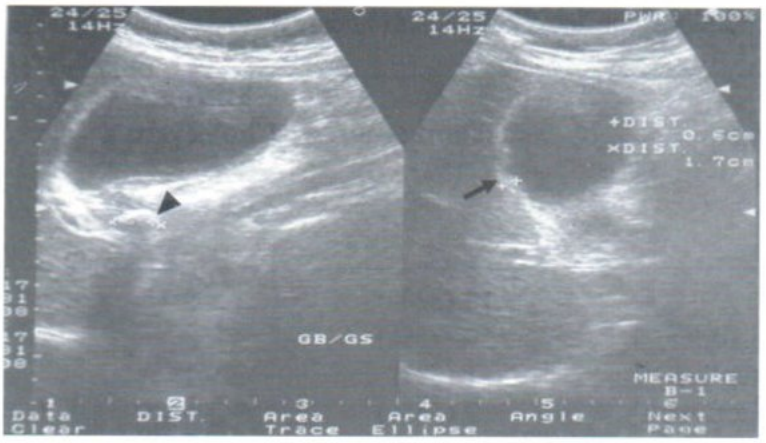

Fig.2 Acute uncomplicated cholecystitis. Ultrasound demonstrates distended gallbladder with thickened wall (arrow). There is a shadowing stone (arrowhead) in the gallbladder neck.

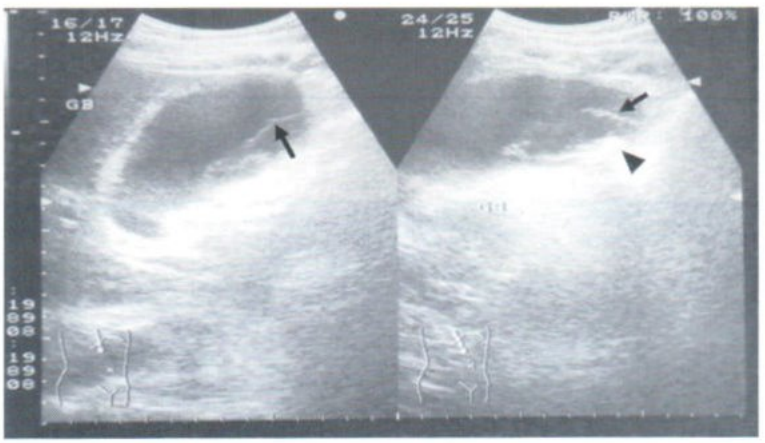

Fig.3 Gangrenous cholecystitis. Ultrasound demonstrates distended gallbladder with intraluminal membrane (arrows). Gallstones (arrowhead) are seen.

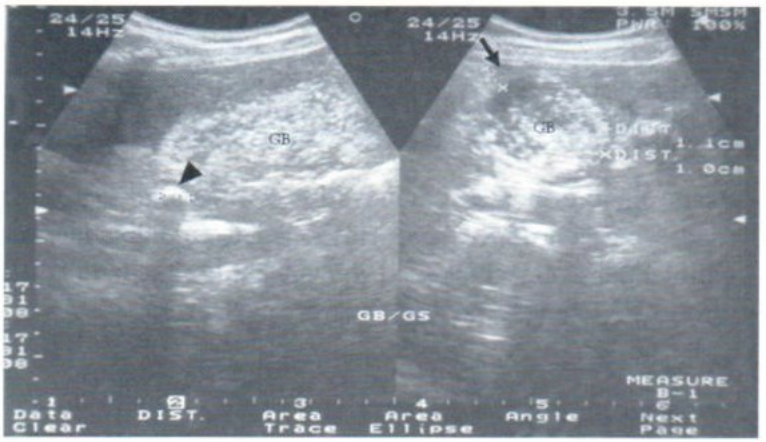

Fig.4 Gangrenous cholecystitis. Ultrasound demonstrates distended gallbladder with thickened wall (arrow) and diffuse echogenicity in the gallbladder lumen (GB). A shadowing gallstone (arrowhead) is seen.

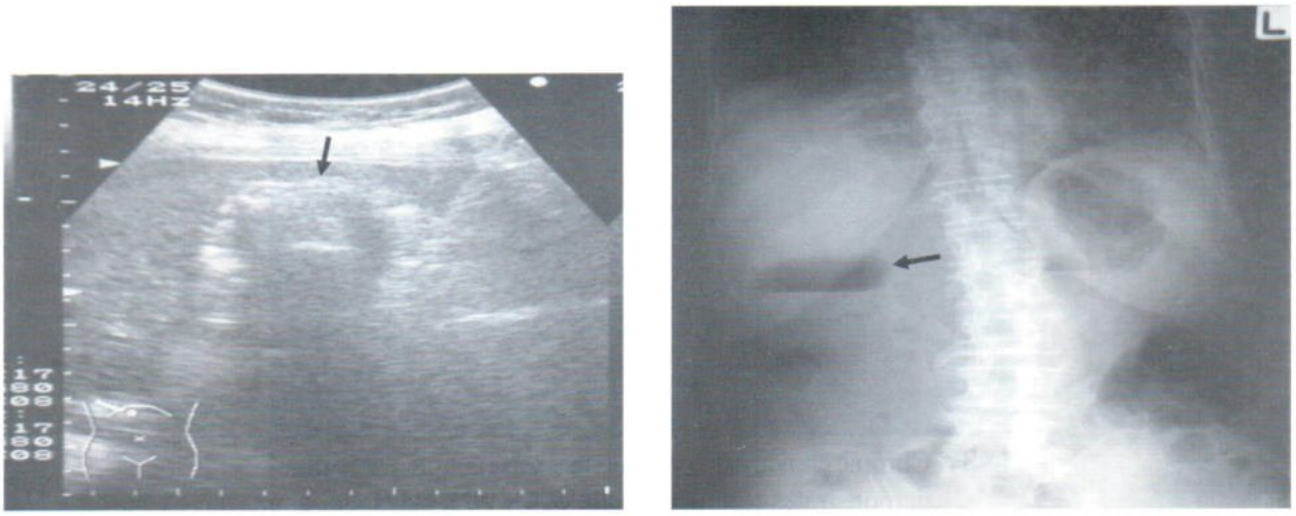

5A 5B

Fig.5 Emphysematous cholecystitis.
A Ultrasound demonstrates reflective echoes in the gallbladder fossa with associated reverberation artifact (arrow).
B Upright radiograph of the abdomen confirms air-fluid level in the gallbladder lumen (arrow).

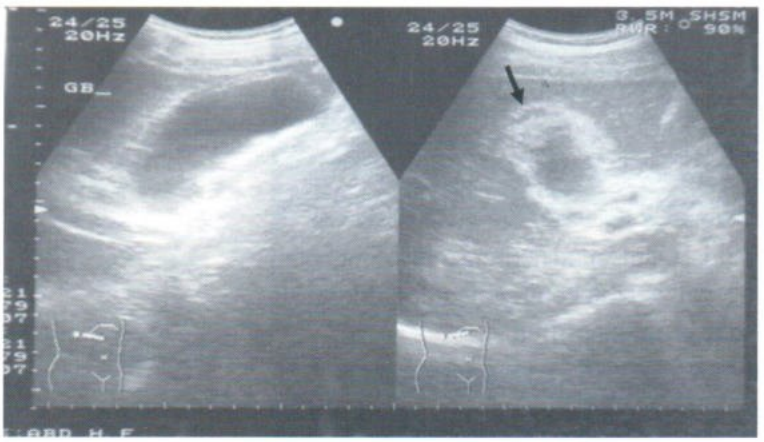

Fig.6 Gallbladder perforation. Ultrasound demonstrates ill-defined gallbladder wall with complex pericholecystic fluid collection (arrow).

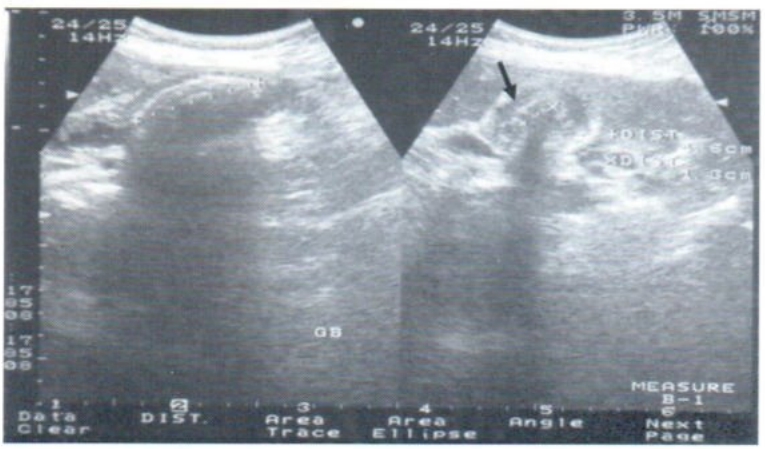

Fig.7 Chronic cholecystitis. Ultrasound demonstrates stone in contracted gallbladder (+--+,x--x). Diffuse gallbladder wall thickening (arrow) is seen.

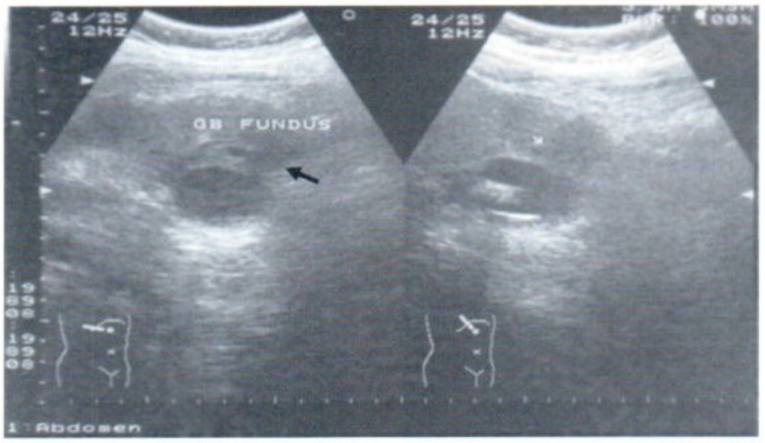

Fig.8 Chronic cholecystitis with acute exacerbation. Ultrasound demonstrates contracted gallbladder with gallstone. The gallbladder wall is thickened with anechoic zone in the wall (blackarrow).

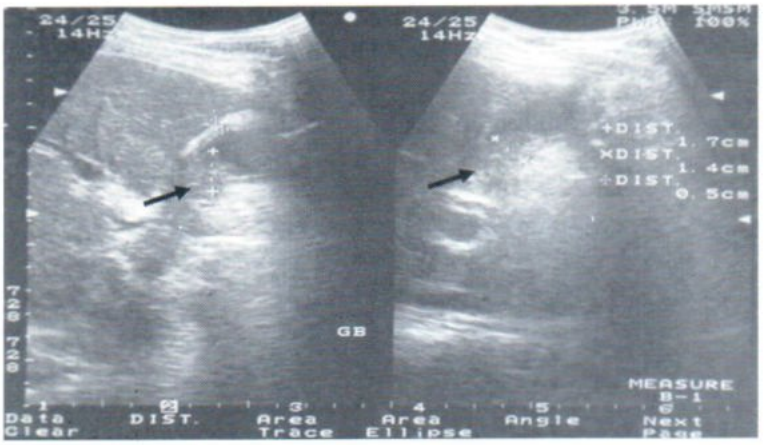

Fig.9 Chronic cholecystitis. Ultrasound demonstrates contracted gallbladder with localized thickening of gallbladder wall (arrows). Gallstone is not identified.

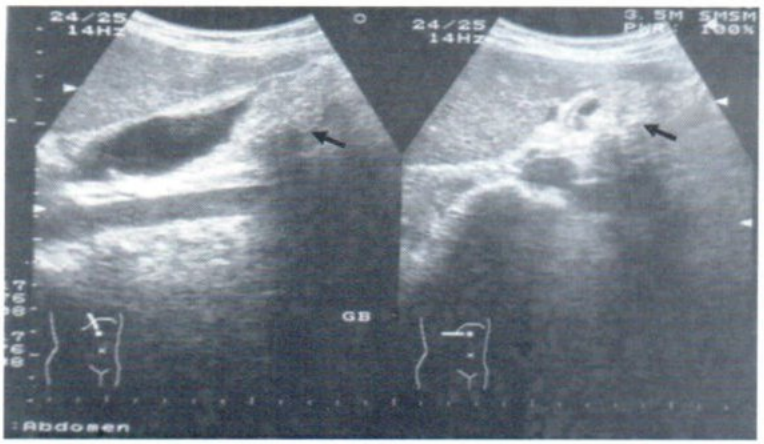

Fig.10 Chronic cholecystitis with muddy gallstone. Ultrasound demonstrates localized thickening of gallbladder wall (arrows) at fundus. This finding is confirmed in operation where there is muddy gallstone in the gallbladder.

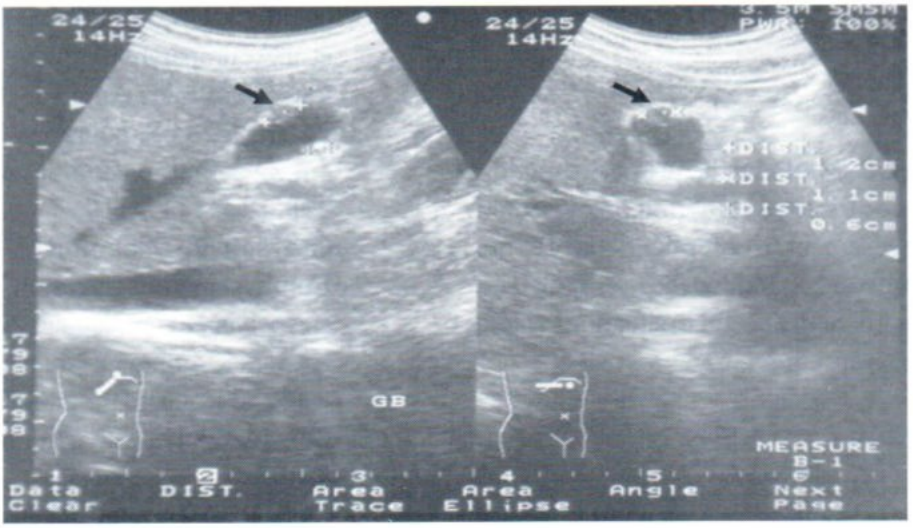

Fig.11 Chronic cholecystitis with mucus cyst. Ultrasound demonstrates contracted gallbladder with a hypoechoic nodule at anterior wall (arrows).

DISCUSSION

The role of CT in the evaluation of abdominal pain continues to be expanded. CT allows for more comprehensive evaluation of the abdomen and pelvis and can identify various inflammatory processes. But ultrasound should be the first imaging modality used when suspecting cholecystitis. It's non-invasive, fast, no radiation, easily tolerated by the patient and reliable in the hands of an experienced operator. Ultrasound is also superior to CT as the initial imaging investigation for assessment of biliary diseases causing acute right upper quadrant pain.[1]

Ultrasound findings in acute uncomplicated cholecystitis are including gallstones, which often impacted in gallbladder neck or cystic duct, a positive sonographic Murphy's sign, gallbladder distention, wall thickening and pericholecystic fluid.[2-4] In the present study, all cases had gallstones and wall thickening. Gallbladder distention and pericholecystic fluid were seen less than half of the cases. I saw gallbladder distention more often in acute cholecystitis with complications. Early detection of the complications reduces morbidity and mortality.[5] In the present study, complications,were detected in 50% of the cases., mostly having gallstones. Ultrasound findings of acute cholecystitis with complications in the present study were not different from the previous reports ; sloughing of gallbladder wall and intraluminal membrane in gangrenous cholecystitis, intraluminal gas in emphysematous cholecystitis and ill-defined gallbladder wall with complex pericholecystic fluid collection in gallbladder perforation.[6-9] Abdominal radiographs were reviewed to confirm intraluminal/intramural air in emphysematous cholecystitis.

Sonographic features of chronic cholecystitis are gallstones and gallbladder wall thickening.[10-11] In the present study, most had gallstones and contracted lumen. Diffuse gallbladder wall thickening were seen half of the cases. Localized thickening of the gallbladder wall that mimicked gallbladder carcinoma were identified in 3 cases. Ultrasound findings in cases of chronic cholecystitis with acute exacerbation were similar to cases of acute cholecystitis. Both cases had gallstones and diffuse gallbladder wall thickening with anechoic zone. Diffuse echogenicity in gallbladder lumen which were seen in acute complicated cholecystitis was found in one case.

In the present study, all of acute cholecystitis were diagnosed by ultrasonography and only 2 cases (17%) of chronic cholecystitis need CT for more

information.

CONCLUSION

Ultrasound should be the primary imaging modality of choice for the evaluation of suspected cholecystitis. Assessment of complications of acute cholecystitis is valuable to reduce the morbidity and mortality. CT is particularly useful in situations where ultrasound findings are equivocal.

REFERENCES

1. Harvey RT, Miller WT, Jr. Acute biliary disease: initial CT and follow-up US versus initial US and follow-up CT. Radiology 1999; 213: 831-836.
2. Bennett GL, Balthazar EJ. Ultrasound and CT evaluation of emergent gallbladder pathology. Radiol Clin North Am. 2003; 41: 1203-1216.
3. Middleton WD. Gallbladder. In: Goldberg BB, eds. Textbook of abdominal ultrasound. Maryland: Williams & Wilkins, 1993; 116-145.
4. Martinez A, Bona X, Velasco M, et al. Diagnostic accuracy of ultrasound in acute cholecystitis. Gastrointest Radiol 1986; 11: 334-338.
5. Jeffrey RB, Laing FC, Wong W, et al. Gangrenous cholecystitis: diagnosis by ultrasound. Radiology 1983; 148: 219-221.
6. Simeone JF, Brink JA, Mueller PR, et al. The sonographic diagnosis of acute gangrenous cholecystitis: importance of the Murphy sign. AJR Am J Roentgenol 1989; 152: 289-290.
7. Mentzer RM, Jr, Golden GT, Chandler JG, et al. A comparative appraisal of emphysematous cholecystitis. Am J Surg 1975; 129: 10-15.
8. Parulekar SG. Sonographic findings in acute emphysematous cholecystitis. Radiology 1982; 145: 117-119.
9. Grayson DE, Abbott RM, Levy AD, et al. Emphysematous infections of the abdomen and pelvis. RadioGraphics 2002; 22: 543-561.
10. Kimura K, Fujita N, Noda Y, et al. Localized wall thickening of the gallbladder mimicking a neoplasm. Digestive Endoscopy 2004 ; 16: 54-57.
11. Finberg HJ, Birnholz JC. Ultrasound evaluation of the gallbladder wall. Radiology 1979; 133: 693-698.
12. Pandy M, Sood BP, Shukla RC, et al. Carcinoma of the gallbladder : role of sonography in diagnosis and staging. J Clin Ultrasound 2000; 28: 227 - 232.
13. Soyer P, Gouhiri M, Boudiaf M, et al. Carcinoma of the gallbladder : imaging features with surgical correlation. AJR 1997; 169: 781-785.
14. Rosenthal SJ, Cox GG, Wetzel LH, et al. Pitfalls and differential diagnosis in biliary sonography. RadioGraphics 1990; 10: 285-311.

ULTRASONOGRAPHIC EVALUATION OF PALPABLE BREAST MASSES

Piyadara KHONGPIBOONKIT, MD[1]

ABSTRACT

PURPOSE : To retrospectively evaluate the sonographic findings and the diagnostic value of sonography in palpable breast masses at Phayao Hospital by using terminology of the Breast Imaging Reporting and Data System (BI-RADS) in order to categorize lesions from the sonograms and compare them with the histopathologic reports of the masses.

MATERIALS AND METHODS : Sonographic studies of 27 patients with palpable breast mass(es) which were histopathologically proven between January 1, 2007 and October 31, 2007 at Phayao Hospital were retrospectively reviewed. Each lesion was evaluated using the sonographic BI-RADS terminology and assigned a final BI-RADS category. The final assessment of sonographic BI-RADS and biopsy results were compared.

RESULTS : The sonographic BI-RADS classifications of all 27 patients were as follows : BI-RADS 5 in 7 patients,BI-RADS 4 in 6 patients,BI-RADS 3 in 8 patients and BI-RADS 2 in 6 patients. Of the 7 patients in the BI-RADS 5 category, 4 patients had malignant tumors, 2 patients had mastitis with abscesses, and 1 patient had fibroadenoma. One patient in the BI-RADS 4 ,one patient in the BI-RADS 3 and one patient in the BI-RADS 2 categories had chronic inflammation, hemolysed blood,and lipoma,respectively. The remaining 17 patients in the BI-RADS 2,3,4 categories had fibroadenomas or fibrocystic changes.

CONCLUSION: Ultrasound is a useful available and inexpensive method in the early detection and diagnosis of palpable breast masses, particularly in small hospitals which do not have mammographic x-ray equipment and in which most of the patients have economic problems. The sonographic BI-RADS descriptors and categories are also very helpful in catagorizing lesions, making management recommendations and differentiating between benign and malignant masses.

INTRODUCTION

Although mammography is recognized as the best method of screening for breast cancer, ultrasonography of the breast also plays a critical role in the diagnostic evaluation for screening, detection of palpable masses. Ultrasound with a high frequency transducer is essential for accurate, noninvasive diagnosis of breast cysts and has shown promises in differentiating between benign and malignant solid masses.[7,8] In light of widespread uses of sonography, the American College of Radiology (ACR) recently developed the Breast Imaging Reporting and Data System (BI-RADS) for breast sonography to standardize the characterization of sonographic lesions.[14,15] This BI-RADS includes descriptors of various features such as mass shape, orientation, margin, and posterior acoustic transmission, and other sonographic features.

[1] Department of Radiology, Phayao Hospital, Phayao, THAILAND 56000

The purpose of this study was to evaluate the sonographic findings and the usefulness of sonography in palpable breast masses at Phayao Hospital by using sonographic BI-RADS descriptors and categories. The final BI-RADS assessments were compared with the histopathologic reports.

MATERIALS AND METHODS

The ultrasonographic studies of 46 patients with palpable breast mass (es) obtained between January 1, 2007 and October 31, 2007 at Phayao Hospital were retrospectively reviewed. None of the patients received a mammographic examination before sonographic examination, due to the lack of mammographic x-ray equipment in Phayao Hospital.

All patients were examined with real-time sonography equipment (Logiq 5 Pro GE Mediacal Systems) using a multifrequency linear array 7.5 -12 MHz transducer.

19 patients were excluded from the study due to having no tissue diagnosis. Sonographic studies in these patients were interpreted as benign mass (es) in the BI-RADS 2 category. Their treatment was giving directory advices, follow up sonography and follow up physical examinations.

The study group included 27 females from 16 to 51 years of age.

The median age of these patients was 31.3 years.

All 27 patients of the study group had histopathologically proven masses. The assessments of the breast masses by sonography were grouped into seven broad categories based on sonographic BI-RADS descriptors,[3, 11] as follows: mass shape (Oval, round, irregular), mass margin (well-circumscribed, microlobulated, speculated, angular, indistinct), posterior echo (enhanced, unaffected,shadowing, or combined), mass echogenicity (hyperechoic, isoechoic, mildly hypoechoic, markedly hypoechoic, complex, anechoic), lesion boundary (abrupt, echogenic halo), mass orientation (parallel, or not) and presence of calcifications.

The sonographic diagnoses were recorded according to their sonographic ACR BI-RADS category. **Table 1.**

Table 1 : US BI-RADS Categories and Interpretation

US BI-RADS category	Interpretation.
0	Need additional imaging
1	Negative study.
2	Benign Findings
3	Probably Benign Findings: Short interval follow up suggested.
4	Suspicious Abnormality: Biopsy should be considered.
5	Highly Suggestive of Malignancy

The US BI-RADS 0 and 1 categories were not included in this study.

The final BI-RADS assessments were compared with the histopathologic reports.

RESULTS

All 27 patients included in the study had histopathologic diagnosis.

Among these patients, 6 patients were diagnosed as BI-RADS 2 category, 8 patients were diagnosed as BI-RADS 3 category, 6 patients were diagnosed as BIRADS 4 category and 7 patients were diagnosed as BIRADS 5 category.

The sizes of all breast masses were ranging from 1 cm. to 9 cm.

All 20 patients in the BI-RADS 2,3,4 categories were benign in the histologic diagnosis, as follows:

- 1 patient in the BI-RADS 2 category had lipoma,
- 1 patients in the BI-RADS 3 category had a hematoma with hemolysed blood in the breast and had a history of recent breast trauma.Sonopraphic study showed a mass with irregular shape and complex echogenicity.
- 1 patient in the BI-RADS 4 category had a history of breast masses and breast pain. Sonography showed a mass with inhomogeneous echo and indistinct margin. FNA was performed and the pathologic report showed chronic inflammatory process from possible granulomatous mastitis.
- The remaining 17 patients had pathologically proven fibroadenoma or fibrocystic changes.

In the 7 patients in BI-RADS 5, malignancy was revealed in 4 cases, mastitis with abscess formation in 2 cases and a fibroadenoma in 1 case. **Table 2**

TABLE 2 : BI-RADS category compared with histopathology

Final BI-RADS assessment (category)	Number of patients (cases)	**Histopathology**
BI-RADS 2 (6 cases)	5	Fibroadenoma, Fibrocystic changes.
	1	Lipoma
BI-RADS 3 (8 cases)	7	Fibroadenoma, Fibrocystic changes.
	1	Hemolysed blood.
BI-RADS 4 (6 cases)	5	Fibroadenoma, Fibrocystic changes.
	1	Chronic inflammatory processes, possible granulomatous mastitis.
BI-RADS 5 (7 cases)	4	Malignancy (Intraductal carcinoma, Invasive ductal carcinoma, Papillary ductal carcinoma in situ,and infiltrating ductal carcinoma, respectively.)
	2	Mastitis with abscess formation.
	1	Fibroadenoma.
Total	27	

TABLE 3 : Mass descriptions of each sonographic BI-RADS category

US BI-RADS category. / Mass Descriptors	BIRAD2 (No of cases)	BIRAD3 (No of cases)	BIRAD 4 (No of cases)	BIRAD5 (No of cases)
Mass shape				
-Oval	6	7	4	2
-Round	-	-	1	-
-Irregular	-	1	1	5
Mass margin				
-Well-circumscribed	6	8	5	-
-Microlobulation.	-	-	-	1
-Angular	-	-	-	1
-Spiculation.	-	-	-	2
-Indistinct	-	-	2	3
Mass exhogenicity				
-Hyperechoic.	1	-	-	-
-Isoechoic	-	-	-	-
-Mildly hypoechoic.	-	5	4	1
-Markedly hypoechoic.	3	2	2	3
-Complex.	-	1	-	3
-Anechoic	2	-	-	-
Lesion Boundary				
-Abrupt	6	8	6	7
-Echogenic halo.	-	-	-	-
Acoustic transmission.				
-Enhanced	5	5	1	-
-Normal	-	3	3	1
-Shadowing	1	-	2	3
-Combined	-	-	-	3
Mass orientation				
-Parallel	6	8	6	5
-Not parallel	-	-	-	2
Calcifications within mass				
-Present	-	-	-	-
-Absent	6	8	6	7

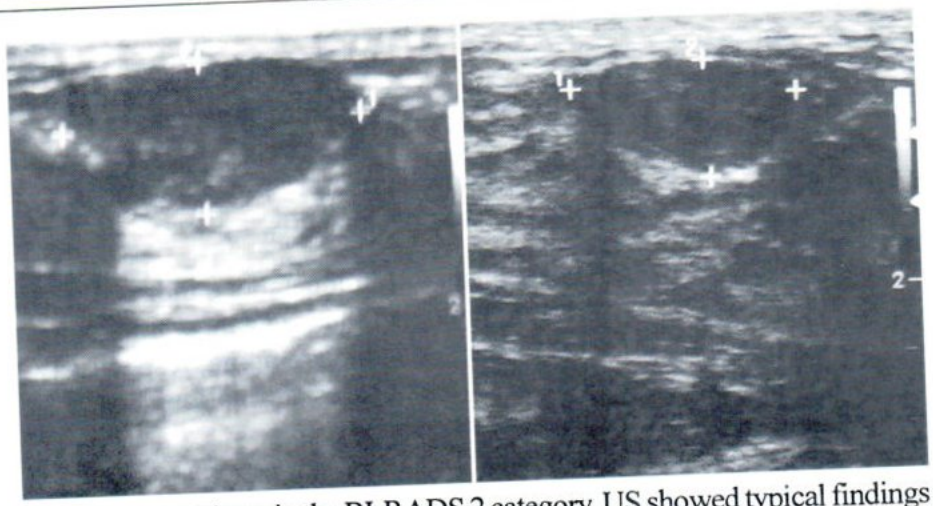

Fig.1 Two patients in the BI-RADS 2 category. US showed typical findings of benign masses: oval shape, well-circumscribed, hypoechoic, abrupt boundary and posterior enhancement. **US : Ultrasonography**

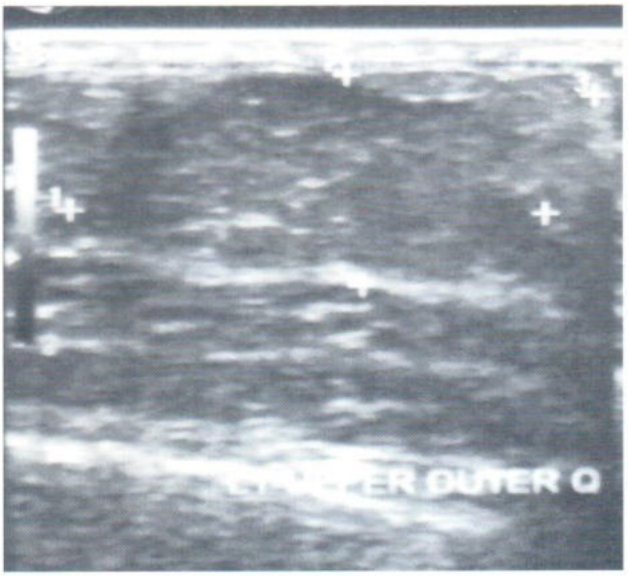

Fig.2 Sonography in a 28-year-old woman showed an oval-shaped mass with indistinct margin and inhomogeneous echo: BI-RADS 4 category. Tissue diagnosis was chronic inflammatory process, possible granulomatous mastitis.

DISCUSSION

Although there has been some controversy regarding the utility of sonography when evaluating solid breast masses for the likelihood of malignancy,[9,10] several studies have suggested that sonographic appearance can be useful in differentiating benign from malignant solid breast masses.[5,7]

The addition of the BI-RADS lexicon for ultrasonography is helpful and can be used with good agreement among radiologists, even those without specific training in the new terminology.[11]

The sonographic findings suspicious for malignancy included shadowing, solid nodule, spiculation, angular margins, thick echogenic halo, microlobulation,taller-than-wide, hypoechogenicity, calcifications and duct extension or branch pattern.[7]

Sonographic evidence of spiculated margin suggests infiltrating growth of the lesion into the surrounding tissue, whereas an irregular shape can indicate inconsistent growth and advancement of the lesion edge. Nonparallel orientation on sonography can suggest spread of the lesion through tissue-plane boundaries. All of these characteristics are more likely to be associated with malignant lesions. In contrast, circumscribed margin and oval shape representing smooth uniform growth without involvement of surrounding tissue are associated more with a benign lesion.[11]

In this study all patients in the BI-RADS 2,3 and 4 categories were benign in the histologic diagnoses. All 6 cases in BI-RADS 4 showed some findings of suspicious malignancy such as posterior shadowing in 2 patients,indistinct margins in 2 patients and irregular mass shape in 1 patient. So tissue diagnosis had to be performed to exclude malignancy.

Among the 7 patients in BI-RADS 5 group:

4 patients had typical sonographic evidences of malignancy and no doubt in the diagnosis,

1 patient had a large fibroadenoma , that showed some malignancy findings (lobulated margin, combined posterior shadowing and complex echogenicity)

2 patients had mastitis with breast abscesses, these conditions being difficult to be the differentiated from malignancy by ultrasound alone, particularly if there were no signs of inflammation.

Breast abscess and inflammatory breast carcinoma may have identical clinical and mammographic findings. Quick use of aspiration biopsy may expedite appropriate patient care.[12]

Most patients included in this study were more concerned about having a malignant breast mass than about their cosmetic appearance. So the patients and the clinicians preferred to have tissue diagnosis of the occult palpable breast masses together with follow up studies.

Mammographic studies were not done in most patients due to economic problems and lack of

mammographic x-ray equipment in Phayao Hospital. Treatment planning and treatment decisions by the clinicians usually depended on sonographic findings and physical examinations.

Statistic analysis was not done in this study because of the small number of patients.

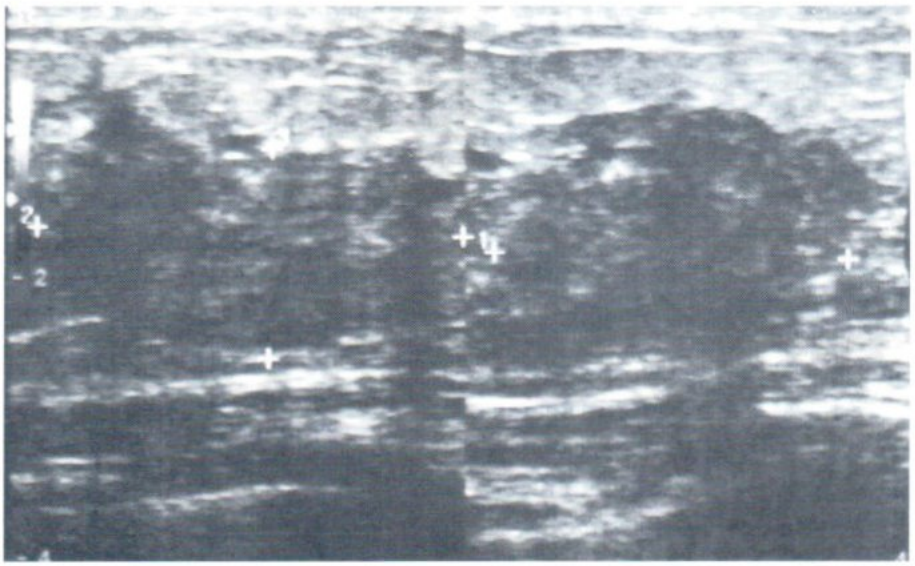

Fig.3 US in a 34-year-old woman showed a mass with irregular shape, indistinct margin and complex echo: BI-RADS 5 category. Tissue diagnosis was mastitis with abscesses formation.

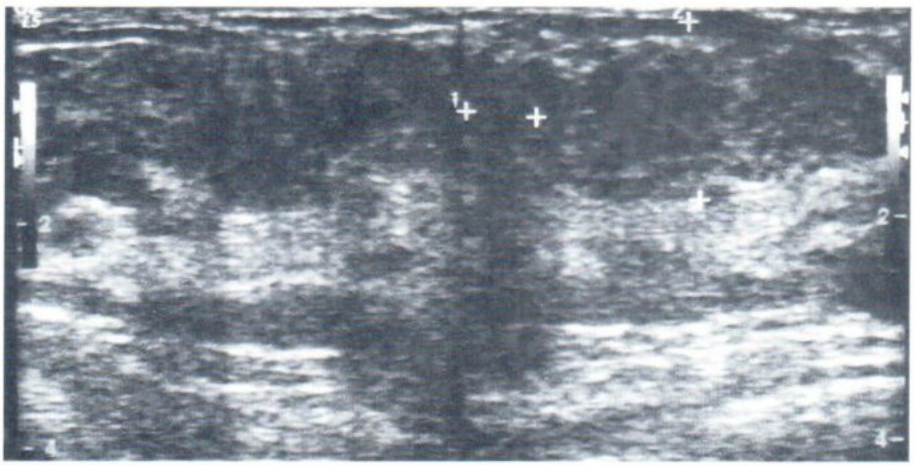

Fig.4 US in a 29-year-old woman. Final assessment was BI-RADS 5 category. Tissue diagnosis was mastitis with abscesses formation.

Fig.5 US in a 48-year-old woman showed a small mass (1 cm.) with spiculated margin and posterior shadowing: BI-RADS 5 category. Tissue diagnosis was intraductal carcinoma.

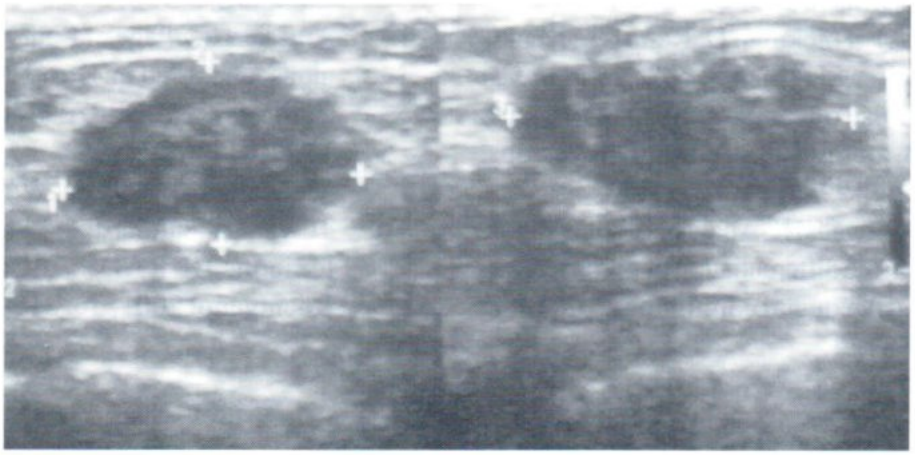

Fig.6 US in a 34-year-old woman showed an inhomogeneous hypoechoic mass with spiculate margin : BI-RADS 5 category. Tissue diagnosis was invasive ductal carcinoma.

CONCLUSION

Ultrasound is a useful, available and inexpensive method in the early detection and diagnosis of palpable breast masses, particularly in small hospitals which do not have mammographic x-ray equipment or other advanced imaging equipment and in which most of the patients have economic problems. The sonographic BI-RADS descriptors and categories are also very helpful in characterizing lesions, making management recommendations and differentiating between benign and malignant breast masses, but are less helpful in differentiating between breast abscess and inflammatory breast cancer or malignant breast masses in the BI-RADS 5 category.

REFERENCES

1. Teresa G. Odle, B.A. Breast Ultrasound. Radiologic Technology, 2007; 78: 222-242
2. D.J. Nelsen, G.A. Rouse, and M. De Lange. Sonographic Evaluation of Solid Breast Masses. Journal of Diagnostic Medical Sonography 1994; 10(6): 312-316

3. A.S. Hong, E.L. Rosen, M.S. Soo, and J.A. Baker. BI-RADS for Sonography: Positive and Negative Predictive Value of Sonographic Features. AJR 2005; 184(4)1260-1265
4. Joo Hee Cha et al. Characterization of Benign and Malignant Solid Breast Masses. Comparison of Conventional US and Tissue Harmonic Imaging: Radiology 2006; 242: 63-69
5. AP Harper, E Kelly-Fry,JS Noe, JR Bies and VP Jackson. Ultrasound in the Evaluation of Solid Breast Masses. Radiology 1983; 146 (3) 731-736
6. Jay A.Baker, Phyllis J.Kornguth, Mary Scott Soo, Ruth Walsh, Patricia Mengoni. Sonography of Solid Breast Lesions: Observer Variability of Lesion Description and Assessment. AJR 1999; 172: 1621-1625
7. Stavors AT, Thickman D, Rapp CL, Dennis MA, Parker SH, Sisney GA. Solid breast nodules: use of sonography to distinguish between benign and malignant lesions. Radiology 1995; 196: 123-134.
8. Skaane P,Engedel K. Analysis of sonographic features in the differentiation of fibroadenoma and invasive ductal carcinoma. AJR 1998; 170: 109-144
9. Jackson VP: Management of solid breast nodules: what is the role of sonography ?. Radiology 1995; 196: 14-15
10. Hall FM. Sonography of the breast: controversies and opinions.AJR 1997; 169: 1635-1636
11. Elizabeth Lazarus, MarthaB. Mainiero, et.al. BI-RADS lexicon for US and mammography: Interobserver variability and positive predictive value. Radilogy 2006; 239: 385-391
12. Patricia L. Abbitt. Breast. Ultrasound: A pattern approach,international edition.Florida 1995; 433-442
13. Malai Muttarak. Abscess in the non-lactating breast: Radiodiagnostic aspects.Australasian Radiology; 1996; 223-225
14. American Collage of Radiology. BI-RADS: ultrasound, 1st ed.in: Breast imaging reporting and data system: BI-RADS atlas,4th ed. Reston, VA: ACR, 2003
15. Mendelson EB, Berg WA, Merritt CRB. Toward a standardized breast ultrasound lexicon, BI-RADS: ultrasound. Semin Roentgenol 2001; 36: 217-225